

IMPACT OF INTERFERENCE ON CONNECTIVITY AND OUTAGE
PERFORMANCES IN WIRELESS COMMUNICATION NETWORKS:
INTERFERENCE-BASED CHANNEL MODELS

by

Constantine Mukasa

A Thesis Submitted to the Faculty of
The College of Engineering and Computer Science
in Partial Fulfillment of the Requirements for the Degree of
Master of Science

Florida Atlantic University

Boca Raton, Florida

August 2013

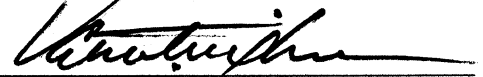
IMPACT OF INTERFERENCE ON CONNECTIVITY AND OUTAGE
PERFORMANCES IN WIRELESS COMMUNICATION NETWORKS:
INTERFERENCE-BASED CHANNEL MODELS

by

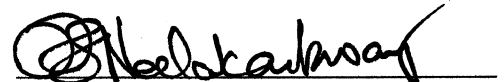
Constantine Mukasa

This thesis was prepared under the direction of the candidate's thesis advisor, Dr. Valentine Aalo, Department of Computer & Electrical Engineering and Computer Science, and has been approved by the members of his supervisory committee. It was submitted to the faculty of the College of Engineering and Computer Science and was accepted in partial fulfillment of the requirements for the degree of Master of Science.

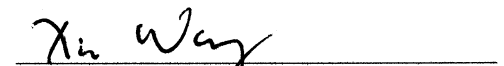
SUPERVISORY COMMITTEE:



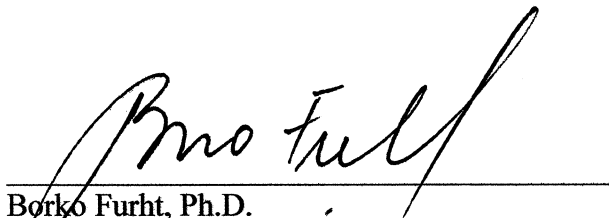
Valentine Aalo, Ph.D.
Thesis Advisor



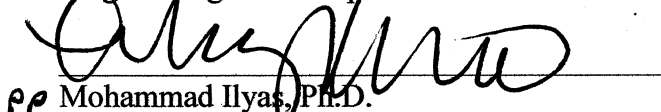
Perambur S. Neelakanta, Ph.D.



Xin Wang, Ph.D.



Borko Furht, Ph.D.
Chair, Department of Computer & Electrical
Engineering and Computer Science



PP Mohammad Ilyas, Ph.D.
Dean, College of Engineering and Computer Science



Barry T. Ross, Ph.D.
Dean, Graduate College

July 18, 2013
Date

ACKNOWLEDGEMENTS

To accomplishment this work, there is a group of people whose contributions provided the support necessary to reach this goal. I am indebted to many people for supporting and helping me along the way. I will endeavor to acknowledge these special individuals, but I am sure to miss some for which I apologize.

First, I wish to express sincere thanks and love to my thesis supervisor, Dr. Valentine Aalo for providing me with the precise balance of guidance and independence during my research. I am greatly indebted to him for his dedicated mentoring, support, encouragement, and advice in various matters. His extensive expertise and splendid intuition have been a great source of motivation to me throughout this process and his remarks and criticisms are deeply reflected throughout the presentation of this thesis.

I am also grateful to Dr. Perambur S. Neelakanta and Dr. Xin Wang for their immense help and support. I am thankful to my classmate Jene Rene Neptune for his friendship and support in the past few years.

Support for this thesis was provided in part by a grant from Tecore Networks and FAU Foundation via the NSF/IUCRC program.

Above all, I am extremely grateful to my family members for their consistent support throughout my career.

ABSTRACT

Author: Constantine Mukasa
Title: Impact of Interference on Connectivity and Outage Performances in Wireless Communication Networks: Interference-based Channel Models
Institution: Florida Atlantic University
Thesis Advisor: Dr. Valentine Aalo
Degree: Master of Science
Year: 2013

In recent years, a plethora of wireless applications such as Bluetooth and Ultra-wide band (UWB) radio have emerged. This drastic increase has overly congested the spectrum. So, new networks such as cognitive radios that can solve the spectrum congestion have emerged. But in such networks, interference is introduced at the physical layer. We study and develop an interference model capable of capturing the intrinsic characteristics of the coexistence of such wireless applications. We investigate the effect of interference using device isolation probability or outage probability in presence Rayleigh and Nakagami- m fading at the physical layer and the impact of lognormal shadowing. We assume that the devices are either deterministically placed or randomly distributed according to a Poisson point process. We derive explicit expressions for the isolation probability and outage probability that give insight into how these channel impairments affect communication in these applications. We use computer simulations to validate our analytical results.

DEDICATION

This manuscript is dedicated to Philonella, D'mitra, and Mary.

IMPACT OF INTERFERENCE ON CONNECTIVITY AND OUTAGE
PERFORMANCES IN WIRELESS COMMUNICATION NETWORKS:
INTERFERENCE-BASED CHANNEL MODELS

List of Figures	ix
List of Notations	xii
List of Acronyms	xv
Chapter 1: Introduction	1
1.1 General Overview	1
1.2 Challenges in Wireless Communication	2
1.3 Interference Modeling	4
1.4 Interference Mitigation.....	5
1.4.1 Interference Cancellation.....	6
1.4.2 Diversity	6
1.4.3 Power Control.....	7
1.5 Performance Measures	7
1.6 Thesis Objective.....	7
1.7 Thesis Organization.....	8
Chapter 2: System Models	10
2.1 Introduction	10
2.2 Propagation Models.....	10

2.3 Channel Models.....	11
2.3.1 Multipath Fading Models	12
2.3.1.1 Rayleigh Fading.....	12
2.3.1.2 Nakagami Fading.....	13
2.3.2 Shadow Fading	14
2.3.3 Composite fading.....	15
2.3.4 Generalized Gamma Distribution.....	18
Chapter 3: Interference Models and Performance Measures	20
3.1 Introduction	20
3.1.1 Fixed Number of Interferers	21
3.1.2 Random Number of Interferers.....	21
3.2 Interference Models.....	22
3.2.1 Collision Channel Model.....	22
3.2.2 Protocol Interference Model.....	23
3.2.3 Capture Threshold Model	23
3.2.4 Additive Interference Model	23
3.3 Performance Measures	25
3.3.1 Average SNR.....	25
3.3.2 Outage Probability.....	26
3.3.3 Device Isolation Probability	26
Chapter 4: Performance Analysis Using Connectivity	28
4.1 Introduction	28
4.2 Noise Limited Systems.....	29

4.2.1 Effect of Path-loss Only	29
4.2.2 Effect of Path-loss, Multipath, and Shadow Fading.....	31
4.3 Systems With Fixed Number of Interferers	33
4.3.1 Effect of Path-loss Only	33
4.3.2 Effect of Path-loss, Multipath, and Shadow Fading.....	35
4.3.2.1.1 PDF Approach	36
4.3.2.1.2 Geometric Mean Approximation	38
4.4 Systems With Random Number of Interferers	40
4.4.1 Effect of Path-loss Only	40
4.5 Effect of Path-loss, Multipath, and Shadow Fading.....	42
4.6 Simulation Results.....	43
Chapter 5: Performance Analysis Using Outage Probability	57
5.1 Introduction	57
5.2 Outage Probability.....	58
5.2.1 Fixed Number of Interferers	58
5.2.1.1 PDF Based Approach.....	59
5.2.1.1.1 Rayleigh Fading Case.	59
5.2.1.1.2 Nakagami Fading Case.	60
5.2.1.2 MGF Based Approach	61
5.2.1.2.1 Rayleigh Fading Case	61
5.2.1.2.2 Nakagami Fading Case	62
5.2.2 Random Number of Interferers.....	65
MGF Based Approach	65

Aggregate Interference Is Alpha-stable.	66
5.2.2.1.1 Rayleigh Fading Case	67
5.2.2.1.2 Nakagami Fading Case	68
Chapter 6: Applications/Systems.....	71
6.1 Cellular Networks	71
6.2 Sensor Networks (Self-Organizing Networks).....	75
6.3 Cognitive Radio Networks	77
6.4 VANET	80
Chapter 7: Analytical and Computer Simulation Results	84
7.1 Computer Simulation	84
7.2 Numerical Analysis	85
Chapter 8: Summary and Conclusion	93
8.1 Summary of Main Results.....	93
8.2 Conclusion.....	95
8.3 Suggestions for Future Work	96
Appendix A.....	97
Appendix B	105
B.1 Fox's H -function [46].....	105
B.2 Meijer's G -function [30]	105
Appendix C	106
Bibliography	108

LIST OF FIGURES

Figure 1: Wireless communication system network architecture [8].	1
Figure 2: CCI and ACI in a cellular network [27].	3
Figure 3: a) Generalized model geometry [56] and b) self-interference components.	3
Figure 4: a) Square, b) Triangular, and c) Hexagon network topologies [43].	5
Figure 5: Distribution of interfering transmitters around the receiver.	20
Figure 6: Deterministic circular disk of transmission model.	30
Figure 7: Illustration of network topology with $\lambda = 10^{-2} \text{ m}^{-2}$ and $\beta = 10 \text{ dB}$. The blue circles denote device location and the red asterisk denotes the receiver	45
Figure 8: Illustration of isolated devices when $\lambda = 10^{-3} \text{ m}^{-2}$, $\lambda = 10^{-2} \text{ m}^{-2}$, $\lambda = 10^{-1.5} \text{ m}^{-2}$, $\lambda = 10^{-1} \text{ m}^{-2}$ respectively and $\beta = 3 \text{ dB}$. The blue circles denote device location, the red diamonds denote isolated devices, and the dotted lines indicate various connections between devices.	46
Figure 9: Comparison of different network topologies. Top: $\lambda = 10^{-2} \text{ m}^{-2}$, bottom: $\lambda = 10^{-1} \text{ m}^{-2}$ for $\beta = 5 \text{ dB}$ and $\beta = 10 \text{ dB}$ respectively.	47
Figure 10: Effects of shadowing on isolation probability using (4.27) when $\lambda = 10^{-4} \text{ m}^{-2}$, $\beta = 3 \text{ dB}$, $\eta = 3.5$, $\bar{\gamma}_z = 2 \text{ dBm}$, and $m_0 = 3$, and $m_z = 2$	48
Figure 11: Impact of lognormal fading on isolation probability when $\beta = 10 \text{ dB}$, $\eta = 3.5$, $\bar{\gamma}_0 = 10$, and $m_0 = 3$ using (4.8).	49

Figure 12: Impact of interferers present on isolation probability using (4.27) when	
$\sigma = 5, \beta = 3 \text{ dB}, \eta = 3.5, \bar{\gamma}_z = 2 \text{ dBm}, \text{ and } m_0 = 3, \text{ and } m_z = 2$.	50
Figure 13: Device isolation probability when the interference area is varied, $\beta = 5$,	
$\eta = 3.5, \sigma_R = 2, m_0 = 3, \text{ and } m = 2$ using (4.32).	51
Figure 14: Illustration of the impact of path-loss, multipath, and shadow fading on	
isolation probability using (4.32) when the interference disk has a radius	
$C = 8 \text{ m}, \beta = 5, N = 5, \eta = 3.5, \sigma_R = 2, m_0 = 3, \text{ and } m_z = 2$.	52
Figure 15: Illustration of how the interference region affects isolation probability.	53
Figure 16: Effect of path-loss coefficient on isolation probability where $\beta = 5$, ,	
$m_0 = 3, \text{ and } m_i = 2$.	54
Figure 17: Comparing the SNR and SINR cases ($N = 0$) when $\beta = 5 \text{ dB}$ and	
$\beta = 10 \text{ dB}, \bar{\gamma}_0 = \bar{\gamma}_z = 1, W = 0.01 \text{ mW}, \eta = 3.5, m_0 = 3, \text{ and } m_i = 2$.	55
Figure 18 : Device isolation probability when the average power ratio is varied,	
$\lambda = 10^{-3} \text{ m}^{-2}, \eta = 3.5, \sigma_R = 2, m_0 = 3, \text{ and } m = 2$ using (4.45).	56
Figure 19: Illustration of a cellular concept.	72
Figure 20: Reuse cluster of size 4 cells (1,2,3,4) and reuse cluster of size 7 cells	
(1,2,3,4,5,6,and 7).	73
Figure 21: Demonstration of first, second and third tiers of co-channel interfering	
cells for a cell at the center [42].	74
Figure 22: a) Illustration of cognitive radio network architecture [7], b) Use of	
cognitive abilities to detect the best available alternate route without	
harming PU.	80

Figure 23: a) VANET ideal communication range scenario shown by the black dotted line, b) VANET realistic communication range scenario shown by the solid blue line.....	83
Figure 24: Plot of outage probability in (5.5) when only one interferer is present and $\eta = 3.5$ in a Rayleigh fading channel.	85
Figure 25: Plot of outage probability in (5.5) while varying the number of interferers, N when $\beta = 5$ and $\eta = 3.5$ in a Rayleigh fading channel.....	86
Figure 26: Plot of outage probability (5.7) against the average power ratio while varying the threshold when $N = 6$, $\eta = 3.5$, $m_0 = 3$, and $m_z = 2$	87
Figure 27: Comparing the PDF (5.5) and MGF (5.10) approach analysis results when $N = 6$ and $\eta = 3.5$ in a Rayleigh fading channel.	88
Figure 28: Comparing the results obtained by PDF (5.7) and MGF (5.16) approach analysis when $N = 6$, $\eta = 3.5$, $m_0 = 3$, and $m_z = 2$	89
Figure 29: Illustration of the impact of interference on outage probability given in.....	90
Figure 30: The outage probability; a comparison of the fading parameter when $N = 6$, $\eta = 3.5$, $\beta = 5$, and $m_z = 2$	91
Figure 31: Illustration of the impact of interference on outage probability in a Rayleigh fading (5.28) when $\lambda = .05$ and β is varied accordingly.	92

LIST OF NOTATIONS

A	Antenna gain
P_χ	Average power of RV χ
P_{tx}	Transmit power
P_R	Received power
P_i	Power received from the i -th transmitter
Y	Instantaneous Power
Λ	Average power ratio
γ	Instantaneous SNR/SIR/SINR
$\bar{\gamma}$	Received average SNR/SIR/SINR
R	Radius of cell
M	Cluster reuse size
\mathcal{R}	Communication range
r	Transmitter-receiver distance
η	Path-loss exponent
j	$\sqrt{-1}$
m_χ	Nakagami fading parameter for RV χ
$\mathbb{M}_\chi(\cdot)$	Moment generating function of RV χ

$\mathcal{D}_{\chi}^k(f(\chi))$	k^{th} derivative of $f(\chi)$ w.r.t χ
$\mathbb{E}(\chi)$	Expectation operation on RV χ
$\mathbb{E}_{\chi}(\cdot)$	Expectation w.r.t RV χ
$\mathbb{P}(\chi)$	Probability operator on RV χ
\mathcal{Q}_{χ}	Probability of RV χ
$p_{\chi}(\cdot)$	PDF of RV χ
$F_{\chi}(\cdot)$	CDF of RV χ
N	Number of interferers
Z	Aggregate interference power
α_i^2	Multipath faded power for the i^{th} link
u_i	Shadow faded power for the i^{th} link
β	Power threshold
W	Noise power at the receiver
\mathcal{A}	Area
\mathfrak{D}	Co-channel reuse distance
λ	Intensity of Poisson process
\mathcal{N}	Random point process
$\Gamma(\cdot)$	Gamma function
$\Gamma(\cdot, \cdot)$	Upper incomplete Gamma function
$\mathcal{G}(\cdot, \cdot)$	Lower incomplete Gamma function

\mathbb{N}^+	Natural numbers without zero
\mathbb{R}^2	2-Dimensional real space
${}_aF_b(\cdot)$	Generalized hypergeometric function
$U(a; b; x)$	Confluent hypergeometric function of the second kind
$G_{p,q}^{m,n}(\cdot)$	Meijer's G - function
$H_{p,q}^{m,n}(\cdot)$	Fox's H - function

LIST OF ACRONYMS

AWGN	Additive white Gaussian noise
ACI	Adjacent-channel interference
BS	Base station
BSC	Base station controller
CCI	Co-channel interference
CDF	Cumulative distribution function
CDMA	Code division multiple access
CNs	Cognitive networks
CRU	Cognitive radio user
dB	Decibels
DSRC	Dedicated short-range communication
EGC	Equal gain combining
FCC	Federal Communications Commission
ITS	Intelligent transportation systems
LOS	Line of sight
MAC	Media access control layer
MGF	Moment generating function
MRC	Maximal ratio combining
PDF	Probability density function

PIC	Parallel interference cancellation
PPP	Poisson point process
PU	Cognitive radio primary user
RVs	Random variables
SIC	Successive interference cancellation
SIR	Signal-to-interference ratio
SINR	Signal-to-interference plus noise ratio
SNR	Signal-to-noise ratio
SU	Cognitive radio secondary user
V2I	Vehicle-to-infrastructure communication
VANET	Vehicular ad hoc networks
VLSI	Very large scale integration
V2V	Vehicle-to-vehicle communication
WSNs	Wireless sensor networks

CHAPTER 1

INTRODUCTION

1.1 General Overview

Enormous improvements in very large scale integration (VLSI) and fabrication processes made in previous years have led to great advancements in electronics such that reliable, complex, and sensitive wireless communication systems are available to aggressively utilize spectral resources. Examples of such systems are cellular systems, self-organizing networks, cognitive radio networks, satellite networks, broadband wireless access systems, and vehicular ad hoc networks (VANET); see Figure 1.

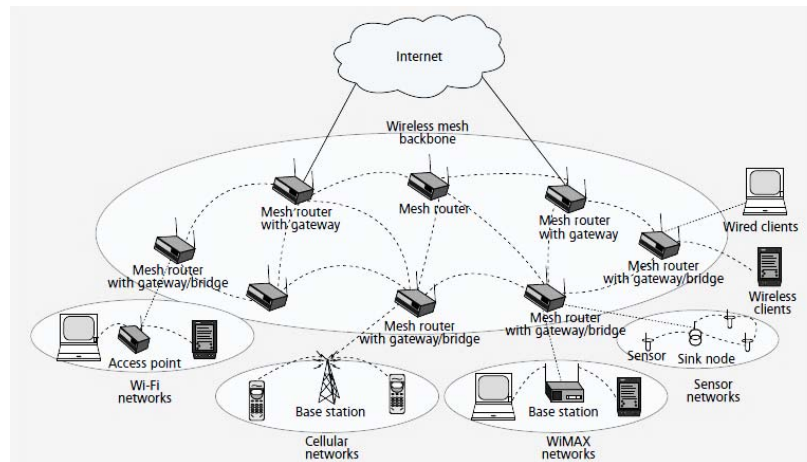


Figure 1: Wireless communication system network architecture [8].

Communication in most of these systems relies on the reuse of the spectral resource and the physical nature of the wireless channel.

1.2 Challenges in Wireless Communication

Communication over the wireless channel is impaired by factors such as wireless propagation effects, thermal noise, and interference. The wireless propagation effects may comprise of transmitted signal attenuation due to distance-dependency (path loss), large objects blocking the transmitted signal (shadow fading), and receiving several copies of the original transmitted signal (multipath fading). Thermal noise is due to the receiver electronics where the electrons in the conductors move constantly in all directions at random velocities and introduce sporadic currents. Thermal noise is mostly modeled in the literature as additive white Gaussian noise (AWGN).

Spectral resource reuse is used to enhance network capacity; but on the other hand, it introduces interference such as co-channel interference (CCI), adjacent-channel interference (ACI), and self-interference. Interference occurs at the receiver's physical layer and is due to undesired transmissions from other transmitters in the network impeding the proper reception of the desired signal. These interfering signals can severely degrade performance of the system by dropping the signal to interference ratio (SIR) of the received signal below acceptable levels. Interference also introduces the near-far effect phenomenon, where nearby signals are stronger and impede proper reception of weaker far away signals.

CCI occurs when transmitters in separate cells that are in different clusters transmit using the same frequency (frequency reuse). ACI occurs when transmitters in a given cluster transmit using different but close channel frequencies whose side-lobes overlap. See Figure 2 that illustrates the origins of ACI and CCI. ACI is mainly due to filter imperfections at the receiver that hinder the filtration of the nearby frequencies; thus

letting them to creep into the pass-band.

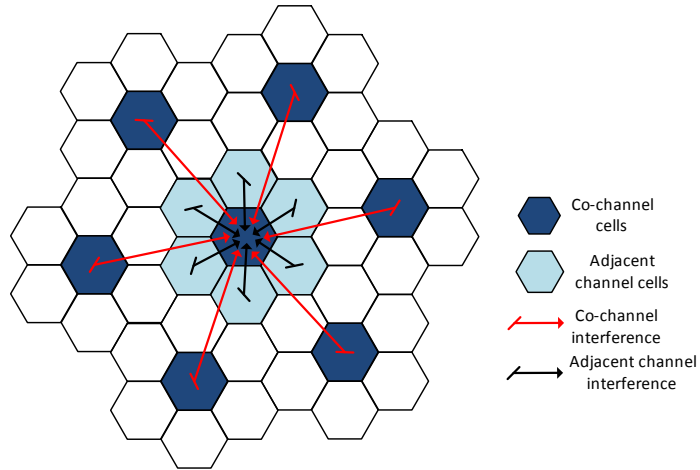


Figure 2: CCI and ACI in a cellular network [27].

When a wireless device can operate in a full duplex mode, the local transmit power appears at the receiver as part of the received signal. But, the transmit power level is much greater than the received signal power; thus drowning the received signal. This is called self-interference (SI).

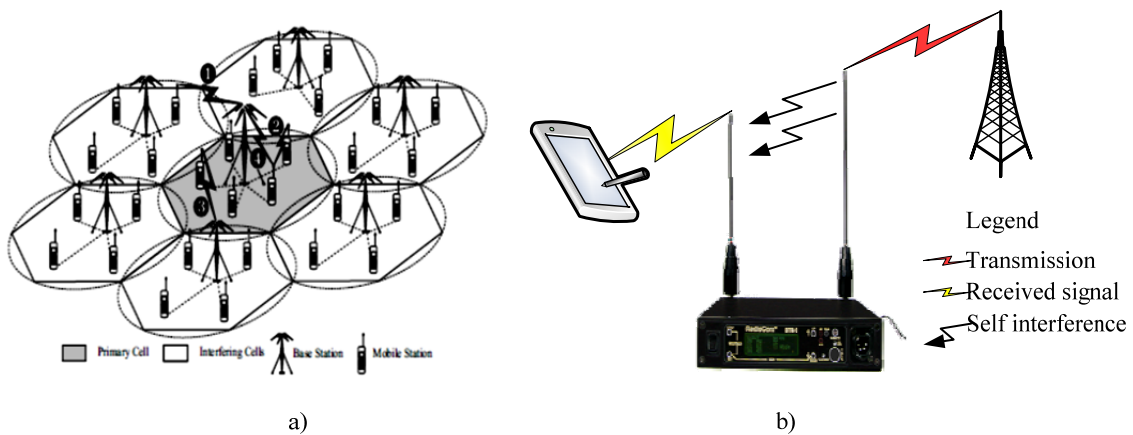


Figure 3: a) Generalized model geometry [56] and b) self-interference components.

1.3 Interference Modeling

Recently, there has been significant interest in accurate and efficient interference modeling techniques in the literature. This is mainly due to the fact that interference modeling plays a significant role in the understanding and analyzing the impact of interference, and designing and developing excellent interference mitigation techniques for wireless communication systems. According to [16, 74], a good interference model should capture the following fundamental components: a propagation model that describes the propagation effects the received signal experiences such as path loss, fading, shadowing, and interference; a spatial distribution of the interferers that takes into account the spatial distribution of the transmitters in the network; and a network operation model that describes the transmission characteristics of the network terminals such as medium access control techniques (random access and deterministic access), power control, and modulation techniques.

Spatial distribution of the interferers is vital in the analysis of the impact of interference on network performance. The location of the interferers plays a significant role in the analysis. The distribution of the locations of the interferers may be deterministic, random, or a hybrid of both. The deterministic scheme is where the placement of the interfering devices follows a regular pattern. Thus, the position of each device and its neighbors are known.

For example, in square, triangular, and hexagon position grids as seen in Figure 4, the devices are placed at the corresponding vertices such that the distance between close neighbors is the same and each device has exactly the same number of nearest neighbors. For example, some systems such as cellular networks and ad hoc networks are considered

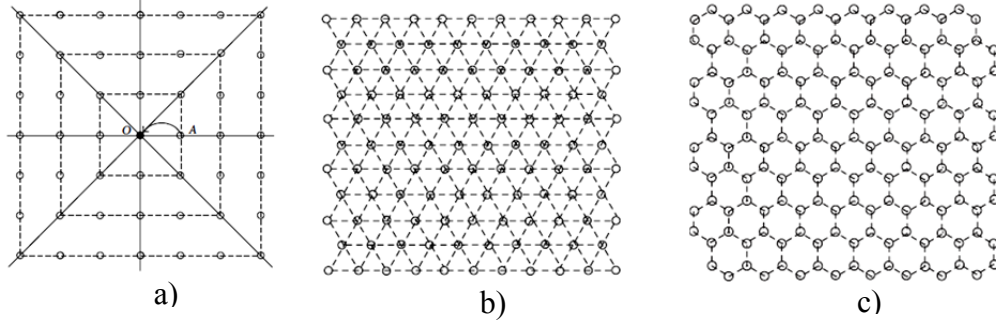


Figure 4: a) Square, b) Triangular, and c) Hexagon network topologies [43].

deterministic because the locations of the devices are known exactly

In a random scheme, there is less control on the placement or location of the devices. For example, in a case where the devices are dropped out of a plane or fired using a gun; their actual locations are unknown. Since the location of the devices in the network are unknown, it is lucid to assume that a device is equally likely to be somewhere within the network and its position is independent from the positions of all the other devices. Thus the location of the interferers can be statistically described. To capture the actual positions of the devices adequately, a suitable probability distribution must be selected. Examples of distributions used for such topologies are Poisson point process (PPP), Binomial point process, and Matern point process. In [33], the benefits and tradeoffs of using either regular or random network topologies are presented. The authors in [43] analyzed the throughput and transmit probability for both regular and random networks.

1.4 Interference Mitigation

In order to improve data throughput, signal-to-interference ratio, and increase co-existing users, various mitigation techniques have been used in different communication applications. Simple mitigation techniques for ACI may include use of superior band-

pass filter design techniques for the receiver, use of transmission schemes with low out-of-bound emissions, assigning channel frequencies that are further apart, and use of digital signal processing equalizer techniques [27]. The techniques discussed include interference cancellation, diversity, and power control.

1.4.1 Interference Cancellation

Successive interference cancellation (SIC) and parallel interference cancellation (PIC) are some of the most commonly employed cancellation techniques at the receiver. SIC is a simple but powerful iterative scheme that orders the received signals according to their likelihood of being decoded with the strongest signal being first. The decoded signal is reconstructed and subtracted from the received signal. The whole process is repeated for all the other signals. In this scheme, the weak signals profit from the stronger signals being canceled out before the weak ones are decoded. PIC is an iterative scheme that uses multiple decoders to decode and cancel out multiple signals simultaneously. PIC helps to combat the time delay experienced by SIC technique.

1.4.2 Diversity

Diversity can be achieved by transmitting and receiving multiple replicas of the signal. The received signals are presumed to experience independent or uncorrelated fading. Since the transmit power will be different for each signal, the received signal-to-noise ratio (SNR) fluctuates randomly. At the receiver end, different linear detection techniques such as maximal ratio combining (MRC) and equal gain combining (EGC) can be used to coherently combine the replicas of the originally transmitted signal to

enhance reliable reception. Multiple-input, multiple-output (MIMO) systems are good examples of systems that benefit from using diversity.

1.4.3 Power Control

High transmitting power levels are known to improve the quality of the received signal at a cell site; but this introduces the near-far effect within the cell and interference in the neighboring cell sites. To combat these effects, power control techniques are used where the power levels transmitted are constantly adjusted to meet the minimum power required to maintain a good quality link. An example is the power control scheme in code division multiple access (CDMA) where the system capacity is maximized if the transmit power of each user is controlled so that the transmitted signals arrive at the cell site with the minimum required signal to noise ratio [57]. Power control helps also to increase the device's battery life.

1.5 Performance Measures

In any wireless communication application, it is imperative to identify a method to quantify the performance of the system. There are several measures of performance used to evaluate real communication systems; namely, average SNR, outage probability, connectivity, and so on.

1.6 Thesis Objective

In wireless ad hoc and sensor networks, multihop transmissions are essential in improving the throughput and extending coverage. So, connectivity of a node to a neighboring node is necessary to successfully relay the transmitted message from the

source to the destination. However in such networks there many simultaneous transmissions such that the signals transmitted at the same time will mutually interfere with each other. Therefore, excellent and efficient analysis, design, and implementation of interference mitigation schemes are needed to ensure connectivity. Most of the proposed solutions depend on the complex computation in the media access control (MAC) layer. However, for systems like wireless sensor networks (WSNs), it is impractical for the devices to have the computational sophistication and power to mitigate interference. For some applications such as jamming in battle field environment, it is impractical to assume a deterministic device placement. Thus, the main objective of thesis is to investigate the impact of interference on the isolation probability and the outage probability in such networks.

1.7 Thesis Organization

The thesis begins with a discussion of the system models in Chapter 2. Section 2.1 deals with the topology models for the devices in the network. Propagation models are described in Section 2.2 and channel models are described in Section 2.3. In Chapter 3, interference models and performance measures are discussed. Section 3.1 deals with interference modeling and performance measures for fixed and random number of interferers. The most used interference models were presented in Section 3.2. The various performance measures are discussed in Section 3.3.

In Chapter 4 we discuss the performance analysis of connectivity using device isolation probability. Section 4.1 offers an introduction, Section 4.2, Section 4.3, Section 4.4, covers the propagation effects on connectivity for noise-limited systems, systems

with fixed number of interferers, and systems with random number of interferers, respectively. Computer simulation results are presented in Section 4.6.

In Chapter 5, we analyze the impact of interference on outage probability. Section 5.1 offers an overview and introduction; Section 5.2 discusses the outage probability for both systems with fixed and random number of interferers using the distribution function (PDF) approach and the moment generating function (MGF) approach. In Chapter 6, applications that use our analysis are presented. The simulation results for outage probability are analyzed and discussed in Chapter 7. In Chapter 8 includes summary and conclusion and future research directions.

Appendices include some of the derivations and MATLAB codes used in our analysis. Bibliography includes different technical journals, textbooks, and some other materials that were used in preparing the thesis.

CHAPTER 2

SYSTEM MODELS

2.1 Introduction

Transmissions in wireless environments are exposed to a variety of channel impairments, including path loss, interference, multipath and shadow fading. In this chapter, we discuss models used to capture the effects for path loss, multipath and shadow fading, and interference. Multipath fading models are also known as short-term fading models while shadow fading models also referred to as long-term fading models. In some applications, models that take in account both multipath and shadow fading are preferred; and these are known as composite fading models.

2.2 Propagation Models

A path-loss model accounts for transmitted power dissipation due to the distance travelled by the signal. The received signal power decays exponential with transmitter-receiver distance. Consider a device transmitting at fixed power P_{tx} and the transmitted signal travels a distance r to the desired receiver, through a wireless channel with path-loss coefficient η . The received power P_R at the receiver can be modeled using the simplified path-loss model as [55]

$$P_R = P_{tx} A r^{-\eta} \tag{2.1}$$

where A is a constant that accounts for antenna gains. The path-loss coefficient η takes values in the range $2 \leq \eta \leq 6$, depending on the channel environment. However, some authors have claimed that path-loss coefficient can also be random when the propagation environment changes erratically. For example, in [24] the authors showed that the path-loss coefficient varies randomly from one macro-cell to another.

There are numerous models used to model path-loss. These include free space, ray tracing, Okumura, and Hata Models; each offering performance depending on the application environment [29]. The model described in (2.1) is valid only when the transmitter–receiver distance r is greater than one and collapses due to the singularity at $r = 0$. This is because the received power exceeds the transmitted power and approaches infinity when $r \rightarrow 0$. This received power gain is impossible in real wireless channels. Some techniques have been proposed to address the singularity at $r = 0$ and the power gain when $r < 1$. One technique is to equate the received power to the transmitted power when the transmitter–receiver distance $r = 0$. Thus, (2.1) can be modified as below to address its shortfalls [21, 36]

$$P_R = P_{tx} A (1 + r)^{-\eta}. \quad (2.2)$$

The path-loss model in (2.1) reasonably models power decay and reduces the complexity of the system analysis. Thus we shall use (2.1) in our analysis.

2.3 Channel Models

Channel models capture the intrinsic characteristics of the propagation effects that a received signal experiences as it travels from the source to the sink in a given channel. In this section, we shall consider some of the statistical models that are commonly used to

characterize multipath and shadow fading.

2.3.1 Multipath Fading Models

These models describe the peculiarity of wireless propagation where the amplitude/envelope of the received signal fluctuates rapidly over a short period or travel distance. The signal fluctuations arise because the transmitted signal travels via many multipath paths before these different copies of the same transmitted signal combine constructively or destructively at the receiver. Since these different received copies of the transmitted signal arrive at different times at the receiver, they introduce a time delay spread which is due to the difference in the arrival time between the first to the last received copy of the transmitted signal. This consequently creates rapid amplitude fluctuations at the receiver. Modeling of such rapid amplitude fluctuations is necessary in wireless communication analysis. The received signal power in the presence of multipath fading is given by

$$P_R = P_{tx} A r^{-\eta} \alpha^2 \quad (2.3)$$

where α is the fading envelope and it has an average square value $P_x = \mathbb{E}[\alpha^2]$ and PDF $p_x(x)$. The received instantaneous power is given by α^2 . Depending on the propagation environment, there are several models such as Rayleigh and Nakagami fading models that are used to quantify the statistical behavior for α .

2.3.1.1 Rayleigh Fading

Rayleigh fading distribution is one of the most commonly used distributions to represent the rapid amplitude fluctuations when there is no direct line of sight (LOS)

between transmitter and receiver. In a Rayleigh fading environment, the received signal envelope has the PDF

$$p_x(x) = \frac{2x}{P_x} \exp(-x^2/P_x); \quad x \geq 0. \quad (2.4)$$

The distribution of the instantaneous received signal power ($\gamma = \alpha^2$) is obtained by a change of variable as

$$p_\gamma(\gamma) = \frac{p_x((P_x\gamma/\bar{\gamma})^{1/2})}{2(\bar{\gamma}/P_x)^{1/2}} \quad (2.5)$$

where $\bar{\gamma}$ is the average SNR. Thus using (2.5) and (2.4) yields the PDF of the instantaneous SNR as [29, 65]

$$p_\gamma(\gamma) = \frac{1}{\bar{\gamma}} \exp(-\gamma/\bar{\gamma}); \quad \gamma \geq 0. \quad (2.6)$$

Thus the instantaneous SNR power is an exponentially distributed random variable with mean $\bar{\gamma}$.

2.3.1.2 Nakagami Fading

In many wireless environments, empirical and experimental data fail to fit well with the well-known models such as Rayleigh distributions. This predicament led to the discovery of the Nakagami distribution, which was first used in the early 1940's to characterize rapid fading in long distance HF channels [67]. The Nakagami distribution has adjustable parameters that can be used to modify the tails of the distribution to fit empirical and experimental data. The received signal envelope in a Nakagami fading channel has a PDF given as [13, 67]

$$p_x(x) = \frac{2m^m}{P_x^m} \frac{x^{2m-1}}{\Gamma(m)} \exp\left(-\frac{mx^2}{P_x}\right); \quad m \geq 0.5; x \geq 0. \quad (2.7)$$

The PDF of the instantaneous power follows a gamma distribution given as [29]

$$p_\gamma(\gamma) = \left(\frac{m}{\bar{\gamma}}\right)^m \frac{\gamma^{m-1}}{\Gamma(m)} \exp\left(-\frac{m\gamma}{\bar{\gamma}}\right); \quad \gamma \geq 0. \quad (2.8)$$

where $m = \left[\mathbb{E}(\gamma^2)\right]^2 / \mathbb{E}[\gamma^2 - \mathbb{E}(\gamma^2)]^2 \geq 0.5$, is the fading parameter and $\Gamma(\cdot)$ is the gamma function [4, eq.(6.1.1)]. The Nakagami distribution has the ability to model multipath fading conditions that are either less or more severe than Rayleigh fading. For instance when $m = 1/2$ and $m = 1$, the distribution becomes a one-sided Gaussian distribution and the Rayleigh distribution, respectively [29, 39, 78]. The Nakagami distribution can model more severe fading than Rayleigh when $0.5 \leq m < 1$ and no fading when $m \rightarrow \infty$ [29, 39, 78]. This distribution can also model the log-normal distribution as a limiting case [29, 39, 78].

2.3.2 Shadow Fading

In some applications like satellite and terrestrial mobile systems, the link quality of the receiver is affected by slow variations of the mean signal level due to shadow fading. Shadow fading models take into account the various propagation conditions such as absorption, reflection, diffraction, and scattering that the received signal experiences due to various terrain characteristics of the path that the signal travelled through. The terrain characteristics may consist of large buildings, landscape irregularity, and foliage. These propagation conditions lead to the received power at two receivers located the same distance away from the transmitter to be different. Thus, the local average power varies

randomly from one point to another within a certain terrestrial region. Since the terrain characteristics causing the variations are unknown, statistical models are suitable to quantify the signal attenuations. When the receiver is able to average out multipath fading, the received signal power in the presence of path-loss and shadow fading is given as

$$P_R = P_{tx} A r^{-\eta} u \quad (2.9)$$

where A is a constant, u accounts for shadow fading. In (2.9), we have assumed $\alpha^2 = 1$. The behavior of the random parameter u can be quantified by a shadow fading model such as the log-normal distribution.

The log-normal fading model has been confirmed to accurately represent empirical data of the received power [29] due to the effect of shadow fading in both indoor and outdoor environments. Thus the local mean power P_x for the envelope follows a log-normal distribution and when expressed in decibels (dB), it follows a Gaussian PDF with mean ν_{dB} and variance σ_{dB}^2 given as [79]

$$p_Y(y) = \frac{1}{\sigma_{dB} y \sqrt{2\pi}} \exp \left[-\frac{1}{2} \left(\frac{\ln y - \nu_{dB}}{\sigma_{dB}} \right)^2 \right]; \quad (2.10)$$

where $\nu_{dB} = \mathbb{E}[\ln Y]$, $\sigma_{dB}^2 = \text{variance}[\ln Y]$, $\ln(\cdot) = \log_e(\cdot)$.

2.3.3 Composite fading

When the systems operate in built up urban area or are subjected to slow moving pedestrians, the average received power is usually a random variable. Measurements in such environments show that the classical fading models fit measured data around the

mean or median but fail toward the tail of the distribution. It is known that in such environments, the receiver is unable to average out the effect of multipath fading but reacts to the instantaneous change in the average received power. In such conditions, composite distributions that can encompass both multipath and shadow fading simultaneously are preferred [52, 67]. The received signal power when both multipath and shadow fading are experienced is given as [18]

$$P_R = P_{tx} A r^{-\eta} \alpha^2 u \quad (2.11)$$

where α accounts for the effects of multipath fading on the envelope and u accounts for shadow fading. We denote the effects of multipath and shadow fading by $K = \alpha^2 u$.

When the received signal experiences only fading, the average power is deterministic; but if both multipath and shadow fading are experienced, the average power of the received signal is random. Thus, the consequence of shadow fading is that the mean power for the multipath faded signal loses its deterministic nature [61]. The composite PDF for the received signal power when both multipath and shadow fading are simultaneously experienced is thus computed as

$$p_\gamma(\gamma) = \int_0^\infty p_{\gamma|Y}(\gamma | y) p_Y(y) dy \quad (2.12)$$

where $p_{\gamma|Y}(\cdot | \cdot)$ is the PDF for the received SNR power conditioned on the average signal power Y and $p_Y(\cdot)$ is PDF of the average signal power.

The most commonly used distributions for modeling composite fading are the Suzuki distribution (Rayleigh-log-normal PDF) and the Nakagami-log-normal distribution. However; these distributions are complex to compute and they do not have closed-form

PDFs [10]. In order to obtain an analytically tractable composite distribution, a gamma distribution was proposed in place of log-normal distribution for modeling shadow fading effects. Also, the gamma distribution fits well the analytical and experimental data compared to the log-normal distribution [3, 62, 63]. Therefore, it is reasonable to assume that shadow fading follows the gamma distribution. This change gave rise to \mathcal{K} distribution, the generalized- \mathcal{K} distribution, and the generalized gamma distribution.

We discuss the Generalized- \mathcal{K} distribution that can excellently approximate the Suzuki distribution [10].

In the Generalized- \mathcal{K} model, multipath fading effects on the received signal follow the Nakagami distribution while the shadow fading effects follow the gamma distribution. The PDF of the average power in a gamma-shadowed environment is given as [2]

$$p_Y(y) = \frac{y^{c-1}}{P_y^c \Gamma(c)} \exp\left(-\frac{y}{P_y}\right); \quad y > 0 \quad (2.13)$$

where $c = \mathbb{E}(Y)^2 / \mathbb{E}[Y^2 - \mathbb{E}(Y)]^2$ is the shape parameter and P_y is the scale parameter. In the event when a signal experiences Nakagami multipath fading and gamma shadow fading simultaneously, the average power in equation (2.8) becomes random; thus it is replaced by a random variable Y . The conditional PDF becomes

$$p_{\gamma|Y}(\gamma | y) = \left(\frac{m}{y}\right)^m \frac{\gamma^{m-1}}{\Gamma(m)} \exp\left(-\frac{m\gamma}{y}\right). \quad (2.14)$$

Substituting (2.14) and (2.13) in (2.12) and simplifying yields the composite PDF as [69]

$$p_\gamma(\gamma) = \frac{2(cm/P_y)^{c+m/2}}{\Gamma(m)\Gamma(c)} \gamma^{c+m/2-1} \mathcal{K}_{c-m} \left(2\sqrt{\frac{cm}{P_y}} \gamma \right) \quad (2.15)$$

where $\mathcal{K}_\chi(\cdot)$ is the modified Bessel function of the second kind, eq.(9.6.2) [4] with order χ , c is a shadowing parameter, m is the fading parameter, $P_y = \mathbb{E}[\bar{\gamma}]$ is the mean received power.

2.3.4 Generalized Gamma Distribution

The generalized gamma distribution was first introduced by Stacy [66] as a generalization of the two-parameter gamma distribution. Griffiths and McGeehan [31] presented this statistical distribution as a generalization of the gamma distribution to model radio-wave propagation. This three parameter distribution is a versatile distribution that can be used to model multipath, shadow fading, or both by varying its parameters. The distribution can model both multipath and shadow fading by scaling the multipath faded signal power to produce a shadowed fading case. The composite PDF of the received signal envelope is given as [1]

$$p_x(x) = \frac{2\nu(m/P_x)^m x^{2\nu m-1}}{\Gamma(m)} \exp\left(-\frac{mx^{2\nu}}{P_x}\right)$$

and the composite PDF of instantaneous SNR power is given as [1, 37]

$$p_\gamma(\gamma) = \frac{\nu}{\Gamma(m)} \Omega^m \nu \gamma^{\nu m-1} \exp(-\Omega \gamma^\nu); \quad \gamma \geq 0 \quad (2.16)$$

where $\Omega = [\Gamma(m+1/\nu)/P_y \Gamma(m)]^\nu$, $m \geq 0.5$ is the fading parameter, ν is the shape

parameter, and $P_y = \mathbb{E}[\bar{\gamma}]$ is the power scale parameter. Note that the multipath fading

effect is obtained by simply adjusting νm and the shadow fading effect by adjusting m [19]. It is worth mentioning that the generalized gamma distribution can model other distributions by adjusting the parameters. For instance, when $m = 1 = \nu$ the distribution yields Rayleigh distribution, Nakagami- m distribution when $\nu = 1$, and log-normal as $m \rightarrow \infty$ and $\nu \rightarrow 0$.

CHAPTER 3

INTERFERENCE MODELS AND PERFORMANCE MEASURES

3.1 Introduction

We discuss how the number of interferers, N in the network is obtained depending on the topology of the devices. As discussed in Chapter 1, the parameter N which is the number of interferers may be either fixed and known or random. In practical applications, a receiver has an exclusion zone given by a disk centered at the receiver with radius, B . No interferers are permitted to transmit within this region as seen in Figure 5. The number of interferers in the circular region $(C - B)$ may be fixed or random.

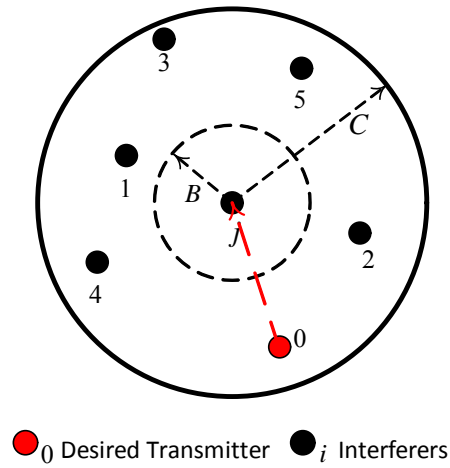


Figure 5: Distribution of interfering transmitters around the receiver.

3.1.1 Fixed Number of Interferers

In the case of fixed number of interferers, the number and location of interferers in the region $(C - B)$ are fixed and known. For instance, in deterministic network topologies such as cellular networks, the number of interfering base stations are known and fixed. In such networks, it is possible to place the transmitters deterministically. So, we consider a network in which N interfering devices are placed deterministically in a two dimensional (2-D) region of area \mathcal{A} . In such a placement, the locations for the devices are known and fixed. Hence, we conclude that the number of interferers in the area \mathcal{A} is fixed and known as N .

3.1.2 Random Number of Interferers

On the other hand, in the case of random number of interferers, the interferers may either be known but vary in time or are totally unknown. This is mainly observed in applications that use random topologies. Thus, for this case the number of interferers located in the region $(C - B)$ is random and unknown. In some networks, it may be impossible to know the exact number of interferers; because the number and location of the interferers vary randomly with time. For example, in cognitive radio systems, the number of interferers is known but at a specific time, the exact number of interfering devices varies with time. We assume that the distribution of the number of interferers, N in the region of area, \mathcal{A} follows a Binomial distribution given as

$$\mathbb{P}[N = k] = \binom{N}{k} p^k (1-p)^{N-k}; \quad k = 0, 1, 2, 3, \dots, N \quad (3.1)$$

where p is the transmission probability of the interfering device.

In some other networks such as environmental monitoring wireless sensor networks, it is difficult or impossible to place the devices deterministically. In such applications, it is difficult to know the exact number of interferers. So, we assume that the number of interferers can randomly take any value between zero and infinity. The number of devices in the network is assumed to belong to a random point process on an infinitely large system plane. Let \mathcal{N} be a 2-D Poisson point process (PPP) over the space \mathbb{R}^2 , with constant spatial intensity of λ . The points of the process denote the location of the terminals and the receiver is assumed to be located at the origin. Thus, the number of active devices in area \mathcal{A} is a random variable that follows a Poisson distribution with an expected value $\lambda\mathcal{A}$ and given as

$$\mathbb{P}[N = k] = \frac{(\lambda\mathcal{A})^k}{k!} \exp(-\lambda\mathcal{A}); \quad k = 0, 1, 2, 3, \dots \quad (3.2)$$

3.2 Interference Models

There are a variety of models that have been used in the literature to quantify the impact of interference at the receiver, and they all depend on how the receiver is able to capture the transmitted signals.

3.2.1 Collision Channel Model

The collision channel model assumes that all transmissions are lost if they were sent simultaneously. It is assumed that the receiver is unable to decode either of the simultaneously received signals, thus there is no successful reception.

3.2.2 Protocol Interference Model

The protocol interference model is based on the condition that a reception at the receiver is successful if the absolute distance between the receiver and the transmitter of the desired signal is less than the absolute distance between the receiver and each of the other interfering transmitters [16]. The transmitter-receiver distance for the desired signal has to be less than any of the other transmitter-receiver distances by a given factor.

3.2.3 Capture Threshold Model

The capture threshold model is based on a capture channel model, where the power of the received signal is compared to the power of every other signal present at the receiver. Let P_i be the signal power received from the i -th transmitter at a given receiver. Then, a receiver can successfully decode the desired message from the 0-th transmitter in the presence of N other messages; if the desired received signal power P_0 is sufficiently stronger than the power P_i of any of the other received signals by a given factor β , that is to say,

$$\frac{P_0}{P_i} > \beta; \quad i = 1, 2, \dots, N. \quad (3.3)$$

This model only considers the impact of individual powers to the desired signal power which is sometimes not satisfactory in many applications.

3.2.4 Additive Interference Model

To consider the impact of all the interfering signals at the receiver, an additive interference model was developed based on physical channel model. Assume that

additive white noise power W is present at the receiver. Then, the receiver is able to decode the desired message from the 0 -th transmitter in the presence of N other messages if the message power P_0 is stronger than the sum of the powers P_i for all the N messages at the receiver plus noise. In other words, this model considers a reception successful even in the presence of interference if the signal-to-interference-plus-noise ratio (SINR), γ , is greater than a threshold, thus

$$\gamma = \frac{P_0}{W + \sum_{i=1}^N P_i} > \beta. \quad (3.4)$$

The additive interference model is more realistic than the protocol model since it considers all interfering signals; but it comes at a cost of higher computational complexity. Let the aggregate interference be $Z = \sum_{i=1}^N P_i$ and note that (3.4) has two special cases. First the noise-limited case where the aggregate interference is assumed to either be so small compared to noise power and hence negligible or the aggregate interference is very large and can be approximated as a Gaussian random variable that can be added to the noise term. This Gaussian approximation follows from the central limiting theorem (CLT) that states that under some conditions, the distribution of the sum of large independent random variables (RVs) is normally distributed. Since Z is a summation of a large number of interferers, it can be approximated to be a normally distributed random variable. This leads to a summation of two Gaussian random variables which yields another Gaussian random variable with different parameters. The CLT argument is accurate as long as there is no dominating interferer [14]. The noise-limited case is obtained by letting $Z = 0$ in (3.4). Secondly, the interference-limited case where

the noise term is assumed to be so small compared to the aggregate interference such that it can be ignored. Thus noise-limited case is obtained by letting $W = 0$ in (3.4).

3.3 Performance Measures

Performance measures are very vital in analyzing the overall fidelity of the system. We discuss in this section the analytical tools that can be used to evaluate the performance of a wireless system in various environments.

3.3.1 Average SNR

Signal-to-noise ratio (SNR) is one of the most understood and commonly used performance measure to assess the overall fidelity of the system. Average SNR is the ratio of the average received power to noise power. Conventionally, noise power in average SNR is considered to be the power of the ubiquitous thermal noise experienced at the receiver; however when the received signal experiences fading, it is appropriate to statistically average SNR to take care of the randomness introduced. In the presence of fading, the received instantaneous SNR (γ) at a given receiver is a random variable (RV). The average SNR is computed using the probability density function (PDF) of γ as [65]

$$\bar{\gamma} = \int_0^{\infty} \gamma p_{\gamma}(\gamma) d\gamma \quad (3.5)$$

where $p_{\gamma}(\gamma)$ is the PDF of γ .

3.3.2 Outage Probability

Outage probability is also a commonly used performance metric for analyzing the performance of wireless system in fading channels. Outage probability is defined as the probability that the output instantaneous SNR, γ falls below a specified threshold, β . Thus, outage probability is computed mathematically as [65]

$$Q_\gamma = \mathbb{P}(\gamma < \beta) = \int_0^\beta p_\gamma(\gamma) d\gamma \quad (3.6)$$

Note that in (3.6), the outage probability turns out to be the cumulative distribution function (CDF) of γ , denoted as $F_\gamma(\gamma)$. Thus, computing the outage probability boils down to finding the CDF, $F_\gamma(\gamma)$.

3.3.3 Device Isolation Probability

In ad-hoc wireless networks, it is essential that the deployed devices form a connected topology. A connected topology is achieved when there is a link from one device to another throughout the entire network. It is difficult in practical applications to obtain a connected topology, but during the planning and designing stages, a good insight on how to obtain a connected topology is necessary. The analysis of a connected topology to account for diversity of paths that link devices in a network is known as connectivity. The connectivity of each device to its next hop neighbor within the network is essential for network coverage. The main concern here is to determine all the single hop links between the device and its neighbors. However, these links are wireless and are affected by factors such as path-loss, fading, and interference. In other words, these

factors will cause some of the existing links to break, leading to some devices having no links to their neighboring devices. Such devices are considered to be isolated. These devices have no single link to any of the other devices in the network. So, analyzing device isolation is one way to quantify connectivity in a network. We define device isolation probability as the probability that a given device is not able to communicate with any of the other devices in the network.

CHAPTER 4

PERFORMANCE ANALYSIS USING CONNECTIVITY

4.1 Introduction

As discussed in Chapter 3, connectivity deals with diversity of paths that link devices in a network. The connectivity of each device to its next hop neighbor within the network is essential for network coverage. One of the first connectivity studies was in [17], where the percolation of a broadcast was investigated. Naserian et al.[50] showed how to attain a connected network using a relationship between the transmission range and the number of devices. In [15], the authors studied the effects of lognormal shadow fading on connectivity in multi-hop radio networks. Hekmat and Van Mieghem [32] studied the effects of lognormal shadowing on connectivity using geometric random graphs. The authors in [48] presented the effects of fading and shadowing on connectivity in sensor networks. Dousse et al [23] used percolation theory to investigate the impact of interference on connectivity in ad-hoc networks. Yang et al [76] use graph theory to derive bound on the connectivity of wireless networks for CSMA systems. Rajagopalan and Varshney [54] discussed the effects of SINR and sensor reliability on connectivity in deterministic network topologies.

There is another source of interference in wireless networks which is intentional interference resulting from sensor jamming attacks [44, 75]. Sensor jamming attacks can

be classified as either active or passive sensor jammers. Active jammers mostly block the transmission channel regardless of the traffic pattern on the channel. Such jammers are effective because they keep the channel busy at all times, but they are easily detected. On the other hand, reactive jammers are usually difficult to detect, since they stay quiet until they sense activity on the channel and thus start to transmit a jamming signal. In general, connectivity of sensor network is severely influenced by the presence of jamming.

In the performance analysis of many wireless networks on the basis of connectivity, it is usually assumed, for analytical simplicity, that the major source of performance impairments is background noise [11, 48]. However, in many practical networks the effect of interference cannot always be ignored [54]. Therefore, in this work we assume that interference is present at the receiver because the sensors are unable to mitigate the impact of interference. Device isolation probability is one of the measures used to quantify connectivity in a network and we denote it by Q_{ip} . We assume that the link between two nodes is either perfectly connected or isolated and the transmit power and antenna gains are assumed to be the same for all devices.

4.2 Noise Limited Systems

4.2.1 Effect of Path-loss Only

When only path loss is considered, there is a deterministic distance called communication range \mathcal{R} such that all the devices within a circular disk of radius \mathcal{R} centered at the transmitting device can receive the sent message successfully. In Figure 6, receivers “1” and “2” can successfully receive a transmission from transmitter “0”; but there

is no link between “0” and “3”, since “3” is out of range. If receiver “3” is not within the communication range of any of the other devices in the network, it is considered to be isolated. In this case there is no fading present in the channel since the signals experience

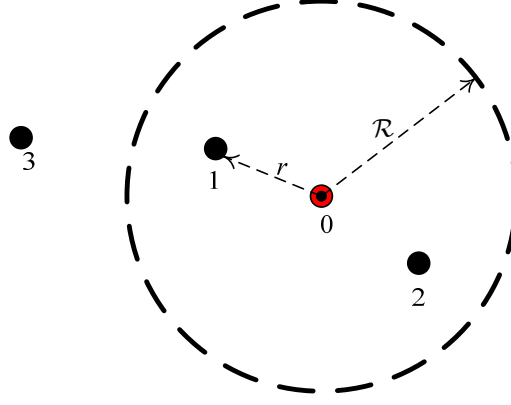


Figure 6: Deterministic circular disk of transmission model.

path-loss only, implying that $K = \alpha^2 u = 1$ in (2.11). It follows that two devices a distance, r_0 apart are not able to communicate (have no link between them) when the received SNR, γ is below the threshold, β ; i.e.

$$\gamma = \frac{P_{tx} AK}{W} r_0^{-\eta} \leq \beta \quad (4.1)$$

where $K = 1$, P_{tx} is the transmit power for the desired signal and W is noise power.

In (4.1), we assume that there is no interference and fading experienced. Thus, we define the communication range \mathcal{R} as the distance at which the Signal-to-noise ratio falls below the threshold. Using (4.1) and rearranging to make r_0 the subject, the communication range is obtained as $\mathcal{R} = [\beta W / AP_{tx}]^{-1/\eta}$ and thus, the device isolation probability for such a case is computed as [20]

$$Q_{IP} = \exp(-\pi\lambda\mathcal{R}^2). \quad (4.2)$$

It follows that the isolation probability for path-loss only without interference is obtain as

$$Q_{IP} = \exp\left(-\pi\lambda\left[\frac{AP_{tx}}{\beta W}\right]^{2/\eta}\right). \quad (4.3)$$

4.2.2 Effect of Path-loss, Multipath, and Shadow Fading

Multipath fading introduces randomness in the path-loss while shadow fading introduces randomness in the mean of the path-loss. Considering a case where a channel presents a random component, that is $K = \alpha^2 u$, the effects of K on path-loss make the communication range \mathcal{R} to become random. The communication range \mathcal{R} , that has CDF $F_{\mathcal{R}}(\cdot)$ and second moment $\mathbb{E}[\mathcal{R}^2]$, determines the probability that two devices separated by a distance, r from each other are able to communicate successfully. In the event that a given receiver has N one-hop neighbors within a distance, r that can communicate with it, Miorandi and Altman [48] showed that the number of one hop neighbors follows a Poisson distribution with intensity, $\lambda\pi\mathbb{E}[\mathcal{R}^2]$. Thus, the device isolation probability becomes [48]

$$Q_{IP} = \exp\left(-\lambda\pi\mathbb{E}[\mathcal{R}^2]\right). \quad (4.4)$$

The received power at a link located a distance, r from the transmitter is assumed to be a random variable that can be modeled taking into account the effects of path-loss, multipath and shadow fading. Substituting (2.11) in (3.4) and rearranging, the SNR for a broken link has to fulfill the condition

$$\gamma = \frac{P_{tx}Ar_0^{-\eta}\alpha_0^2u_0}{W} \leq \beta \quad (4.5)$$

where α_0^2 accounts for multipath fading, u_0 is the desired signal shadow fading parameter, and r_0 is the desired signal transmitter-receiver distance. Considering that \mathcal{R} is the distance at which the SNR, γ falls below a threshold, β , we use (4.5) to obtain the second moment of the communication range as

$$\mathbb{E}[\mathcal{R}^2] = \left(\frac{P_{tx} A}{W \beta} \right)^{2/\eta} \mathbb{E}[\alpha_0^2 u_0]^{2/\eta} \quad (4.6)$$

Assume that the transmitted signals experience path-loss, Nakagami multipath fading with PDF given in (2.8) and mean $\bar{\gamma}_0$, and log-normal shadow fading with zero mean and PDF given in (2.10); then, substituting in the PDFs and performing the expectation operations with the help of [30, eq.(3.326.2.10 and 3.323.2.10)] yields (see Appendix A for details)

$$\mathbb{E}[\mathcal{R}^2] = \frac{\Gamma(2/\eta + m_0)}{\Gamma(m_0)} \left(\frac{A P_{tx} \bar{\gamma}_0}{m_0 W \beta} \right)^{2/\eta} \exp\left[\left(\sqrt{2}\sigma/\eta\right)^2\right]. \quad (4.7)$$

The isolation probability for the SNR case is obtained by substituting (4.7) in (4.4) yielding

$$\mathcal{Q}_{IP} = \exp\left(-\lambda\pi \frac{\Gamma(2/\eta + m_0)}{\Gamma(m_0)} \left(\frac{A P_{tx} \bar{\gamma}_0}{m_0 W \beta} \right)^{2/\eta} \exp\left[\left(\frac{\sqrt{2}\sigma}{\eta}\right)^2\right]\right). \quad (4.8)$$

It is worth noting that in (4.8), the effects of multipath and shadow fading, and path-loss are clearly observable and decoupled. Observe that lognormal shadow fading improves the isolation probability as lognormal spread, σ increases without increasing the transmit power. Even though it is a known fact that a wireless channel cannot amplify a signal, it is worth mentioning that the impact of lognormal shadow fading according to

our analysis in a real environment is unclear. This phenomenon where lognormal shadow fading improves connectivity was also observed in [48] and may be due to the bias that is introduced in $\mathbb{E}(\mathcal{R}^2)$. That is, the average link gain increases with the lognormal spread.

When the signals experience Rayleigh fading, we substitute $m_0 = 1$ in (4.8) which yields the isolation probability for the SNR case as

$$\mathcal{Q}_{IP} = \exp \left(-\lambda \pi \frac{2}{\eta} \Gamma \left(\frac{2}{\eta} \right) \left(\frac{AP_{tx} \bar{\gamma}_0}{W\beta} \right)^{2/\eta} \exp \left[\left(\frac{\sqrt{2}\sigma}{\eta} \right)^2 \right] \right). \quad (4.9)$$

This result was also obtained in [48].

4.3 Systems With Fixed Number of Interferers

4.3.1 Effect of Path-loss Only

Considering the case when interferers are present but no fading, a receiver can successfully capture a signal from the 0 -th transmitter in the presence of other interfering signals, if the received signal-to-interference plus noise ratio (SINR) satisfies the additive interference model condition given in (3.4). Substituting (2.11) in (3.4), the received SINR, γ for a broken link is

$$\gamma = \frac{P_{tx} A K_0 r_0^{-\eta}}{W + \sum_{i=1}^N P_{tx} A K_i r_i^{-\eta}} \leq \beta \quad (4.10)$$

where $K_0 = K_i = 1$ for path-loss only case, N is a constant, W is noise power, and r_i is the transmitter–receiver distance for the i -th interfering transmitter.

When the impact of interference is much more than that of noise, the effects of noise can be ignored. That is, we set $W = 0$. Since the transmit power and antenna gains are the

same for all devices, the distance at which the SIR falls below a threshold, β for the case when N is fixed, is obtained using (4.10) as

$$\mathcal{R}^2 = \left[\left(\frac{1}{\beta} \right)^{2/\eta} \mathbb{E}_r \left\{ \left(\sum_{i=1}^N \frac{K_i}{K_0} r_i^{-\eta} \right)^{-2/\eta} \mid r \right\} \right]. \quad (4.11)$$

We assume that the PDF for the sum is known or can be easily approximated. Next, we discuss how the sum term in (4.11) can be approximated using geometric mean [4, eq.(3.2.1)].

Recognizing the sum term in (4.11) as the harmonic mean of the variables, we may use [4, eq.(3.2.1)] to upper-bound it by the geometric mean of the variables as

$$\left(\sum_{i=1}^N \frac{1}{(K_0/K_i) r_i^\eta} \right)^{-2/\eta} \leq \frac{1}{N^{2/\eta}} \prod_{i=1}^N (K_0/K_i)^{2/(\eta N)} r_i^{2/N}. \quad (4.12)$$

Assuming that the interferers are *i.i.d* and N and r_i are statistically independent of each other, (4.12) simplifies to

$$\left(\sum_{i=1}^N \frac{1}{(K_0/K_i) r_i^\eta} \right)^{-2/\eta} \leq \frac{1}{N^{2/\eta}} \Phi^{2/\eta} r^2 \quad (4.13)$$

where $\Phi = K_0/K$. In (4.13), note that the number of interferers present in the $(C-B)$ disk is fixed and the interferer locations are mutually independent and uniformly distributed in the disk. For ease of our analysis, we do not consider the exclusion zone; thus, without any loss in generality, we assign $B = 0$. The distance for each active transmitter from the receiver is random and has a PDF given as

$$p_r(r) = 2r/C^2; \quad 0 \leq r \leq C. \quad (4.14)$$

Substituting (4.13) in (4.11) and evaluating the expectation using (4.14) yields the communication range as

$$\mathcal{R}^2 \leq \left[C / \left(\sqrt{2} (\beta N)^{1/\eta} \right) \right]^2, \quad (4.15)$$

where $\Phi = 1$ was used. Note that the result in (4.15), is an upper bound on communication range i.e. the communication range can never exceed this value.

Substituting (4.15) in (4.2), we have the isolation probability as

$$Q_{IP} \leq \exp \left(-\pi \lambda \left[C / \left(\sqrt{2} (\beta N)^{1/\eta} \right) \right]^2 \right). \quad (4.16)$$

4.3.2 Effect of Path-loss, Multipath, and Shadow Fading

When the effects of path-loss, multipath and shadow fading are present, $K = \alpha^2 u$ is a random variable. Thus, (4.10) becomes

$$\gamma = \frac{P_{tx} A r_0^{-\eta} \alpha_0^2 u_0}{W + \sum_{i=1}^N P_{tx} A r_i^{-\eta} \alpha_i^2 u_i} \leq \beta \quad (4.17)$$

where α_i is the multipath fading envelope on the i -th link, u_0 is the desired signal shadow fading parameter, r_0 is the desired signal transmitter-receiver distance, u_i is the interfering signal shadowing parameter, and r_i is the interfering signal transmitter-receiver distance. When the effects of noise are ignored, that is $W = 0$, it follows that the communication range is given as

$$\mathcal{R}^2 = \left[\frac{\beta \left(\sum_{i=1}^N P_{tx} A r_i^{-\eta} \alpha_i^2 u_i \right)}{P_{tx} A \alpha_0^2 u_0} \right]^{-2/\eta}. \quad (4.18)$$

The second moment of the communication range is computed as

$$\mathbb{E}[\mathcal{R}^2] = (1/\beta)^{2/\eta} \mathbb{E}[\alpha_0^2 u_0]^{2/\eta} \mathbb{E}\left[\sum_{i=1}^N u_i \alpha_i^2 r_i^{-\eta}\right]^{-2/\eta} \quad (4.19)$$

4.3.2.1.1 PDF Approach

In the PDF approach, we use the definition of the communication and the PDF of the variables to evaluate the expectation

$$\mathbb{E}[\mathcal{R}^2] = (1/\beta)^{2/\eta} \mathbb{E}\left[\frac{\alpha_0^2 u_0}{\sum_{i=1}^N r_i^{-\eta} \alpha_i^2 u_i}\right]^{2/\eta}. \quad (4.20)$$

As seen in (4.20), the expectation is performed on the ratio of two independent random variables. Given two independent random variable \mathcal{U} and \mathcal{V} , the PDF of their ratio, $T = \mathcal{U}/\mathcal{V}$ is computed mathematically as [49]

$$p_T(t) = \int_0^\infty |v| p_u(tv) p_v(v) dv. \quad (4.21)$$

When N is fixed, the r_i 's are deterministic and assuming the received desired signal has mean power $\bar{\gamma}_0$ and fading parameter m_0 , and the N mutually independent interfering signals each has mean power $\bar{\gamma}_i$ and fading parameter m_i experience path-loss and Nakagami fading; then, the aggregate interference power also follows a Nakagami distribution with mean $\bar{\gamma}_z$ and fading parameter m_z . Observe that for this case the numerator and denominator in (4.20) are both gamma random variables; that is a ratio of two gamma random variables. Using (4.21) and [30, eq.(3.241.3.11)], the PDF of the power ratio is given as

$$p_\gamma(\gamma) = \mathbb{E}_{u_0, u} \left\{ \frac{\Gamma(m_0 + m_z N)}{\Gamma(m_0)\Gamma(m_z N)} \left(\frac{m_0}{\Lambda} \right)^{m_0} m_z^{m_z N} \gamma^{m_0-1} \left(\frac{m_0}{\Lambda} \gamma + m_z \right)^{-m_0-m_z N} \left(\frac{u_0}{u} \right)^{2/\eta} \right\} \quad (4.22)$$

where $\Lambda = \bar{\gamma}_0 / \bar{\gamma}_z$ is the mean power ratio and $\Gamma(\cdot)$ is the Gamma function. It follows that using (4.22) and [30, eq.(7.511)] to simply yields the second moment in (4.20) as (see Appendix A for details)

$$\mathbb{E}[\mathcal{R}^2] = \frac{\Gamma(m_0 + 2/\eta)\Gamma(m_z N - 2/\eta)}{\Gamma(m_0)\Gamma(m_z N)} \left(\frac{m_z A P_{tx}}{m_0 B W} \right)^{2/\eta} \exp \left[\left(\sqrt{2\sigma^2} / \eta \right)^2 \right] \quad (4.23)$$

where σ is the lognormal spread. Substituting (4.23) into (4.4), we obtain the isolation probability.

When the effect of noise in the denominator of (4.17) cannot be ignored at the receiver and the desired signal power is given by P_0 . The PDF of the SINR, $\gamma = P_0 / 1 + Z$ where the interfering signal powers are normalized by the noise power W is given as [2]

$$p_\gamma(\gamma) = \frac{(m_0 / \bar{\gamma}_0)^{m_0} (m_z / \bar{\gamma}_z)^{m_z N}}{\Gamma(m_0)\Gamma(m_z N)} \gamma^{m_0-1} \exp \left(-\frac{m_0}{\bar{\gamma}_0} \gamma \right) \times \int_0^\infty (1+t)^{m_0} t^{m_z N-1} \exp \left(-t \left[\frac{m_0}{\bar{\gamma}_0} \gamma + \frac{m_z}{\bar{\gamma}_z} \right] \right) dt; \quad \gamma \geq 0 \quad (4.24)$$

where N is the total number of co-channel interferers and $\Gamma(\cdot)$ is the Gamma function.

The success probability is computed using (4.24) to obtain.

$$Q_s = \frac{(m_0 / \bar{\gamma}_0)^{m_0} (m_z / \bar{\gamma}_z)^{m_z N}}{\Gamma(m_0)\Gamma(m_z N)} \int_0^\infty (1+t)^{m_0} t^{m_z N-1} \exp \left(-\frac{m_z}{\bar{\gamma}_z} t \right) \times \int_\beta^\infty \gamma^{m_0-1} \exp \left(-\frac{m_0}{\bar{\gamma}_0} (t+1) \gamma \right) d\gamma dt \quad (4.25)$$

The expectation is computed with the help of [30, eq.(3.478.1)] and [4, eq.(13.2.5)] to obtain

$$\mathbb{E}[\mathcal{R}^2] = \frac{\Gamma(m_0 + 2/\eta)}{\Gamma(m_0)} \left(\frac{AP_{tx}}{m_0 \beta W} \right)^{2/\eta} \left(\frac{m_z}{\bar{\gamma}_z} \right)^{m_z N} \mathbf{U} \left(m_z N; m_z N + 1 - 2/\eta; \frac{m_z}{\bar{\gamma}_z} \right) \times \exp \left[\left(\sqrt{2\sigma^2}/\eta \right)^2 \right] \quad (4.26)$$

Substituting (4.26) in (4.4) yields the isolation probability as

$$\mathcal{Q}_{IP} = \exp \left(-\lambda \pi \frac{\Gamma(m_0 + 2/\eta)}{\Gamma(m_0)} \left(\frac{AP_{tx}}{m_0 \beta W} \right)^{2/\eta} \left(\frac{m_z}{\bar{\gamma}_z} \right)^{m_z N} \mathbf{U} \left(m_z N; m_z N + 1 - 2/\eta; \frac{m_z}{\bar{\gamma}_z} \right) \exp \left[\left(\sqrt{2\sigma^2}/\eta \right)^2 \right] \right) \quad (4.27)$$

where $\mathbf{U}(a; b; t)$ is the confluent hypergeometric function defined as [4, eq.(13.2.5)].

4.3.2.1.2 Geometric Mean Approximation

When the effects of path-loss, multipath and shadow fading are present, and the number of interferers is fixed, the expectation in (4.20) can be rewritten as

$$\mathbb{E}[\mathcal{R}^2] = \left[\left(\frac{1}{\beta} \right)^{2/\eta} \mathbb{E}_{\alpha, r} \left\{ \sum_{i=1}^N \left\{ \frac{1}{\left[\left(\frac{\alpha_0^2}{\alpha_i^2} \right) \left(\frac{u_0}{u} \right) r_i^\eta \right]} \right\} \mid r, \alpha \right\} \right]^{-2/\eta}. \quad (4.28)$$

To perform the expectation operation in, we use the approximation in (4.13) which yields

$$\mathbb{E}[\mathcal{R}^2] \leq \left[\frac{C}{(\sqrt{2}(\beta N)^{1/\eta})} \right]^2 \mathbb{E}_{\alpha, u} \left\{ \left[\left(\frac{\alpha_0^2}{\alpha^2} \right) \left(\frac{u_0}{u} \right) \right]^{2/\eta} \mid \alpha, u \right\}. \quad (4.29)$$

It follows from (4.29), that the expectation is performed on ratio of two independent random variables. In a Nakagami fading channel when both α_0^2 and α^2 follow gamma distributions given in (2.8) with mean power $\bar{\gamma}_0$ and $\bar{\gamma}$, and fading parameter m_0 and m ,

respectively; the PDF of the power ratio is given in (4.22) and the expectation for the power ratio in (4.29) can be computed with the help of [30, eq.(3.194.3 and 8.384.1)] to obtained

$$\mathbb{E}\left[\left(\frac{\alpha_0^2}{\alpha^2}\right)^{2/\eta}\right] = \frac{\Gamma(m_0 + 2/\eta)\Gamma(m - 2/\eta)}{\Gamma(m_0)\Gamma(m)} \left(\frac{m\Lambda}{m_0}\right)^{2/\eta}. \quad (4.30)$$

Considering that both u_0 and u are zero mean log-normal random variables with PDF given in (2.10) and variances σ_0^2 and σ^2 , respectively; the ratio of these two independent log-normal random variables is itself a log-normal distributed random variable. That is, the power ratio follows a log-normal distribution with zero mean and variance $\sigma_R^2 = \sigma_0^2 + \sigma^2$. Thus, using [30, eq. (3.323.2.10)]; the expectation for the log-normal power ratio is obtained as (see Appendix A for details)

$$\mathbb{E}\left[\frac{u_0}{u}\right]^{2/\eta} = \exp\left[\left(\frac{\sqrt{2\sigma_R^2}}{\eta}\right)^2\right]. \quad (4.31)$$

Substituting (4.30) and (4.31) in (4.29) yields the second moment of the communication range; which is substitute in (4.4) to obtain the isolation probability as

$$\begin{aligned} Q_{IP} \leq \exp\left(-\lambda\pi \frac{\Gamma(m_0 + 2/\eta)\Gamma(m_z - 2/\eta)}{\Gamma(m_0)\Gamma(m_z)} \left(\frac{m_z\Lambda}{m_0\beta N}\right)^{2/\eta}\right. \\ \left.\times \left[\frac{C}{\sqrt{2}}\right]^2 \exp\left[\left(\sqrt{2\sigma_R^2}/\eta\right)^2\right]\right) \end{aligned} \quad (4.32)$$

4.4 Systems With Random Number of Interferers

4.4.1 Effect of Path-loss Only

Considering the case when interferers are present but no fading, we model the positions of the interferers as a Poisson point process. So, the communication range given in (4.11) has a random sum. In this case N is a random variable from a Poisson point process; that is, the number of interferers present in the $(C - B)$ disk is random and the interferer locations are mutually independent and uniformly distributed in the disk. Thus, we condition on the number of interferers present in the disk. The distance for each active transmitter from the receiver is random and has a PDF given in (4.14). The communication range given in (4.11) becomes

$$\mathcal{R}^2 = \left[\left(\frac{1}{\beta} \right)^{2/\eta} \mathbb{E}_{N,r} \left\{ \left(\sum_{i=1}^N \frac{K_i}{K_0} r_i^{-\eta} \right)^{-2/\eta} \mid N, r \right\} \right]. \quad (4.33)$$

We may remove the conditioning on the number of interferers and the random distances by noting that the interferers are uniformly distributed in the space and the distances follow the distribution in (4.14) to obtain the square of the communication range. However, the distribution of the sum term in (4.33) is rather hard to determine.

We assume that the interferers are *i.i.d* and N and r_i are statistically independent of each other. Since N follows a Poisson process with intensity, λ , the sum term is a compound Poisson sum whose distribution can be approximated using a shifted gamma

function [58]. Let $Z = \sum_{i=1}^N \frac{K_i}{K_0} r_i^{-\eta}$, then $Z = k + S$; where $k \in \mathbb{R}$ and S has a gamma

distribution, $\Gamma(\varphi, \theta)$. It follows that Z has a sifted gamma distribution given as

$$p_Z(z) = \frac{(z-k)^{\varphi-1}}{\theta^\varphi \Gamma(\varphi)} \exp\left(-\frac{(z-k)}{\theta}\right); \quad z \geq k \quad (4.34)$$

where $\varphi = \frac{4\lambda\mu_2^3}{\mu_3^2}$, $\theta = \frac{2\mu_2}{\mu_3}$, $k = \lambda\left(\mu_1 - \frac{2\mu_2^2}{\mu_3}\right)$, $\mu_b = \mathbb{E}\left\{\left[\frac{1}{\Phi}r^{-\eta}\right]^b\right\}$ and $b \in \mathbb{R}$. The

moments of Z are given by

$$\mu_1 = \frac{2C^{-\eta}}{\Phi(\eta-2)}; \quad \mu_2 = \frac{C^{-2\eta}}{\Phi^2(\eta-1)}; \quad \mu_3 = \frac{2C^{-3\eta}}{\Phi^3(3\eta-2)}. \quad (4.35)$$

Using the results in (4.35), we have the shifted gamma parameter as

$$k = \frac{\lambda C^{-\eta}}{\Phi} \left(\frac{2}{(\eta-2)} - \frac{(3\eta-2)}{(\eta-1)^2} \right), \quad \varphi = \frac{\lambda(3\eta-2)^2}{(\eta-1)^3}, \quad \text{and} \quad \theta = \frac{\Phi C^{-\eta}(\eta-1)}{(3\eta-2)} \quad (4.36)$$

where $\Phi = 1$ for path-loss only. Observe that the expectation in (4.33) is the negative moment of the sum. Using (4.34) and [4, eq.(13.2.5)], the expectation is performed yielding (see Appendix A for details)

$$\mathbb{E}[\mathcal{R}^2] = \left[\left(\frac{1}{\beta} \right)^{2/\eta} k^{-\nu} \left(\frac{k}{\theta} \right)^\varphi \mathbf{U} \left(\varphi, \varphi+1-\nu, \frac{k}{\theta} \right) \right]. \quad (4.37)$$

where k , θ , φ are given in (4.36), and $\mathbf{U}(a, b, t)$ is the confluent hypergeometric function defined as [4]. Thus, substituting (4.37) in (4.2), we have the isolation probability as

$$\mathcal{Q}_{IP} \approx \exp \left(-\pi\lambda \left[\left(\frac{1}{\beta} \right)^{2/\eta} k^{-2/\eta} \left(\frac{k}{\theta} \right)^\varphi \mathbf{U} \left(\varphi, \varphi+1-2/\eta, \frac{k}{\theta} \right) \right] \right). \quad (4.38)$$

4.5 Effect of Path-loss, Multipath, and Shadow Fading

The second moment of the communication range in (4.19) can be rewritten as

$$\mathbb{E}[\mathcal{R}^2] = (1/\beta)^{2/\eta} \mathbb{E}_{\Phi, N, r} \left\{ \left(\sum_{i=1}^N \frac{1}{\Phi} r_i^{-\eta} \right)^{-2/\eta} \mid N, r, \Phi \right\} \quad (4.39)$$

where $K_0 = \alpha_0^2 u_0$, $K = \alpha^2 u$, and $\Phi = K_0/K$. To perform the expectation operation in

(4.39), we use the shifted gamma approximation with parameters given as

$$k = \lambda C^{-\eta} \Phi \left(\frac{2}{(\eta-2)} - \frac{(3\eta-2)}{(\eta-1)^2} \right), \quad \varphi = \frac{\lambda(3\eta-2)^2}{(\eta-1)^3}, \quad \text{and} \quad \theta = \frac{C^{-\eta}(\eta-1)}{\Phi(3\eta-2)}. \quad (4.40)$$

It follows from the discussion in section (4.3.1.2) that the expectation is given as (refer to Appendix A for details)

$$\mathbb{E}_{\Phi, N, r} \left\{ \left(\sum_{i=1}^N \frac{1}{\Phi} r_i^{-\eta} \right)^{-2/\eta} \mid N, r, \Phi \right\} = \mathbb{E}_{\Phi} \left[k^{-2/\eta} \left(\frac{k}{\theta} \right)^{\varphi} \mathbf{U} \left(\varphi, \varphi+1-2/\eta, \frac{k}{\theta} \right) \right]. \quad (4.41)$$

Referring to (4.40), observe that Φ only appears in k and θ ; thus, substituting in these variables yields

$$\mathbb{E}_{\Phi, N, r} \left\{ \left(\sum_{i=1}^N \frac{1}{\Phi} r_i^{-\eta} \right)^{-2/\eta} \mid N, r, \Phi \right\} = \psi^{\varphi} \mathbf{U}(\varphi, \varphi+1-2/\eta, \psi) \mathbb{E}_{\Phi} [\Phi^{-2/\eta}] \quad (4.42)$$

where $\psi = \lambda \left(\frac{2(3\eta-2)}{(\eta-2)(\eta-1)} - \frac{(3\eta-2)^2}{(\eta-1)^3} \right)$. Substituting in $\Phi^{-1} = (\alpha_0^2/\alpha^2)(u_0/u)$ into

(4.42), we have

$$\mathbb{E}_{\Phi} [\Phi^{-2/\eta}] = \mathbb{E} \left[(\alpha_0^2/\alpha^2)^{2/\eta} \right] \mathbb{E} \left[(u_0/u)^{2/\eta} \right]. \quad (4.43)$$

It follows from (4.43) that the two expectation terms are performed on the ratio of two independent random variables.

In a Nakagami fading channel when both α_0^2 and α^2 follow gamma distributions with mean power $\bar{\gamma}_0$ and $\bar{\gamma}$, and fading parameter m_0 and m , respectively; the expectation for the power ratio is given in (4.30). Considering that both u_0 and u are zero mean log-normal random variables with variances, σ_0^2 and σ^2 , respectively; the expectation for the log-normal power ratio is given in (4.31). Thus, It follows that the second moment of the communication range in (4.39) becomes

$$\mathbb{E}[\mathcal{R}^2] = \left[\psi^\varphi \mathbf{U} \left(\varphi, \varphi + 1 - \frac{2}{\eta}, \psi \right) \frac{\Gamma(m_0 + 2/\eta) \Gamma(m - 2/\eta)}{\Gamma(m_0) \Gamma(m)} \left(\frac{m\Lambda}{m_0\beta} \right)^{2/\eta} \right. \\ \left. \times \exp \left[\left(\sqrt{2\sigma_R^2}/\eta \right)^2 \right] \right] \quad (4.44)$$

The device isolation probability is obtained by substituting (4.44) in (4.4). yielding

$$\mathcal{Q}_{IP} = \exp \left\{ -\lambda \pi \psi^\varphi \mathbf{U} \left(\varphi, \varphi + 1 - \frac{2}{\eta}, \psi \right) \frac{\Gamma(m_0 + 2/\eta) \Gamma(m - 2/\eta)}{\Gamma(m_0) \Gamma(m)} \left(\frac{m\Lambda}{m_0\beta} \right)^{2/\eta} \right. \\ \left. \times \exp \left[\left(\sqrt{2\sigma_R^2}/\eta \right)^2 \right] \right\} \quad (4.45)$$

We observe that the effects of multipath fading, shadow fading, and path-loss are clearly decoupled in (4.45). This phenomenon in the isolation probability, where the effects of either path-loss and multipath or path-loss and shadow fading are decoupled, occurs in both noise-limited and interference-limited cases.

4.6 Simulation Results

In this section we present the numerical result discussed in this chapter and obtain simulation results to validate the numerical results using MATLAB. We have the simulation area topography as a square ($\mathcal{A} = 100\text{m} \times 100\text{m}$). The receiver is assumed to

be located at the center (0,0) of the inscribing circle of the square. Each run of the simulation assumes a random number of interfering devices (N) according to a Poisson point process with intensity (λ). We do not count the 0-th transmitter and receiver when reporting the number of interfering nodes in the simulation. The N devices are uniformly disseminated over the simulation area as seen in Figure 7. We assume that the node location information is known in order to determine the distance to receiver.

The Euclidian distance between the i -th interfering device and the receiver at the center is computed using the Euclidian distance formula. The distance is used to compute path-loss (path-loss coefficient is set to 3.5) experienced by the signal on the i -th link. Multipath and shadow fading are accounted for by appropriate random variables that are multiplied with the path-loss output. The links between the devices are tested to check for isolated nodes. The link between two given nodes is good as long as (4.10) is satisfied. There is a possibility that a node is able to receive a message from another node, but it is not able to transmit successfully to this particular node; that is the link between them is one-way. This is due to the randomness in the channel.

The system parameters are selected as follows: $A = P_{tx} = 1$, $\eta = 3.5$, $W = 10^{-4}$ mW, lognormal spread $\sigma = 2$, and Rayleigh fading with means $\bar{\gamma}_0 = 10$ dBm and $\bar{\gamma}_i = 2$ dBm, $i = 1, 2, \dots, N$. The parameters such as device density, λ that accounts for device concentration within area, A , radius, C for the disk containing all the interferers, and threshold, β are selected or varied suitably. Simulations are performed using the same system parameters. The process is repeated many times and the node isolation probability is computed as an average of 1500 simulation runs.

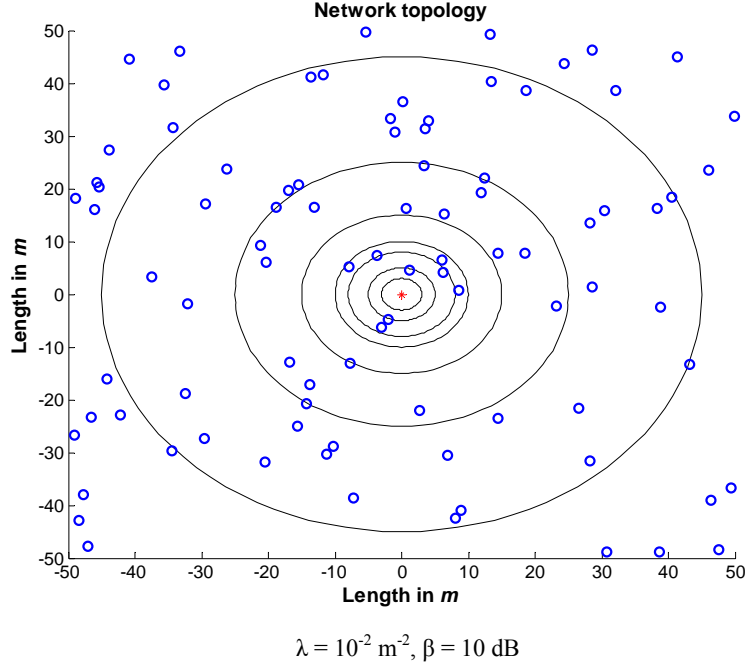


Figure 7: Illustration of network topology with $\lambda = 10^{-2} \text{ m}^{-2}$ and $\beta = 10 \text{ dB}$. The blue circles denote device location and the red asterisk denotes the receiver

In Figure 7, we illustrate a typical device network topology. The receiver is assumed to be at the center and all the other transmitters are uniformly distributed around it. The large circles in Figure 7 represent various disks with radius C ranging from 3 to 45 meters and the small blue bubbles indicate the location of the devices. The location for the interferers within these disks plays a significant role in performance analysis. That is, when all the interferers are located in a circle with a smaller radius, more congestion with more interference are experienced and vice versa.

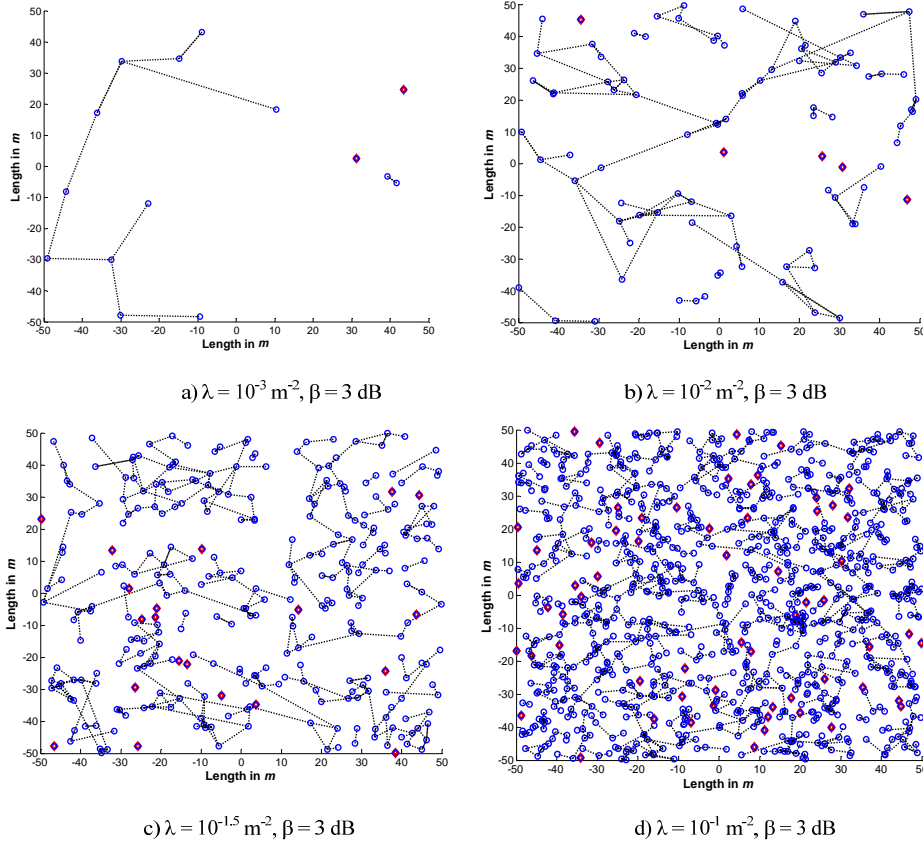


Figure 8: Illustration of isolated devices when $\lambda = 10^{-3} \text{ m}^{-2}$, $\lambda = 10^{-2} \text{ m}^{-2}$, $\lambda = 10^{-1.5} \text{ m}^{-2}$, $\lambda = 10^{-1} \text{ m}^{-2}$ respectively and $\beta = 3 \text{ dB}$. The blue circles denote device location, the red diamonds denote isolated devices, and the dotted lines indicate various connections between devices.

We compare the impact of device population density on connectivity. The red diamonds denote the nodes that are isolated in the network. For example, in a) the nodes located at (30,5) and (45,25) are isolated and in b) the nodes located at (5,5) and (47,-12) are isolated too. We observe that as the device density is increased, the number of devices in the network increase improving connectivity and coverage; but also the number of isolated devices increases too due to interference experienced by the receivers. However, fewer devices in the network compromise coverage because the sensors are further apart as illustrated in Figure 8 a).

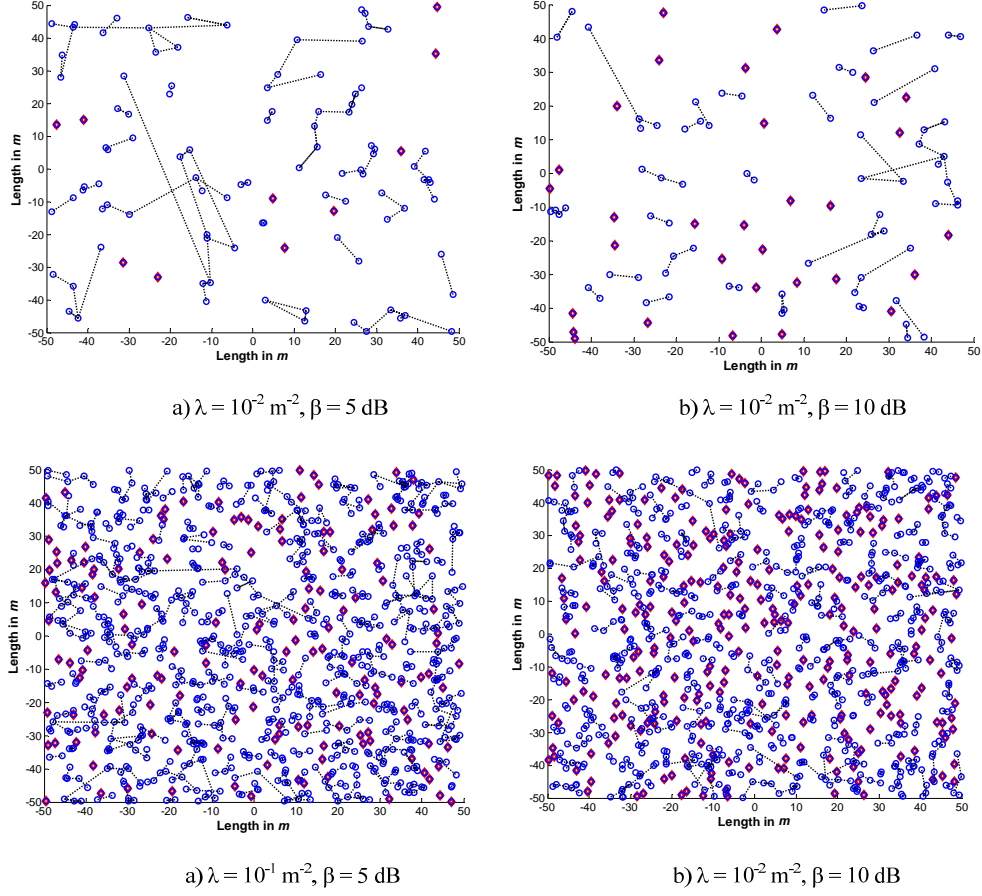


Figure 9: Comparison of different network topologies. Top: $\lambda = 10^{-2} \text{ m}^{-2}$, bottom: $\lambda = 10^{-1} \text{ m}^{-2}$ for $\beta = 5 \text{ dB}$ and $\beta = 10 \text{ dB}$ respectively.

We compare the impact of threshold on connectivity in Figure 9. We observe that increasing the threshold from 5dB to 10 dB, the number of isolated devices in both network topologies increases too as expected.

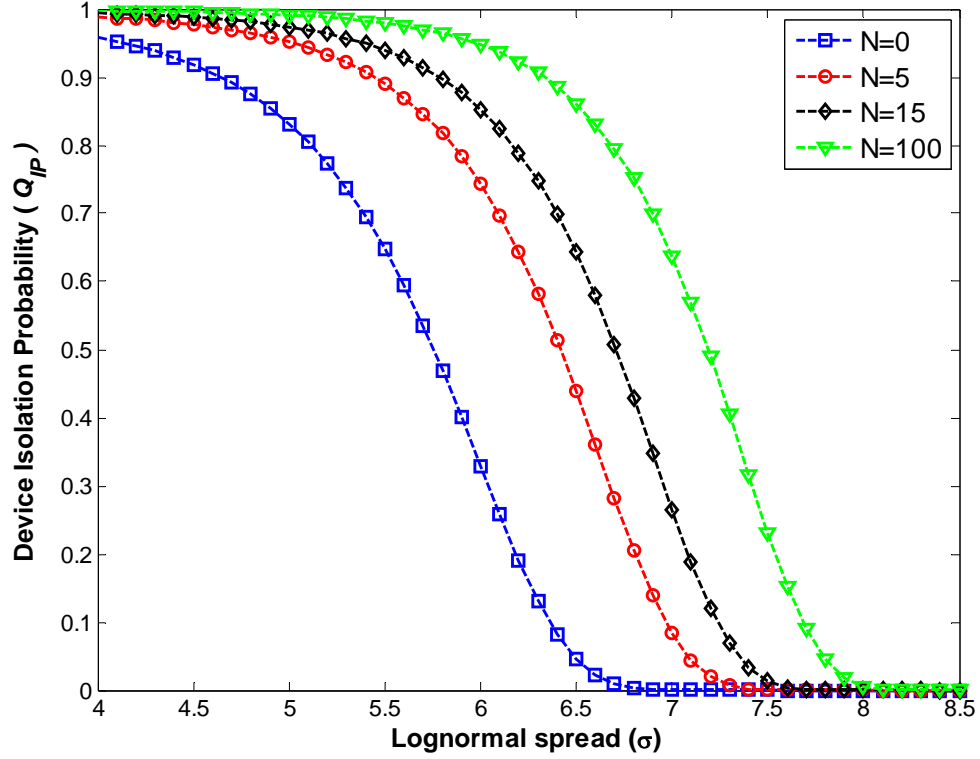


Figure 10: Effects of shadowing on isolation probability using (4.27) when $\lambda = 10^{-4} \text{ m}^{-2}$, $\beta = 3 \text{ dB}$, $\eta = 3.5$, $\bar{\gamma}_z = 2 \text{ dBm}$, and $m_0 = 3$, and $m_z = 2$.

In Figure 10, the isolation probability is plotted against the lognormal spread, for different number of interferers present. We vary σ to capture the effects of log-normal shadow fading on the isolation probability. Observe that the isolation probability monotonically decreases as σ is increased. For example, when $\sigma = 6$, the isolation probability with no interferers are present ($N = 0$) is 0.25 which is an improvement compare to 0.8 when five ($N = 5$) interferers are present. This phenomenon where lognormal shadow fading improves connectivity was also observed in [48] and may be due to the bias that is introduced in $\mathbb{E}(\mathcal{R}^2)$. That is, the average link gain increases with the lognormal spread.

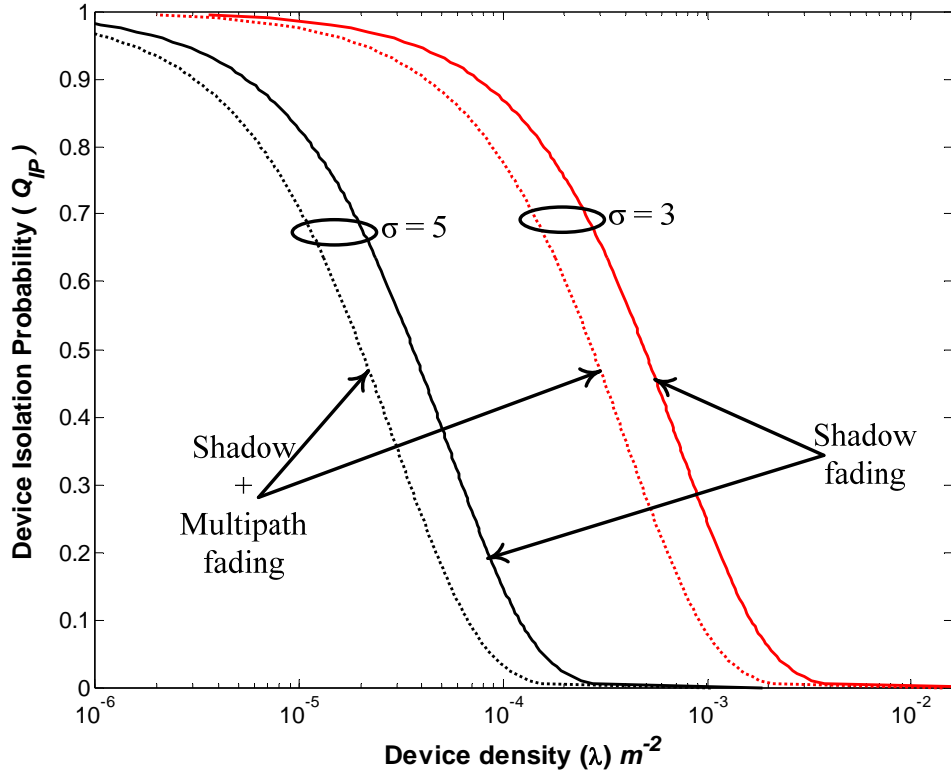


Figure 11: Impact of lognormal fading on isolation probability when $\beta = 10$ dB, $\eta = 3.5$, $\bar{\gamma}_0 = 10$, and $m_0 = 3$ using (4.8).

In Figures 11-17, we plot the isolation probability versus the device density for different propagation environments. In Figure 11, the solid lines represent the log-normal shadow fading effects, while the dashed lines represent multipath and shadow fading. From the curves it is evident that lognormal shadowing may have a tremendous impact on network performance. We observe that multipath fading has a negative impact on isolation probability, but the impact is not so enormous.

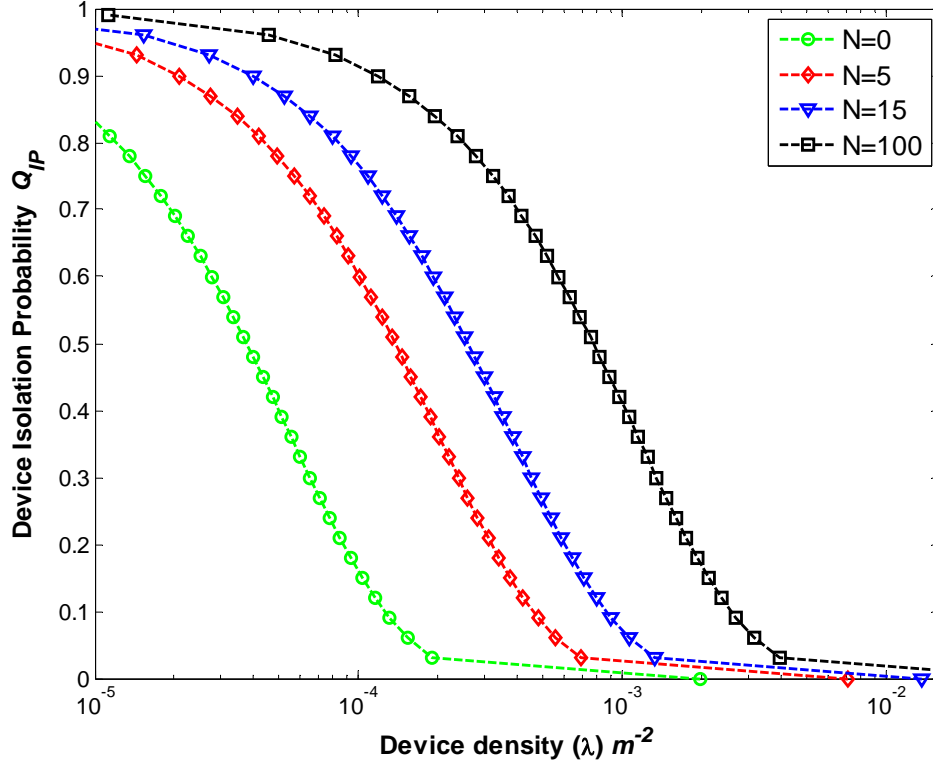


Figure 12: Impact of interferers present on isolation probability using (4.27) when $\sigma = 5$, $\beta = 3$ dB, $\eta = 3.5$, $\bar{\gamma}_z = 2$ dBm, and $m_0 = 3$, and $m_z = 2$.

In Figure 12, we plot the isolation probability versus the device density for different numbers of interferers. In Figure 12, the curve to the left represents fewer interferers present in the network. For example, the green curve represents no interferers in the network ($N = 0$) while the black curve represents 100 interferers in the network ($N = 100$). From the curves it is evident that presence of interference has a tremendous impact on network performance.

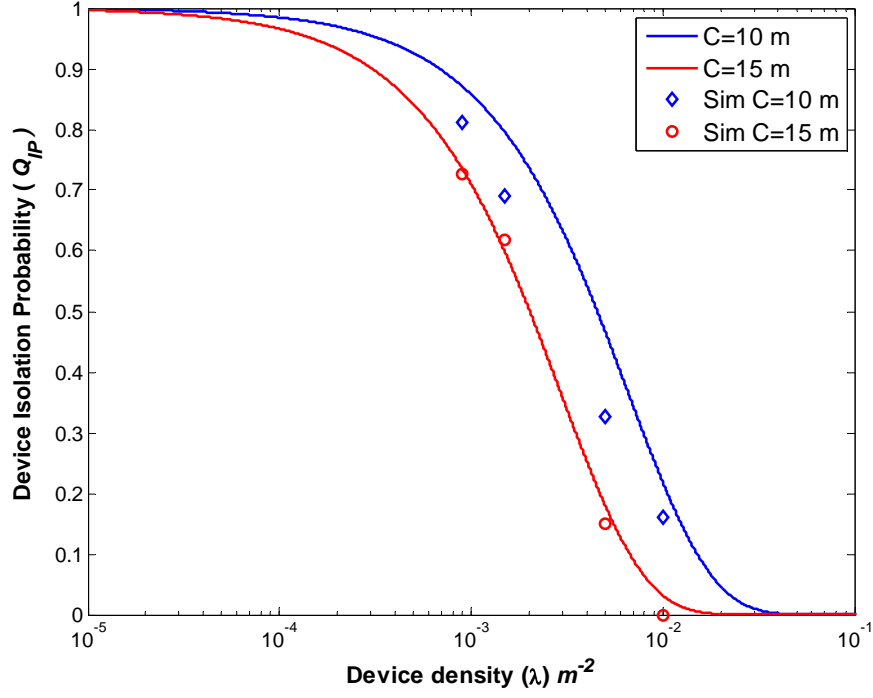


Figure 13: Device isolation probability when the interference area is varied, $\beta = 5$, $\eta = 3.5$, $\sigma_R = 2$, $m_0 = 3$, and $m = 2$ using (4.32).

In Figure 13, we consider the impact of the cell radius C . Note that for a given device density, decreasing C implies a more crowded cell with more interference. The simulation results roughly approximate the analysis results for both interference areas. Note that the analysis results denote the upper bound of isolation probability.

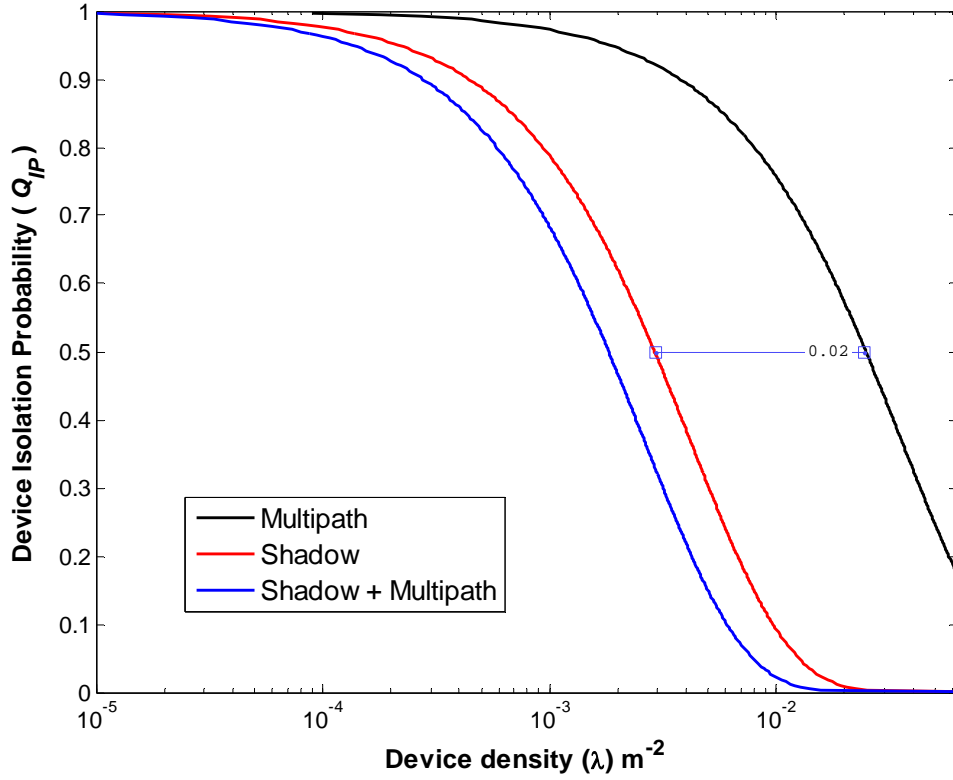


Figure 14: Illustration of the impact of path-loss, multipath, and shadow fading on isolation probability using (4.32) when the interference disk has a radius $C = 8$ m, $\beta = 5$, $N = 5$, $\eta = 3.5$, $\sigma_R = 2$, $m_0 = 3$, and $m_z = 2$.

In Figure 14, notice that Nakagami fading has a negative impact on the connectivity properties of the network, but the impact is very minimal compared to that of lognormal fading. From the graph, when the isolation probability is 0.5, the difference distance between shadow and multipath fading is 0.02 m^{-2} . We observe the same phenomenon where lognormal shadow fading improves connectivity properties of the network as discussed in Section 4.2.2.

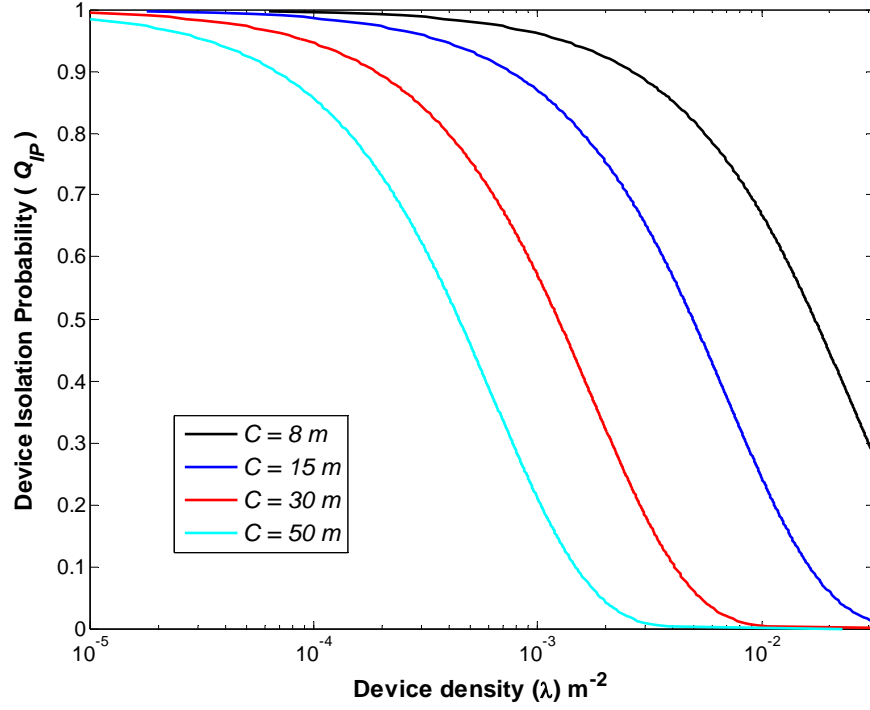


Figure 15: Illustration of how the interference region affects isolation probability.

As the cell radius is increased, the connectivity properties of the network are positively impacted as expected because a smaller radius accounts for congestion with more interference. For example, when the isolation probability is 0.5, the device density for $C = 50 m$ is $3.162 \times 10^{-4} m^{-2}$ compared to $136 \times 10^{-4} m^{-2}$ for $C = 8 m$.

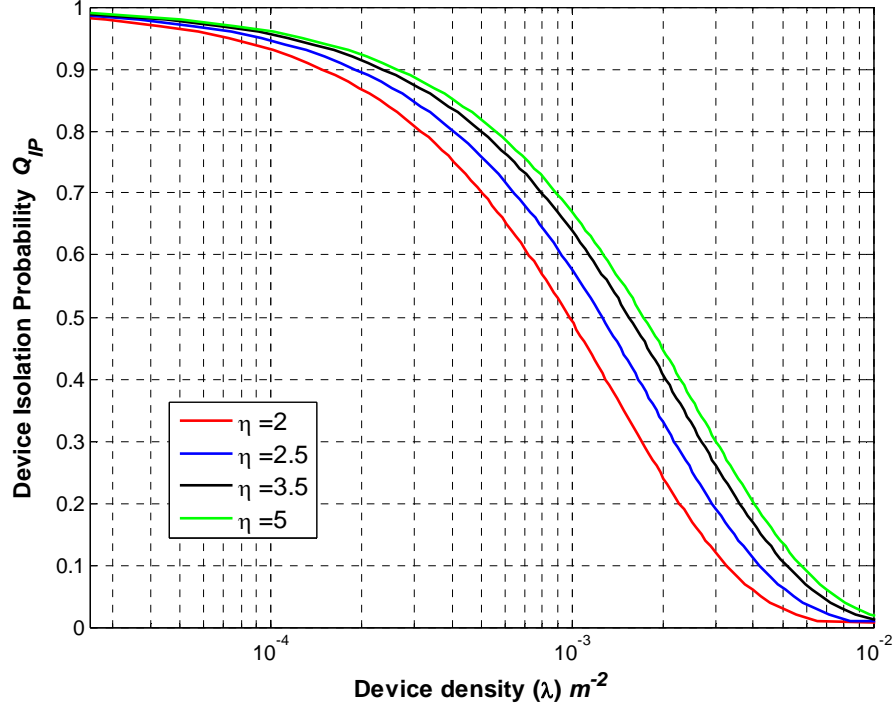


Figure 16: Effect of path-loss coefficient on isolation probability where $\beta = 5$, $m_0 = 3$, and $m_i = 2$.

When $\lambda = 10^{-3} m^{-2}$, we observe that the isolation probability is 0.5 for path-loss coefficient $\eta = 2$ and almost 0.7 for $\eta = 5$. Thus, the isolation probability increase as path-loss exponent increases. This is due to the fact that the signal strength decreases as the path-loss exponent increases, which leads to a low SINR compared to the threshold at the receiver

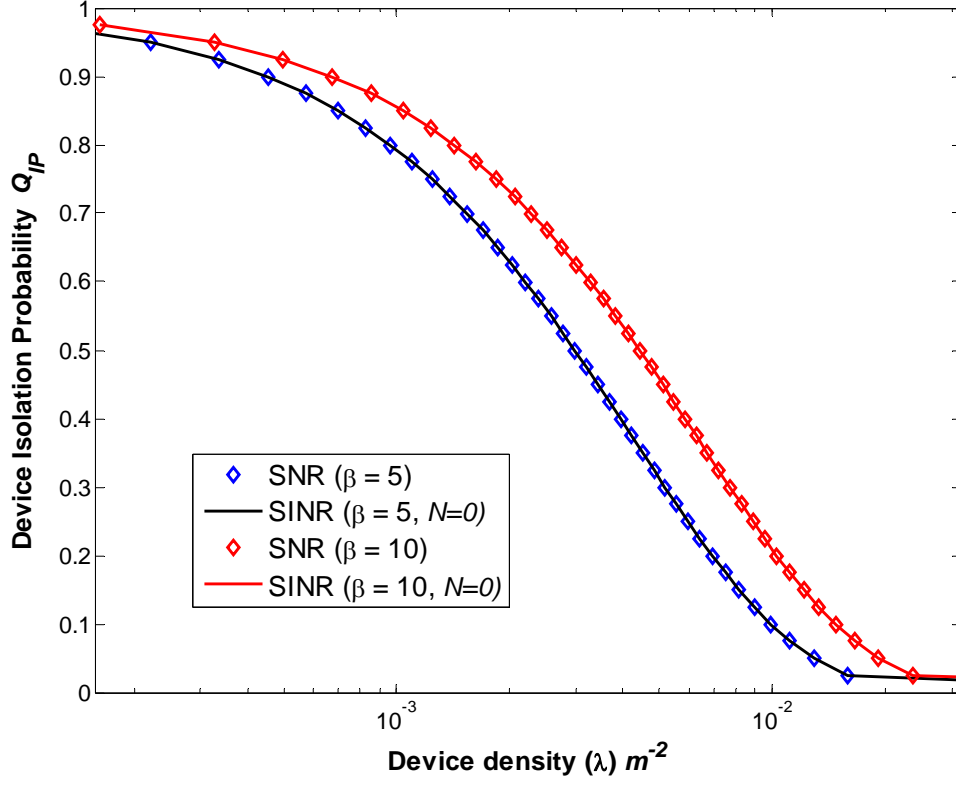


Figure 17: Comparing the SNR and SINR cases ($N = 0$) when $\beta = 5$ dB and $\beta = 10$ dB, $\bar{\gamma}_0 = \bar{\gamma}_z = 1$, $W = 0.01\text{mW}$, $\eta = 3.5$, $m_0 = 3$, and $m_i = 2$.

In Figure 17, we compare the plots for SNR and SINR when there is no interference while varying threshold. We observe that both cases are in agreement when no interference is experienced.

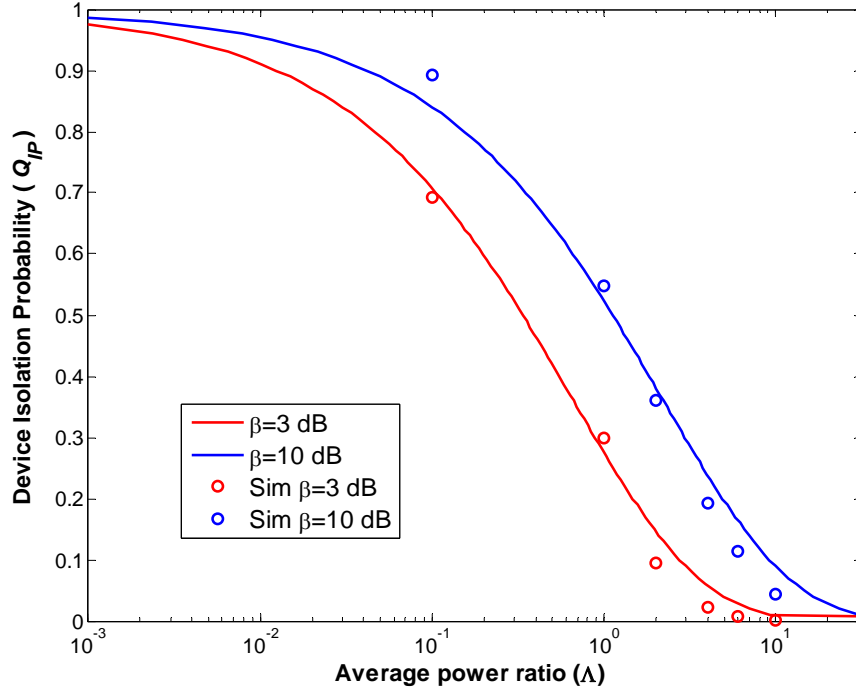


Figure 18 : Device isolation probability when the average power ratio is varied, $\lambda = 10^{-3} \text{ m}^{-2}$, $\eta = 3.5$, $\sigma_R = 2$, $m_0 = 3$, and $m = 2$ using (4.45).

In Figure 18, we evaluate the accuracy of the shifted gamma approximation used to obtain (4.45). Two values of threshold $\beta = 3 \text{ dB}$ and $\beta = 10 \text{ dB}$ were considered. For average power ratio, $\Lambda = 1$, the isolation probability for $\beta = 3 \text{ dB}$ is 0.3 and for $\beta = 10 \text{ dB}$ is 0.55. The simulation results roughly approximate the analysis results for both threshold values. Note that the analysis results displayed were obtained using the shifted gamma approximation.

CHAPTER 5

PERFORMANCE ANALYSIS USING OUTAGE PROBABILITY

5.1 Introduction

In this chapter, we consider a wireless network in which the channel can be modeled using any of the fading and shadowing models discussed in Chapter 2. All the devices in the network are considered to transmit with a constant power level P_{tx} and white noise power W is assumed to be present at the receiver. Both noise and interference are considered to be present without either being overly dominant. A receiver is unable to decode a message from the 0 -th transmitter with N other messages present when the SINR is below the threshold. Therefore, substituting (2.11) in (3.4) and rearranging, the SINR, γ for a failed reception is

$$\gamma = \frac{P_{tx} A r_0^{-\eta} \alpha_0^2 u_0}{W + \sum_{i=1}^N P_{tx} A r_i^{-\eta} \alpha_i^2 u_i} < \beta \quad (5.1)$$

In some cases, the received faded signals are assumed to follow known distributions. For example, the desired signal may follow Rayleigh or Nakagami distributions while the aggregate interference power follows the Gamma distribution. Note that in (5.1), N may be fixed or a random variable.

5.2 Outage Probability

Outage probability is the probability when the output SINR falls below a specified threshold, β .

5.2.1 Fixed Number of Interferers

Considering the additive interference model in (5.1), it is observed the number of interferers plays a significant role in determining the outage probability. When the number of interferers N is fixed, the outage probability is computed as

$$\begin{aligned} Q_{\alpha_0^2} &= \mathbb{P} \left(\frac{P_{tx} A r_0^{-\eta} \alpha_0^2 u_0}{W + \sum_{i=1}^N P_{tx} A r_i^{-\eta} \alpha_i^2 u_i} < \beta \right) \\ &= \mathbb{P} \left(\alpha_0^2 < \beta \left[\frac{u_0 r_0^\eta W}{A P_{tx}} + \sum_{i=1}^N \alpha_i^2 \left(\frac{u_i}{u_0} \right) \left(\frac{r_0}{r_i} \right)^\eta \right] \right) \end{aligned} \quad (5.2)$$

where $\mathbb{P}(\cdot)$ denotes the probability operator. We may express equation (5.2) as

$$Q_{\alpha_0^2} = \mathbb{P}(\alpha_0^2 < \beta [D + Z]) \quad (5.3)$$

where $D = [u_0 r_0^\eta W / A P_{tx}]$, $Z = \sum_{i=1}^N w_i \alpha_i^2$, and $w_i = (u_i / u_0) (r_0 / r_i)^\eta$.

The outage probability for the noise-limited and interference-limited special cases can be obtained from (5.3) either by setting $Z = 0$ or $W = 0$, respectively. In what follows, we consider two approaches in deriving the outage probability. In the PDF approach, we assume that N is known and derive the PDF of the aggregate interference and, consequently, the outage probability. On the other hand, in the MGF approach, we assume that the MGF of the aggregate interference is known.

5.2.1.1 PDF Based Approach

In some systems, the PDF of the signal for the interferer is known or can be easily estimated. Assuming that the interferers are placed in a deterministic topology, then the number of interferers is fixed and known. We also assume that the signals at the receiver only suffer path-loss and multipath fading and that the interfering signals are identical and independently distributed (*i.i.d*). Then, w_i in (5.2) is a constant that can be absorbed in the average power for the total interference. Assume $W = 0$, that is, we only consider the interference limited case. Given that the desired signal follows a distribution denoted by $p_{\gamma_0}(\cdot)$ and the total interference power Z (which is the sum of all the interfering signal powers) follows a distribution denoted by $p_Z(\cdot)$, the signal to interference power ratio ($\gamma = \gamma_0/Z$) is a ratio of two independent random variables with PDF computed mathematical using (4.21).

5.2.1.1.1 Rayleigh Fading Case.

We consider that the desired signal experiences Rayleigh fading as it travels to the receiver. For such a case, the received desired signal power, γ_0 has PDF given in (2.6) with mean power, $\bar{\gamma}_0$. In the event when the existing N mutually independent interfering signals also experience Rayleigh fading; the SNR received for each of the interfering signal is exponentially distributed with mean power, $\bar{\gamma}_i$. The total interference power Z (which is the sum of N exponential random variables) follows a Gamma distribution, with PDF given in (2.13) and mean power, $\bar{\gamma}_z$. Using (4.21), the appropriate distributions

given in (2.6) and (2.13), and using [30, eq.(3.381.4)]; the PDF of the signal-to-interference power ratio becomes

$$p_\gamma(y) = \frac{\Gamma(N+1)}{\bar{\gamma}_0 \bar{\gamma}_z^N \Gamma(N) (1/\bar{\gamma}_z + y(1/\bar{\gamma}_0))^{N+1}} \quad (5.4)$$

Substituting (5.4) in (5.3) yields the SIR outage probability as

$$Q_{\alpha_0^2} = \left(\frac{N\beta}{\Lambda} \right) {}_2F_1 \left(N+1, 1; 2; -\frac{\beta}{\Lambda} \right) \quad (5.5)$$

where $\Lambda = \bar{\gamma}_0/\bar{\gamma}_z$ and [30, eq.(3.194.1)] was used.

5.2.1.1.2 Nakagami Fading Case.

We consider the case when the received signal experiences Nakagami fading as it travels to the receiver. For such a case, the received desired signal power γ_0 has PDF given in (2.8), with mean power, $\bar{\gamma}_0$ and fading parameter m_0 . In the case of Nakagami faded interfering signals, each with mean power, $\bar{\gamma}_i$ and m_i as the fading parameter, the total interference power, Z , which is the sum of the N interfering signals also follow a Nakagami distribution whose PDF is given in (2.8) with parameters $(m_z, \bar{\gamma}_z)$. The PDF of the power ratio is given as [78]

$$p_\gamma(\gamma) = \frac{\Gamma(m_0 + m_z N)}{\Gamma(m_0) \Gamma(m_z N)} \left(\frac{m_0}{\Lambda} \right)^{m_0} m_z^{m_z N} \gamma^{m_0-1} \left(\frac{m_0}{\Lambda} \gamma + m_z \right)^{-m_0 - m_z N} \quad (5.6)$$

where $\Lambda = \bar{\gamma}_0/\bar{\gamma}_z$ is the mean power ratio and $\Gamma(\cdot)$ is the Gamma function. Substituting (5.6) in (5.3) yields the SIR outage probability as [78]

$$Q_{\alpha_0^2} = \frac{\Gamma(m_0 + m_z N)}{m_0 \Gamma(m_0) \Gamma(m_z N)} \left(\frac{m_0 \beta}{m_z \Lambda} \right)^{m_0} {}_2F_1 \left(m_0 + m_z N, m_0; m_0 + 1; -\frac{m_0 \beta}{m_z \Lambda} \right). \quad (5.7)$$

It follows that by setting $m_0 = m_i = 1$ in (5.7) yields the outage probability result obtained for Rayleigh fading given in (5.5).

5.2.1.2 MGF Based Approach

In some systems, the MGF of the signal for the interferer is known or can be easily estimated. Assuming that the interferers are placed in a deterministic topology, then the number of interferers is fixed and known. We also assume that the signals at the receiver only suffer path-loss and multipath fading and that the interfering signals are *i.i.d.* Then, w_i in (5.2) is a constant that can be absorbed in the average power for the total interference. We assume that there is no shadow fading present and a unit transmitter-receiver distance for the 0 -th link, then outage probability can be computed by conditioning on the aggregate interference in (5.3). Then averaging out the aggregate interference Z , we have

$$\mathcal{Q}_{\alpha_0^2} = \int_0^\infty F_{\alpha_0^2|Z}(\beta[D+Z]) p_z(z) dz = \mathbb{E}_Z \left[F_{\alpha_0^2}(\beta[D+Z]) | Z \right] \quad (5.8)$$

$$\text{where } F_{\alpha_0^2|Z}(\beta[D+Z]) = \mathbb{P} \left(\alpha_0^2 \leq \beta \left[\frac{W}{AP_{tx}} + \sum_{i=1}^N \alpha_i^2 \right] | z \right) = \mathbb{P} \left[\alpha_0^2 < [D+Z]\beta | z \right].$$

5.2.1.2.1 Rayleigh Fading Case

Assume $W = 0$, that is, we only consider the interference limited case. When the desired signal experiences Rayleigh fading, α_0^2 is a Rayleigh random variable with

conditioned CDF given as $F_{\alpha_0^2|Z}(\beta Z) = 1 - \exp\left(-\frac{\beta}{\gamma_0} Z\right)$. Thus, we can compute the

outage probability using (5.8) to obtain

$$Q_{\alpha_0^2} = 1 - \int_0^\infty \exp\left(-\frac{\beta}{\bar{\gamma}_0} Z\right) p_Z(z) dz = 1 - \mathbb{M}_Z(\beta/\bar{\gamma}_0) \quad (5.9)$$

where $\mathbb{M}_Z(s) = \mathbb{E}(e^{-sZ})$ is the MGF of Z . We discuss how Z can be modeled. One approach is to assume that the MGF of Z is known or can be easily approximated.

Assuming that the N interfering signals experience Rayleigh fading and their locations are known; then, w_i 's are known constants. The aggregate interference power at the receiver is the sum of exponential random variables that yields a gamma random variable. Therefore, the aggregate interference power at the receiver can be characterized by the MGF given as $\mathbb{M}_Z(\beta/\bar{\gamma}_0) = (1 + \bar{\gamma}_z \beta/\bar{\gamma}_0)^{-N}$ and the outage probability is computed using (5.9) to yield

$$Q_{\alpha_0^2} = 1 - (1 + \beta/\Lambda)^{-N} \quad (5.10)$$

where $\Lambda = \bar{\gamma}_0/\bar{\gamma}_z$. Note that the result in (5.10) was also obtained by Simon and Alouini [65, eq.(10.19)].

5.2.1.2.2 Nakagami Fading Case

When the desired signal experiences Nakagami fading, the power received has a CDF given as

$$F_{\alpha_0^2}(\gamma) = \left\{ \frac{1}{\Gamma(m_0)} \mathcal{G}\left(m_0, \frac{m_0 \gamma}{\bar{\gamma}_0}\right) \right\} = 1 - \left\{ \frac{1}{\Gamma(m_0)} \Gamma\left(m_0, \frac{m_0 \gamma}{\bar{\gamma}_0}\right) \right\} \quad (5.11)$$

where $\mathcal{G}(a, \chi) = \int_0^\chi t^{a-1} \exp(-t) dt$ is the lower incomplete gamma function [4, eq.(6.5.2)].

But, we can use [4, eq.(8.353.5)] and (5.11) to express the conditioned CDF as

$$F_{\alpha_0^2|Z}(\beta z) = 1 - \frac{z^{m_0}}{\Gamma(m_0)} \int_0^\infty \left(t + \frac{m_0 \beta}{\bar{\gamma}_0} \right)^{m_0-1} \exp \left[- \left(t + \frac{m_0 \beta}{\bar{\gamma}_0} \right) z \right] dt \quad (5.12)$$

where $m_0 > 1$.

By setting $W = 0$ in (5.8), the outage probability for the interference limited case can be computed by substituting (5.12) in (5.8) to obtain

$$\mathcal{Q}_{\alpha_0^2} = 1 - \frac{1}{\Gamma(m_0)} \int_0^\infty \left(t + \frac{m_0 \beta}{\bar{\gamma}_0} \right)^{m_0-1} \mathbb{E}_Z \left\{ z^{m_0} \exp \left[- \left(t + \frac{m_0 \beta}{\bar{\gamma}_0} \right) z \right] \right\} dt \quad (5.13)$$

By use of the convolution theorem [4, eq.(29.2.10)], the expectation operation can be replaced by m_0 -th derivative of the MFG to obtain

$$\mathcal{Q}_{\alpha_0^2} = 1 - \frac{(-1)^{m_0}}{\Gamma(m_0)} \int_0^\infty \left(t + \frac{m_0 \beta}{\bar{\gamma}_0} \right)^{m_0-1} \mathcal{D}_s^{m_0} \mathbb{M}_Z \left[\left(t + \frac{m_0 \beta}{\bar{\gamma}_0} \right) s \right] \Big|_{s=1} dt \quad (5.14)$$

where $\mathcal{D}_k^n(\cdot)$ is the n^{th} derivative with respect to k . We now discuss an example where the outage probability in (5.14) can be applied.

Let the N interferers also experience Nakagami fading; then, each interfering signal power seen at the receiver is a gamma random variable. Assuming that the locations are fixed, the aggregate interference Z whose average power is $\bar{\gamma}_z$ and fading parameter m_z seen at the receiver is characterized by a MGF

$$\mathbb{M}_Z \left(\left(t + m_0 \beta / \bar{\gamma}_0 \right) s \right) = \left(1 + \frac{\bar{\gamma}_z \left(t + m_0 \beta / \bar{\gamma}_0 \right) s}{m_z} \right)^{-Nm_z} \quad (5.15)$$

Thus, we use (5.15) to compute the derivative term in (5.14) first, then the result is substituted back into (5.14) and simplified using [30, eq.(3.194.2.6)] to obtain the outage

probability as (see Appendix A for details)

$$Q_{\alpha_0^2} = 1 - \left\{ \frac{(m_z \Lambda / m_0 \beta)^{Nm_z} \Gamma(m_0 + Nm_z)}{(Nm_z) \Gamma(m_0) \Gamma(Nm_z)} {}_2F_1 \left(Nm_z + m_0, Nm_z; Nm_z + 1; -\frac{\Lambda m_z}{m_0 \beta} \right) \right\} \quad (5.16)$$

where $\Lambda = \bar{\gamma}_0 / \bar{\gamma}_z$.

When noise cannot be ignored and the interferers are *i.i.d.*, we use equations (5.3) and (5.22) to obtain the outage probability as

$$Q_{\alpha_0^2} = \mathbb{E}_Z \left[F_{\alpha_0^2}(\beta[D+Z]) | Z \right] \text{ where } Z = w \sum_{i=1}^N \alpha_i^2 \text{ and } w \text{ is a constant that can be set}$$

equal unit without loss of generality. Assuming a Nakagami fading channel, the outage probability can be expressed as

$$Q_{\alpha_0^2} = \mathbb{E}_Z \left\{ \frac{1}{\Gamma(m_0)} \mathcal{G} \left(m_0, \frac{m_0 \beta (D+Z)}{\bar{\gamma}_0} \right) \right\} \quad (5.17)$$

Using [4, eq.(6.5.12;13.2.1)], and Laplace transform identities; equation (5.17) is expressed as an integral of the derivative of the MGF as below

$$Q_{\alpha_0^2} = \frac{1}{\Gamma(m_0)} \int_0^1 y^{-1} \left\{ (-1)^{m_0} \mathcal{D}_s^{m_0} \mathbb{M}_{m_0 \beta y (D+Z)/\bar{\gamma}_0}(-s) \right\} \Big|_{s=1} dy \quad (5.18)$$

To compute the outage probability, the MGF is required. So, the interference is characterized by a gamma random variable with known MGF. To perform the derivative term in the above equation, we use the MGF identities, differentiation properties, and [4, eq.(13.1.10)] to obtain the derivative as

$$\begin{aligned} \mathcal{D}_s^{m_0} \mathbb{M}_{m_0 \beta y (D+Z)/\bar{\gamma}_0}(s) \Big|_{s=1} &= (-1)^{m_0} \left(\frac{m_0 \beta y D}{\bar{\gamma}_0} \right)^{m_0} \left(\frac{m_0 \beta y}{\Lambda m_z} \right)^{-Nm_z} \exp \left(-\frac{m_0 \beta y D s}{\bar{\gamma}_0} \right) \sum_{k=0}^{\infty} (-1)^k \binom{m_0}{k} \\ &\times \left(-\frac{m_0 \beta y D}{\bar{\gamma}_0} s \right)^{-k} (-Nm_z)_k \left(\frac{\Lambda m_z}{m_0 \beta y} \right)^{-Nm_z-k} \left(1 + \frac{m_0 \beta y}{\Lambda m_z} s \right)^{-Nm_z-k} \end{aligned} \quad (5.19)$$

where $\Lambda = \bar{\gamma}_0/\bar{\gamma}_z$. By substituting equation (5.19) into (5.18) and using [4, eq.(13.1.10)],

we have outage probability (as shown in Appendix A) as

$$\begin{aligned} Q_{\alpha_0^2} = & \frac{1}{\Gamma(m_0)} \left(\frac{m_0 \beta D}{\bar{\gamma}_0} \right)^{m_0} \left(\frac{m_z D}{\bar{\gamma}_z} \right)^{Nm_z} \int_0^1 y^{m_0-1} \exp \left(-\frac{m_0 \beta y D}{\bar{\gamma}_0} \right) \\ & \times U \left(Nm_z, Nm_z + m_0 + 1; -; \frac{m_z D}{\bar{\gamma}_z} \left(1 + \frac{m_0 \beta y}{\Lambda m_z} \right) \right) dy \end{aligned} \quad (5.20)$$

Equation (5.20) is not in closed form but can be easily computed numerically.

5.2.2 Random Number of Interferers

In some applications the number of interferers may be finite and known, but the number varies randomly with time; and in other networks, it may not be possible to know the exact number of interferers present at a particular time. In either case, we assume that the number of interferers present is random and follows either a binomial or Poisson distribution, accordingly. The devices in the network are assumed to be distributed according to a random point process on an infinitely large system plane. Thus, when N is random; the outage probability in (5.2) becomes

$$Q_{\alpha_0^2} = \mathbb{P} \left(\alpha_0^2 < \beta \left[\frac{u_0 r_0^\eta W}{AP_{tx}} + \sum_{i \in \mathcal{N}} \alpha_i^2 \left(\frac{u_i}{u_0} \right) \left(\frac{r_0}{r_i} \right)^\eta \right] \right) \quad (5.21)$$

where \mathcal{N} denotes the random process defining the number of interfering devices.

MGF Based Approach

In some systems, it may not be possible to know the number of interferers present, but the MGF for the aggregate interference may be easily known or approximated. In the event when the interfering signals experience both multipath and shadow fading and the

total number and location of the interferers are not known; the outage probability is obtained by conditioning on the random event. Using (5.21), the outage probability for SINR case is given as

$$\begin{aligned} Q_{\alpha_0^2} &= \mathbb{E}_{\alpha_0^2, u, N, r} \left\{ \mathbb{P} \left(\alpha_0^2 < \beta \left[\frac{u_0 r_0^\eta W}{AP_{tx}} + \sum_{i \in \mathcal{N}} \alpha_i^2 \left(\frac{u_i}{u_0} \right) \left(\frac{r_0}{r_i} \right)^\eta \right] \right) \right\} \\ &= \mathbb{E}_{\alpha_0^2, u, N, r} \left\{ F_{\alpha_0^2} \left(\beta [D + Z] \right) \right\} \end{aligned} \quad (5.22)$$

where D and Z are defined in (5.3) and $\alpha_0^2, \alpha_i^2, u_0, r_i, N$, and u_i are all random variables whose PDFs or MGFs are known or can be approximated.

Aggregate Interference Is Alpha-stable.

In cases when the number of interferers is unknown, the transmitter-receiver distances are random, and the received signals suffer path-loss and either multipath or shadow fading; then, w_i is random and the aggregate interference Z is considered to follow an alpha stable distribution (α – stable distribution). A wealth of literature discussing interference modeling suggest that when the interferers are distributed according to a 2-D PPP in a plane; the distribution of the aggregate interference follows the heavy-tailed family of α – stable distributions [35, 53, 77]. If we assume that the receiver treats all interfering signals as shot noise (shot noise is an after-effect of an impulse train generated from a PPP exciting a memory-less linear filter) the magnitude of interference seen by the receiver at the origin can be compared to the amplitude of the shot noise. The amplitude can be characterized as an infinite sum of impulse responses that may be either deterministic or random. Thus, the shot noise amplitude characterizing the interference at the receiver is given as [45, 72]

$$Z = \sum_{i \in \mathcal{N}} K_i r_i^{-\eta} \quad (5.23)$$

where \mathcal{N} denotes the PPP defined by the interfering devices, r_i is the random distance of the i -th transmitter from the origin, and $K_i = \alpha_i^2 u_i$ is a random variable that accounts for the other channel propagation effects experienced by the i -th interferer. For example, $K_i = 1$ which is a constant in the case of deterministic path loss only and it is a random variable with an appropriate PDF in the event of either multipath or shadow fading or both. The MGF of such a sum in (5.23) can be shown to be given as [72]

$$\mathbb{M}_Z(s) = \exp\left[-\pi\lambda \mathbb{E}_K\left[K^{2/\eta}\right] \Gamma(1-2/\eta) s^{2/\eta}\right] \quad (5.24)$$

The MGF in (5.24) can be expressed as

$$\mathbb{M}_Z(s) = \exp\left[-\Theta s^{2/\eta}\right] \quad (5.25)$$

where $\Theta = \pi\lambda \mathbb{E}_K\left[K^{2/\eta}\right] \Gamma(1-2/\eta)$. Comparing (5.25) with the definition of an α – stable distribution, it can be concluded that the aggregate interference Z follows an α – stable distribution with characteristic exponent, $2/\eta$. The characteristic exponent determines the heaviness of the tail of the distribution.

5.2.2.1.1 Rayleigh Fading Case

It follows that when Z follows the alpha-stable distribution given in (5.24) and the desired signal is a Rayleigh random variable, using (5.24) in (5.9) the outage probability is given by

$$\mathcal{Q}_{\alpha_0^2} = 1 - \exp\left[-\left\{\left(\pi\lambda \mathbb{E}_K\left[K^{2/\eta}\right] \Gamma(1-2/\eta) (\beta/\bar{\gamma}_0)^{2/\eta}\right) + (W\beta/AP_{tx})\right\}\right]. \quad (5.26)$$

Next we consider some special cases of (5.26).

i). When the interfering signals experience only path-loss, that is no multipath or shadow fading; we set $K_i = 1$, without loss of generality, i.e., $\mathbb{E}_K [K^{2/\eta}] = 1$ and the outage probability in (5.26) reduces to

$$\mathcal{Q}_{\alpha_0^2} = 1 - \exp \left[- \left\{ (W\beta/AP_{tx}) + \left(\pi\lambda (\beta/\bar{\gamma}_0)^{2/\eta} \Gamma(1-2/\eta) \right) \right\} \right]. \quad (5.27)$$

ii). In the event of Rayleigh fading with no shadow fading, K_i is an exponential random variable, thus $\mathbb{E}_K [K^{2/\eta}] = \Gamma(1+2/\eta) \bar{\gamma}_z^{2/\eta}$, and the outage probability is given as

$$\mathcal{Q}_{\alpha_0^2} = 1 - \exp \left[- \left\{ (W\beta/AP_{tx}) + \left(\pi\lambda (\beta/\Lambda)^{2/\eta} \Gamma(1+2/\eta) \Gamma(1-2/\eta) \right) \right\} \right] \quad (5.28)$$

where $\Lambda = \bar{\gamma}_0 / \bar{\gamma}_z$.

5.2.2.1.2 Nakagami Fading Case

In the event that the MGF for Z follows the alpha stable distribution given in (5.25), we may use (5.14) and (5.25) to obtain the derivative term as

$$\mathcal{D}_s^{m_0} \left\{ \mathbb{M}_Z \left[\left(t + \frac{m_0\beta}{\bar{\gamma}_0} \right) s \right] \right\} \Big|_{s=1} = \mathcal{D}_s^{m_0} \left\{ \exp \left(-\Theta \left(t + \frac{m_0\beta}{\bar{\gamma}_0} \right)^{2/\eta} s^{2/\eta} \right) \right\} \Big|_{s=1} \quad (5.29)$$

The exponential function in (5.29) can be expressed as a contour integral, and the solution to such a derivative is a Fox's H -function (see Appendix A). The Fox's H -function is not easily computable because the function is not readily available in any standard mathematical packages. Thus, we consider a special case when $\eta = 2n$; where $n \in \mathbb{N}^+$, the Fox's H -function can simplify into the more easily computable Meijer's G -function. The outage probability for the special case was determined to be (see Appendix A for details)

$$Q_{SIR} = 1 - \left\{ \frac{\sqrt{n(2\pi)^{(1-n)}}}{\Gamma(m_0)} \left(\frac{m_0 \beta}{\bar{\gamma}_0} \right)^{m_0} \right. \\ \left. \times G_{2,n+2}^{n+1,1} \left(\left(\pi \lambda \mathbb{E}_K [K^{1/n}] \Gamma(1-1/n) / n \right)^n \left(\frac{m_0 \beta}{\bar{\gamma}_0} \right) \middle| \begin{matrix} 0, (1-m_0) \\ -m_0, \Delta(n, 0), m_0 \end{matrix} \right) \right\} \quad (5.30)$$

where $G_{p,q}^{k,l}(\cdot)$ is a Meijer G -function defined in (B.2) and

$$\Delta(a, b) = \left(\frac{b}{a}, \frac{b+1}{a}, \dots, \frac{b+a-1}{a} \right). \text{ We now consider some special cases for (5.30)}$$

i). When the interfering signals experience only path-loss, i.e. no multipath or shadow fading; the outage probability simplifies to

$$Q_{SIR} = 1 - \left\{ \frac{\sqrt{n(2\pi)^{(1-n)}}}{\Gamma(m_0)} \left(\frac{m_0 \beta}{\bar{\gamma}_0} \right)^{m_0} \right. \\ \left. \times G_{2,n+2}^{n+1,1} \left(\left(\pi \lambda \frac{\Gamma(1-1/n)}{n} \right)^n \left(\frac{m_0 \beta}{\bar{\gamma}_0} \right) \middle| \begin{matrix} 0, (1-m_0) \\ -m_0, \Delta(n, 0), m_0 \end{matrix} \right) \right\} \quad (5.31)$$

ii). Similarly, for Rayleigh fading with no shadow fading, we have

$$\mathbb{E}_k [K^{1/n}] = \Gamma(1+1/n) \bar{\gamma}_z^{-1/n}, \text{ and thus the outage probability becomes}$$

$$Q_{SIR} = 1 - \left\{ \frac{\sqrt{n(2\pi)^{(1-n)}}}{\Gamma(m_0)} \left(\frac{m_0 \beta}{\bar{\gamma}_0} \right)^{m_0} \right. \\ \left. \times G_{2,n+2}^{n+1,1} \left(\left(\pi \lambda \frac{\Gamma(1+1/n) \Gamma(1-1/n)}{n} \right)^n \left(\frac{m_0 \beta}{\Lambda} \right) \middle| \begin{matrix} 0, (1-m_0) \\ -m_0, \Delta(n, 0), m_0 \end{matrix} \right) \right\} \quad (5.32)$$

iii). In the event of Nakagami fading, $\mathbb{E}_K [K^{1/n}] = \Gamma(m_z + 1/n) \bar{\gamma}_z^{-1/n} / \Gamma(m_z)$ and the outage probability is given as

$$\begin{aligned}
Q_{SIR} = & 1 - \left\{ \frac{\sqrt{n(2\pi)^{(1-n)}}}{\Gamma(m_0)} \left(\frac{m_0 \beta}{\bar{\gamma}_0} \right)^{m_0} \right. \\
& \times \left. G_{2,n+2}^{n+1,1} \left(\left(\pi \lambda \frac{\Gamma(1-1/n) \Gamma(m_z + 1/n)}{n \Gamma(m_z)} \right)^n \left(\frac{m_0 \beta}{\Lambda} \right) \middle| \begin{matrix} 0, (1-m_0) \\ -m_0, \Delta(n, 0), m_0 \end{matrix} \right) \right\}.
\end{aligned} \tag{5.33}$$

CHAPTER 6

APPLICATIONS/SYSTEMS

6.1 Cellular Networks

In a cellular network, a mobile user (MU) establishes a wireless communication link with the nearest base station (BS). A number of base stations are connected to a base station controller (BSC) via microwave links or leased lines. The BSC is responsible for transferring an ongoing call from one base station to another as a mobile user travels from cell to cell. The BSC is then connected to a mobile switching center (MSC) by either cable or microwave radio links that switches calls to connect mobile users to other users. The MSC is connected to the public switched telephone network (PSTN) that uses fiber optics cables, telephone lines, and microwave radio links and so on to connect a user anywhere in the world to communicate with another user, as illustrated in Figure 19.

A cell site typically covers a radius of approximately one to ten miles. The network consists of several overlapping cell sites located in close proximity to each other to provide seamless connectivity and continuous coverage for all mobile users. A base station sometimes cannot cover all the area required due to fading. One way to improve coverage area is to increase transmit power. However, increasing transmit power also introduces interference that leads to poor reception and thus creating reception gaps in the covered area. This solution negates the intended goal. Another solution is to explore the

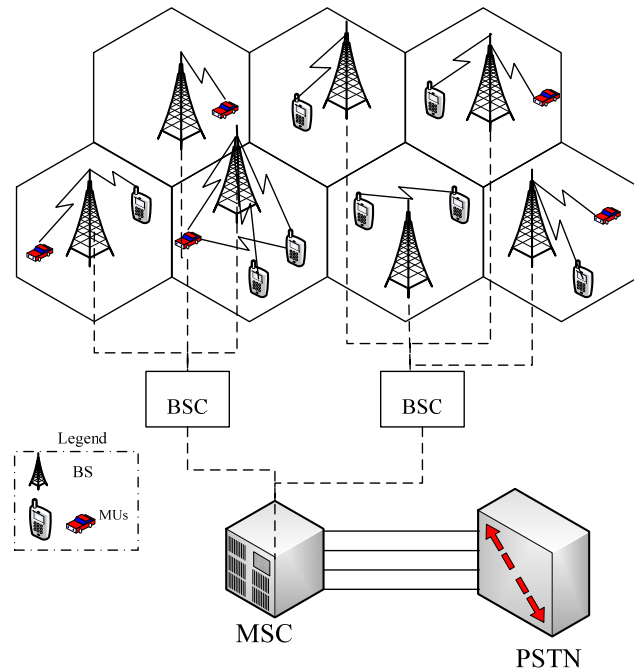


Figure 19: Illustration of a cellular concept.

cell shapes, which in practice, are irregular distorted and overlapping areas. Routinely a circle is chosen to represent a cell site coverage area but a hexagon is more preferred because it eliminates gaps and overlapping regions within the entire coverage area. The hexagon cell shape also offers ease of concept analysis, close approximation of a circle, and the largest coverage area. Consequently, hexagon cell shapes require less cell sites and base stations [55], compared to other shapes. The merits of a hexagon cell shape are illustrated in Figure 20.

Frequency reuse is a core concept in cellular networks, where a particular radio channel/frequency used in one cell site is used again in another cell site as long as the minimal separation distance is met. When the minimal separation is not satisfied and communication takes place on that channel, co-channel interference is experienced on the channel. The minimal separation to minimize interference depends on several factors

such as number of co-channel cell sites, the terrain configurations, antenna height, and cell site transmit power for the entire network. The network may consist of several clusters, where a cluster is defined as a collection of cells that use the complete set of available channels. Therefore, a cluster reuse of size M cells has to satisfy the condition below [55]

$$M = e^2 + ef + f^2; \quad e \geq f \quad (6.1)$$

where $e, f \in \mathbb{N}$. It is observable that frequency reuse is limited by co-channel interference; hence, the reuse separation should be determined such that co-channel interference is minimized.

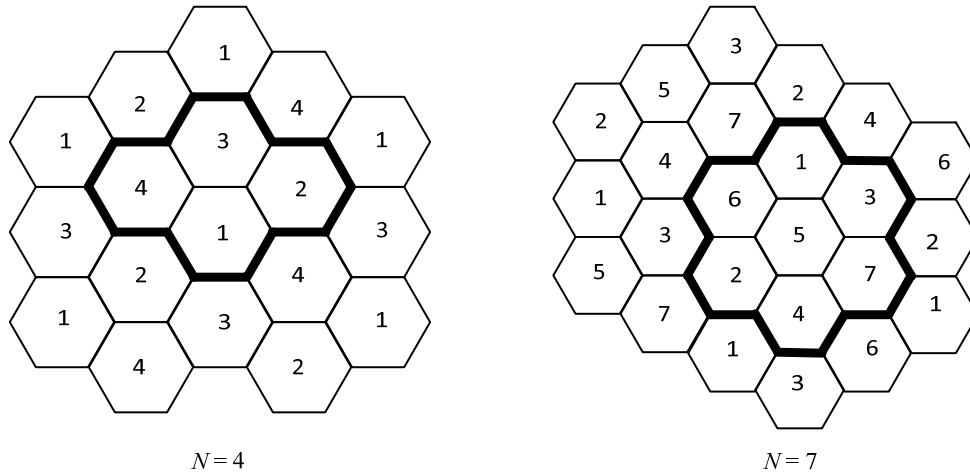


Figure 20: Reuse cluster of size 4 cells (1,2,3,4) and reuse cluster of size 7 cells (1,2,3,4,5,6,and 7).

When the hexagonal cells are approximately equal in size, the co-channel interference is independent of the transmitted power. But co-channel interference depends on the cell radius, R and frequency reuse separation (\mathfrak{D}_i) between cells using the same carrier frequencies. Thus, the co-channel reuse factor can be expressed as

$\mathfrak{D}_i/R = \sqrt{3M}$ where $i = 1, 2, \dots$ is the tier number and $M = 4, 7, 12, 19, \dots$ is the allowable

cluster size as per equation (6.1)[67]. The reuse distance when $i = 1$ represents the reuse distance of the first tier, $i = 2$ is for the second tier, and so on. From Figure 21, it is observable that the first tier has six cells using co-channel at the reuse distance \mathfrak{D}_1 . The second tier will have 12 cells using co-channel at the reuse distance \mathfrak{D}_2 , and so on.

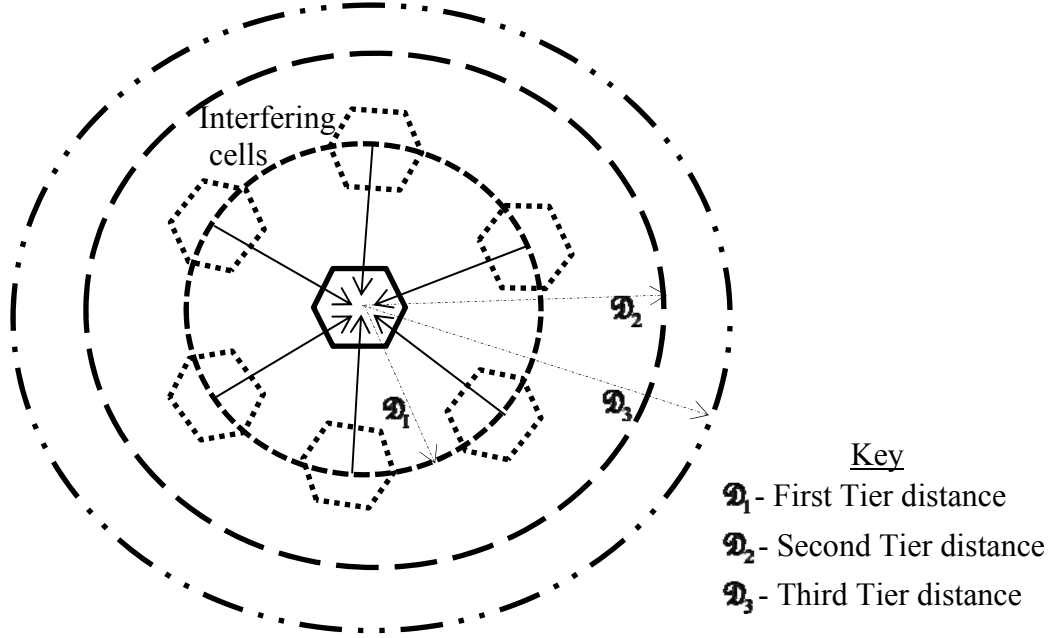


Figure 21: Demonstration of first, second and third tiers of co-channel interfering cells for a cell at the center [42].

The most effective interfering cells are located in the first tier, followed by those in the second, third, and higher tiers. Thus, the total number of interfering cells is given by a recursive formula as

$$N_i = 2N_{i-1} \quad (6.2)$$

where $i = 1, 2, 3, \dots$ is the tier number and $N_0 = 3$ is the initial condition. The effects of the co-channel interfering cells in the second, third, and higher tiers are negligible because their interference contributions are much smaller (about 1% of the total interference) compared to the first tier [5, 27]. Thus, we can assume that the number of effective

interferers in equation (6.2) to be only six (6) and the SIR for a mobile user in a cellular network is given as

$$\gamma = P_0 / \sum_{i=1}^6 P_i \quad (6.3)$$

where P_0 is the desired signal power from the desired base station and P_i is the interference power from the i^{th} interfering co-channel cell base station. Hence, for a wireless link to meet the required quality of service (QOS), the received SIR in (6.3) has to exceed a preset threshold; otherwise, the link quality is unacceptable and the mobile user experiences outage.

6.2 Sensor Networks (Self-Organizing Networks)

Recently, there has been a great deal of interest in the field of wireless sensor networks (WSNs). This is no surprise due to WSNs' potential in various fields such as military surveillance systems, security, environment and traffic monitoring, disaster recovery, hazard and structural monitoring (structural stability, air quality and ventilation monitoring), inventory management in production environment, and health related applications [2, 12, 51].

WSNs have been made possible due to great advancements in electronics; thanks to very large scale integration (VLSI) and improved fabrication processes that have made manufacturing of very tiny, sensitive, cheap, and reliable sensor systems that can be used to create a network. Like ants, individually, each sensor node may not accomplish much; but working collectively, they have the potential to monitor large areas, and detect required events [9]. Wireless sensor networks are thus formed by tiny sensors/nodes that

can communicate with each other in a peer-to-peer fashion through a wireless link. We use sensor and node interchangeably. These sensors are decentralized, self-organizing and capable of collecting, storing, and processing information without depending on a pre-existing network infrastructure. There must be a link between the nodes for them to communicate with each other. To maintain full connectivity in the coverage area, there must be a link from one node to another, throughout the entire network [32, 34, 60].

Considerable research has been done in various areas such as developing a computationally fast and accurate methodology to evaluate the error, detection, and false alarm probabilities for networks of arbitrary sizes (small, medium, and large number of sensors) [9]. Since WSNs depend on wireless channel for communication, the networks experience such propagation effects as interference, path loss, multipath, and shadow fading. Similar to cellular networks, WSNs are driven by coverage and connectivity. For a sensor to be able to increase its communication range, it must increase its transmit power significantly. This power increase introduces interference within the network. Also, deploying many sensors within the coverage area introduces interference; but, fewer sensors will compromise the area's coverage by leaving portions of the area not covered. This is due to sensors having either overlapping communication ranges in the case of too many sensors or farther apart communication ranges for fewer sensors.

Sensors that are out of communication range of each other can still communicate with each other by if there are other sensors between them that can be used as relays to forward the information from the source to destination. An effective WSN will require optimal balance on the exact number of nodes required to cover the area. During the design and implementation phases of the WSN, appropriate models for interference,

capacity evaluation, performance degradation, and signal processing protocols have to be determined to alleviate impairments from propagation effects [16].

In WSNs such as military surveillance systems, the number of interferers, N is usually unknown and changes at each particular instant. This may be due to jamming, some sensors being dead, some sensors did not experience the phenomenon of interest, or some being out of range. No matter what the reason may be, the number of sensors N , is a random variable from a Poisson point process [43, 47, 51, 70]. We assume that the nodes remain static once deployed. The nodes transmit with fixed power P_{tx} and use omnidirectional antennas. All transmissions are exposed to either path-loss, multipath or shadow fading or a combination. We assume either Rayleigh or Nakagami fading environment and, thus, a desired transmission is successfully received if equation (5.1) is satisfied [64].

6.3 Cognitive Radio Networks

In recent years, there has been increased interest in cognitive radios due to the development of intelligent and adaptive wireless devices enhanced by the introduction of secondary spectrum licensing. The spectrum in wireless networks is regulated by a fixed assignment policy. Government agencies regulate and assign a portion of the spectrum to a license holder on a long term basis within a given geographical region. For example, in the United States of America, the Federal Communications Commission (FCC) has licensed most of the useful wireless communication frequency bands; which has led to search for other bands due to dramatic increase of mobile services accessing the limited spectrum. So, the industrial scientific and medical (ISM) or 2.4 and 5GHz bands are

regulated but unlicensed bands and mainly used for wireless computer networking. The popular Bluetooth and Wi-Fi technologies operate in these ISM bands [25] and with most gadgets using these technologies, the bands are usually congested and strained. Since the licensed and unlicensed spectrum bands are fully overcrowded, there has been ongoing research to avoid the looming spectrum crisis. However, recent spectral analysis shows that for almost 90% of the time, large portions of the licensed bands are unused and underutilized [22]. This has led the FCC to approve dynamic and secondary spectrum licensing to utilize the large portions of the unused spectrum. The unused and underutilized spectrum portions are known as white spaces or spectrum holes or fallow [22].

Cognitive radio networks (CRNs) are defined as wireless networks that consist of several types of users namely: a primary or incumbent user (PU) who is the license holder of a specific portion of the spectrum, and a secondary user (SU) or cognitive radio user (CRU) who uses spectrum holes in a resourceful way [22, 26]. In licensed bands, the PU has priority to access and use the allocated band or channel; while CRU can access the channel to search for potential spectrum holes. Research on CRNs is ongoing because CRNs have the potential to solve the spectrum overload problem. For example, Akan et al [6] discussed the use of cognitive radio opportunistic spectrum access ability in WSN's to eliminate collision and excessive contention delay that densely populated networks experience. Authors in [26], discussed how the openness of CRNs leads to various security issues and threats. Kusaladharma and Tellambura [40] investigated aggregate interference at the PU when SU are distributed in a finite ring.

The concept of CRNs is possible because the CRU's are designed with cognitive abilities to sense for PUs existence in their surroundings and adapt to the environment as needed to search for spectrum holes. Generally SUs' spectrum detection techniques can be classified as: i) primary transmitter detection where SUs detect a weak signal from the PU, ii) primary receiver detection where the SUs search within their communication range for all PUs that are receiving data, and iii) interference temperature management where the SUs' compare how many new interferences are received to the interference limit. It is assumed that upon sensing the existence of the PU, the SUs either remain silent or employ their cognitive abilities to dynamically adjust their operating parameters to detect an alternate route to minimize harm to the PUs. In Figure 22, the architecture and cognitive abilities that enable SUs to operate in the licensed and unlicensed bands are illustrated. When the PU is sensed in the current route, the SUs can search and hop to the best available alternate route as long as the link meets the performance criteria. Despite CRU's abilities, there are other factors such as multipath and shadow fading that will lead to poor reception of the PU's beacon. Poor beacon reception by the CRU leads to wrong parameter adjustment; which in turn, leads to multiple transmissions causing interference at the PU's end. Hence, aggregate interference modeling at the PU is essential to characterize degradation of performance quality. We consider interference in the context of CRUs transmissions interfering on a reception at the PU and the reverse is negligible because the CRUs are designed to operate under higher levels of interference from PUs.

In the network, the PU is located at the origin and the SUs are assumed to be randomly located according to a Poisson point process. The SUs are assumed to be uniformly distributed in a circular area with radius, \mathcal{R} that can extend to infinity. \mathcal{R} is

considered to be PU's communication range. Thus, the number of SUs in the circular region is assumed to follow a Poisson distribution with parameter that denotes the average number, λ of transmitting SUs per unit area [28, 73]. All SUs are assumed to be transmitting in the same frequency as the PU transmitter. Thus, the interfering

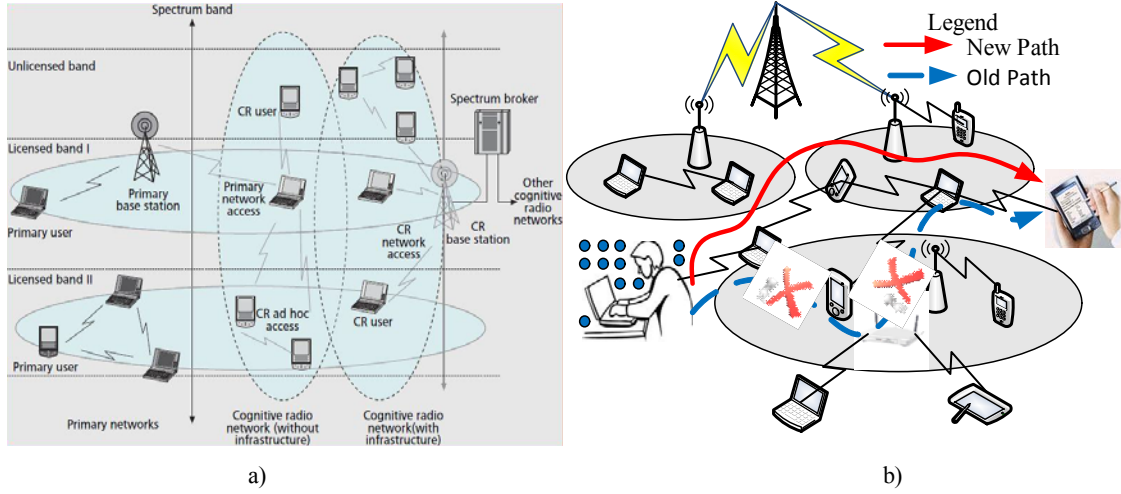


Figure 22: a) Illustration of cognitive radio network architecture [7], b) Use of cognitive abilities to detect the best available alternate route without harming PU.

transmissions from devices outside \mathcal{R} are assumed to be negligible. A certain minimum SINR ratio is required for a licensed device (PU) to successfully operate in the presence of multiple SUs. The SINR for a failed reception is expressed in (5.1).

6.4 VANET

Until recently, a driver in a vehicle was limited by his/her field of view about the surrounding. That is, a driver can only react to situations that are visible to him/her. Clearly, this has significantly played a part in the skyrocketing numbers of deaths caused by vehicle accidents in the United States (US). Considerable research is ongoing on how to reduce accident rate. One suggestion is to improve the field of view by implementing

communication between vehicles, thus the birth of Vehicular Ad Hoc networks (VANETs). VANETs are prospective technologies for intelligent transportation systems (ITS) that have the technological potential to reduce the alarming number of accidents by creating a network on the road with vehicles equipped with wireless communication devices.

VANET aims at providing safety and comfort applications through dedicated short-range communication (DSRC) that includes vehicle-to-vehicle (V2V) or vehicle-to-infrastructure (V2I) communication. V2V enables communication between vehicles without infrastructure and V2I enables communication of vehicles with existing infrastructure. Safety applications may include collision avoidance, safe merge assistance, emergency vehicles approaching, and hazardous warning; comfort applications may include congestion avoidance, internet access, and entertainment. Safety applications are motivated by improving driving safety and can be grouped in either periodic or event-driven messages. Periodic messages are generated occasionally to inform surrounding vehicles about the vehicle's current status such as speed, acceleration, position, and direction; while event-driven messages are emergency messages that are critical and of high priority. These messages are sent to inform drivers of detected unsafe situations. Safety messages are vital to all vehicles surrounding the sender and if not well controlled; their broadcasts may grow exponentially leading to a broadcast storm. This can happen when all surrounding vehicles rebroadcast the received message and the vehicles that receiver the rebroadcast also rebroadcast and so on. This kind of scenario leads to channel congestion, packet collisions, and packet loss. The

concept of VANETs is built around the fact that vehicles have the ability to exchange information with each other and/or the road-side equipment.

Research is ongoing in this field even though some progress has been made. For example, the investigation in [59] determined that the messages suffered a degradation of 50% to 70% due to interference and further, that degradation was experienced when the messages also suffered shadow fading. Similarly, Lee and Lim [41] showed that interference due to multi-hop routing and broadcasting reduced throughput and increased packet loss rate. It was observed that the probability of reception decreased in the presence of Nakagami fading and in saturation conditions, the probability of reception of broadcast messages was as low as 20% - 30% at distances of 100m or greater from the sender [68]. In [71], a cooperative retransmission algorithm was proposed that overcomes shadow fading caused by blocking objects such as heavy vehicles and interference caused by retransmissions.

We are motivated by the fact that the desired broadcasted message will not only have to compete with interfering messages from other vehicles but will suffer from path-loss, multipath, and shadow fading. Figure 23 shows how multipath and shadow fading impact the transmission range of a vehicle. In an idealistic VANET system, vehicles within the circular disk are assumed to receive the message; but in the presence of fading, the shaded areas between the dashed and solid lines is out of range while the clear areas between the solid and dashed lines are within the communication range of vehicle 1. All vehicles have the same communication range and transmit with the same power P_{tx} . Vehicle mobility is neglected since it remains almost stationary within a message transmission time [38]. Assume that a spectator standing at a random point on a road is

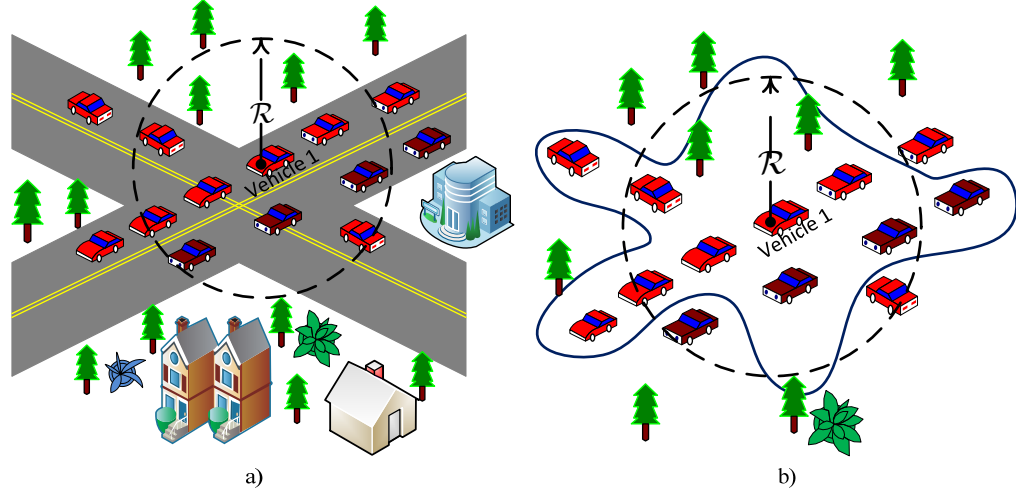


Figure 23: a) VANET ideal communication range scenario shown by the black dotted line, b) VANET realistic communication range scenario shown by the solid blue line.

able to count the number of vehicles passing by; the number of vehicles passing him/her per unit time, say one hour, follows a Poisson distribution with a certain intensity. Thus we assume that the vehicles are dispersed in the highway/road according to a Poisson process with a parameter of λ nodes per area \mathcal{A} . The vehicles' locations on the highway/road are uniformly distributed and the number of interfering vehicles, N is we assume that the vehicles are dispersed in the highway/road according to a Poisson process with a parameter of λ nodes per area \mathcal{A} . The vehicles' locations on the highway/road are uniformly distributed and the number of interfering vehicles, N is random. So, a vehicle located at distance r from a transmitting vehicle is unable to successfully receive the sent message if equation (5.1) is satisfied.

CHAPTER 7

ANALYTICAL AND COMPUTER SIMULATION RESULTS

7.1 Computer Simulation

In this chapter, we conduct extensive computer simulations to validate the analytical results developed in chapters 5 and 6. In the simulation, we consider a topology with N wireless sensors placed deterministically on a square region of area, $\mathcal{A} = 100 \text{ m} \times 100 \text{ m}$. To validate our mathematical analysis, we performed simulations in MATLAB environment. The system parameters are selected as follows: $A = P_{tx} = 1$, $\eta = 3.5$, $W = 0.01 \text{mWatt}$, $m_0 = 3$, and $m_z = 2$. The parameters such as N, λ, Λ, w , and β are selected or varied suitably. Simulations are performed using the same system parameters. For random networks, we choose a random number of sensors according to a two dimensional Poisson point process that are placed over the simulation area according to a uniform distribution. The links between the sensors are tested to check for outage links. The process is repeated many times and the outage probability is computed as an average of 1500 simulation runs.

7.2 Numerical Analysis

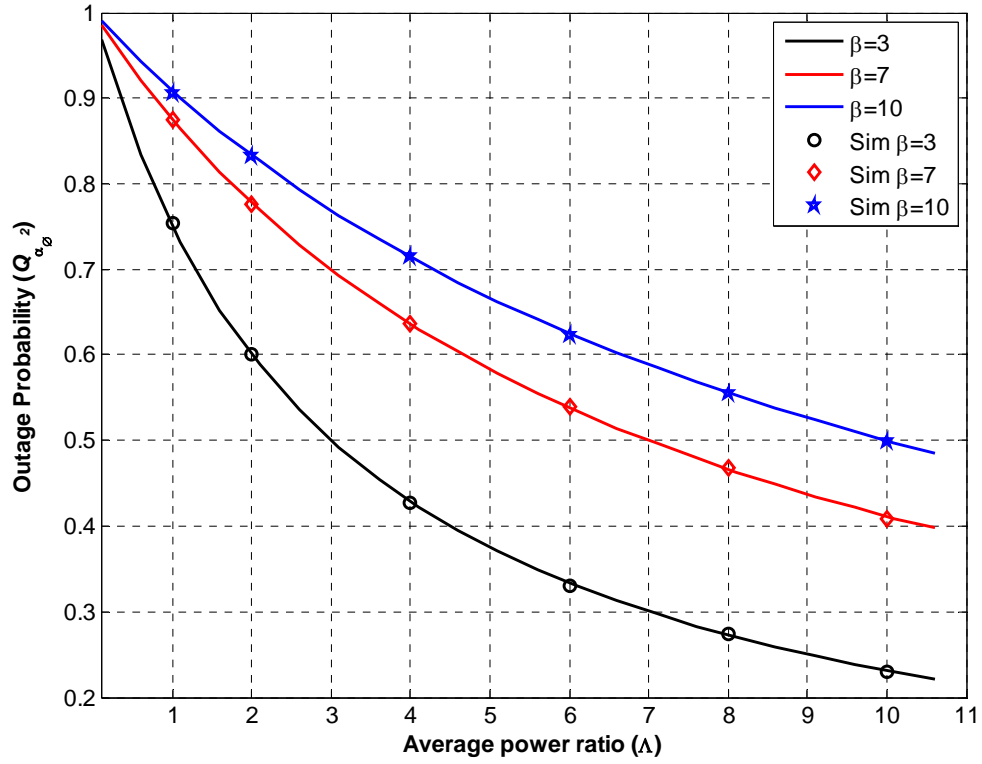


Figure 24: Plot of outage probability in (5.5) when only one interferer is present and $\eta = 3.5$ in a Rayleigh fading channel.

In Figures 24-31, we plot outage probability verses the average power ratio for different propagation environments. In Figure 24, we vary the threshold values when there is one dominant interferer in a Rayleigh fading channel. When the average power, $\Lambda = 10$, the outage probability is 0.23 for a threshold $\beta = 3$ and 0.50 for a threshold $\beta = 10$. Computer simulations were performed and are in agreement with the analytical results.

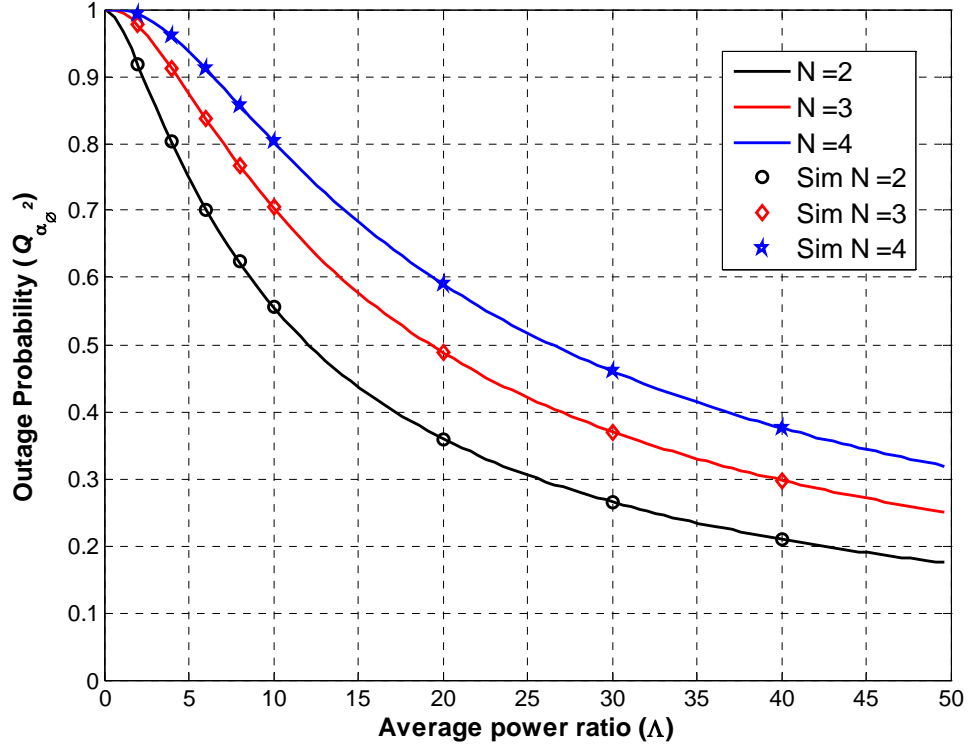


Figure 25: Plot of outage probability in (5.5) while varying the number of interferers, N when $\beta = 5$ and $\eta = 3.5$ in a Rayleigh fading channel.

In Figure 25, we plot the outage probability against the average power ratio while varying the number of interferers, N in a Rayleigh fading channel. When the average power, $\Lambda = 40$, the outage probability is 0.20 for $N = 2$ and 0.38 for $N = 4$. Observe that the simulation and the analysis agree.

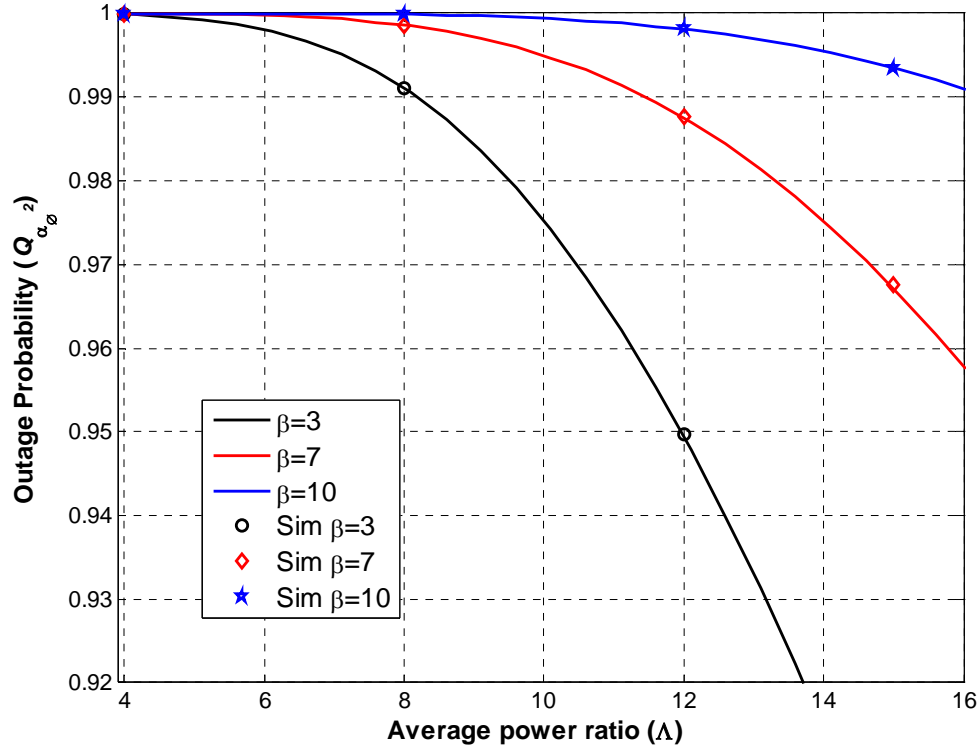


Figure 26: Plot of outage probability (5.7) against the average power ratio while varying the threshold when $N = 6$, $\eta = 3.5$, $m_0 = 3$, and $m_z = 2$.

In Figure 26, we vary the threshold values when there are six (6) interferers in a Nakagami fading channel. When the average power, $\Lambda = 12$, the outage probability is 0.95 for a threshold $\beta = 3$ and 0.998 for a threshold $\beta = 10$. Computer simulations were performed and are in agreement with the analytical results.

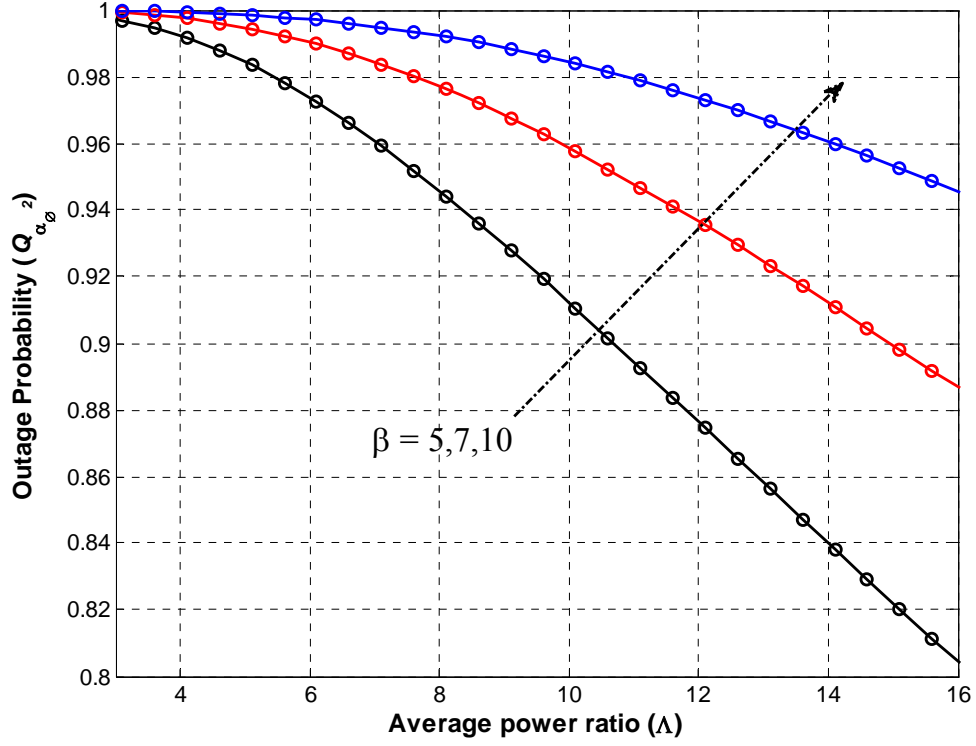


Figure 27: Comparing the PDF (5.5) and MGF (5.10) approach analysis results when $N = 6$ and $\eta = 3.5$ in a Rayleigh fading channel.

In Figures 27 and 28, we compare the results obtained by the two methods, that is to say the PDF and MGF approaches. The solid lines are for equation the PDF approach for (5.5) and the circles are for the MGF approach for (5.10) when $N = 6$ and the threshold β is varied in a Rayleigh fading channel. Observe that the results obtained for the two approaches agree.

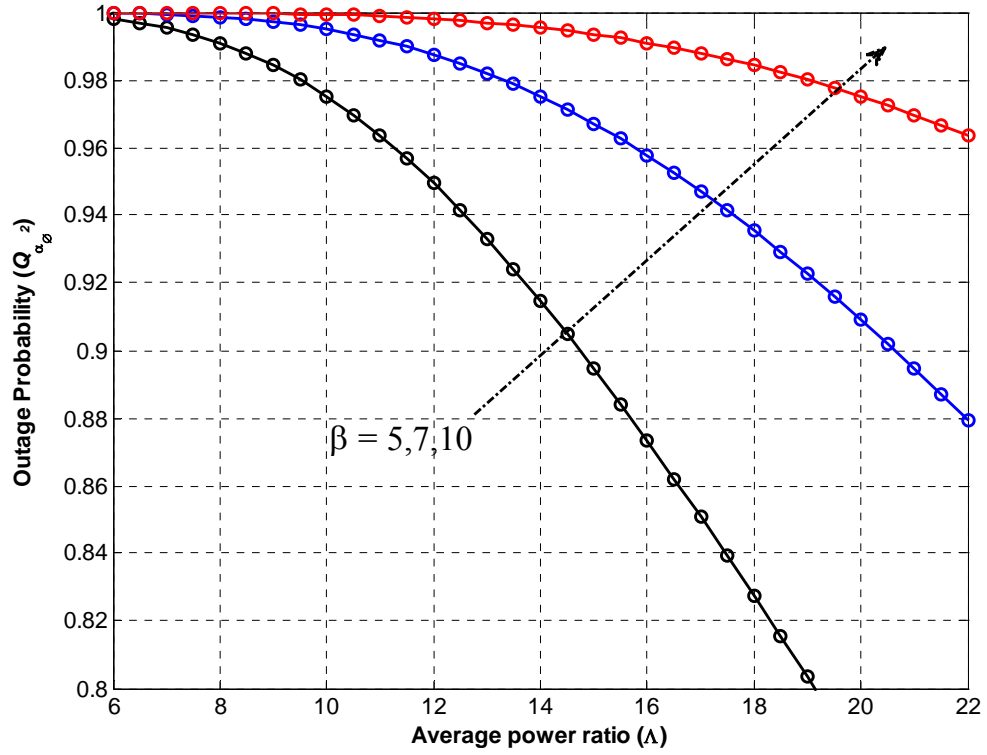


Figure 28: Comparing the results obtained by PDF (5.7) and MGF (5.16) approach analysis when $N = 6$, $\eta = 3.5$, $m_0 = 3$, and $m_z = 2$.

In Figure 28, the solid lines are for equation the PDF approach for (5.7) and the circles are for the MGF approach for (5.16) when $N = 6$ and threshold β is varied in a Nakagami fading channel. Observe that the two approaches are in agreement.

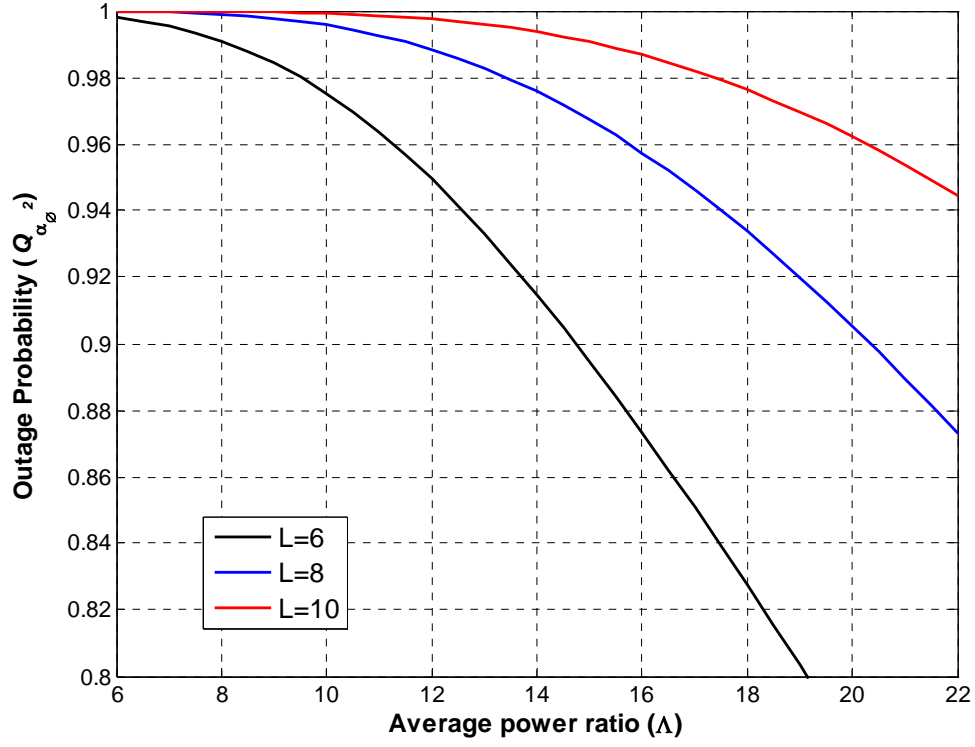


Figure 29: Illustration of the impact of interference on outage probability given in (5.16) for $\beta = 5$, $\eta = 3.5$, $m_0 = 3$, and $m_z = 2$. and N is varied accordingly.

In Figure 29, we plot the outage probability against the average power ratio while varying the number of interferers, N in a Nakagami fading channel. When the average power, $\Lambda = 16$, the outage probability is 0.87 for $N = 6$ and 0.99 for $N = 10$.

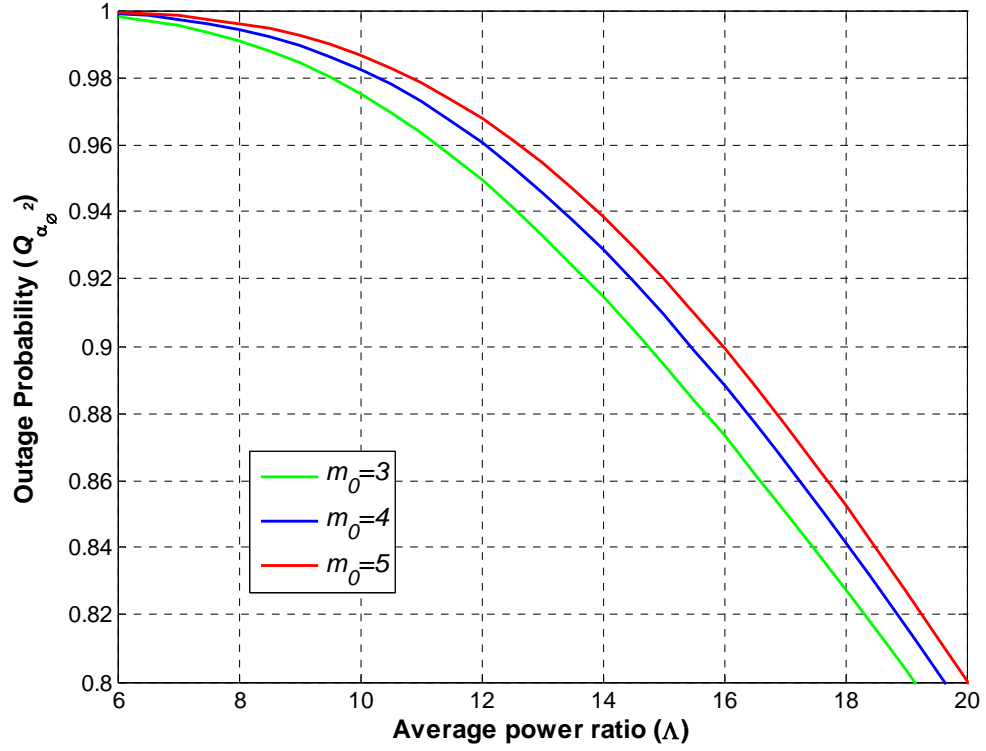


Figure 30: The outage probability; a comparison of the fading parameter when $N = 6$, $\eta = 3.5$, $\beta = 5$, and $m_z = 2$.

In Figure 30, we vary the fading parameter for the desired signal. When the average power, $\Lambda = 16$, the outage probability is 0.87 for $m_0 = 3$ and 0.9 for $m_0 = 5$. Observe that the Nakagami fading parameter has minimal impact on the outage probability.

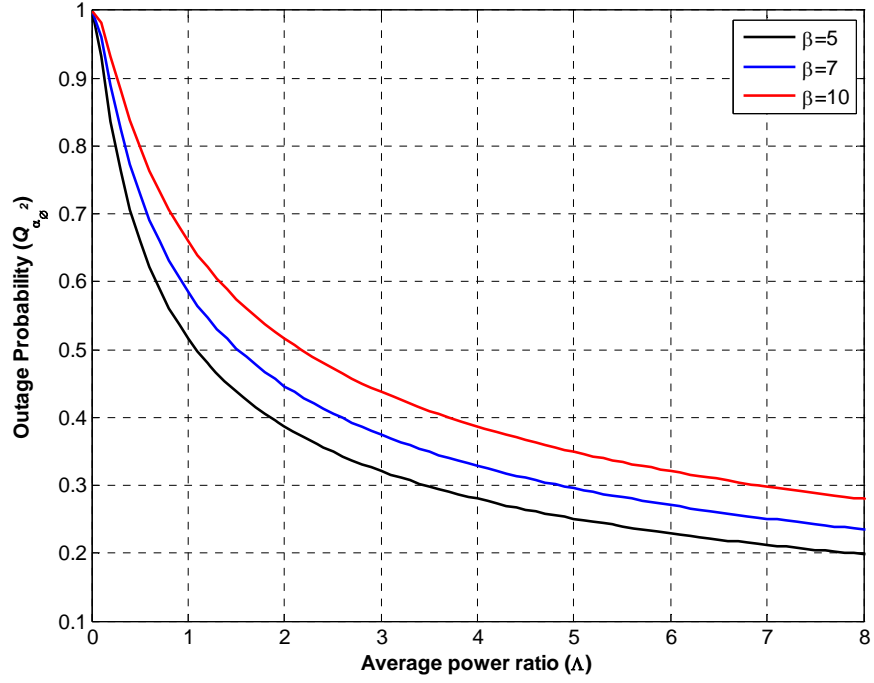


Figure 31: Illustration of the impact of interference on outage probability in a Rayleigh fading (5.28) when $\lambda = .05$ and β is varied accordingly.

In Figure 31, we consider the impact of threshold, β , in a Rayleigh fading channel when the number of interferers is random and follows a Poisson distribution with intensity $\lambda = .05$. When the average power, $\Lambda = 7$, the outage probability is 0.21 for $\beta = 5$ and 0.3 for $\beta = 10$.

CHAPTER 8

SUMMARY AND CONCLUSION

8.1 Summary of Main Results

In this chapter, a summary of the results from the analysis with regards to the impact of interference on device isolation probability and outage probability are presented. The scope of such analysis, motivation and objectives were elucidated in Chapter 1. In Chapter 2, we discussed the system models that included the propagation and channel models. Fading models and practical environments in which each model is useful in quantifying the statistical behavior of the received signal are discussed. In Chapter 3, the interference models and the importance of performance measures used in wireless communication, especially outage probability and device isolation probability were considered. In Chapter 4, we derived in closed-form expression the isolation probability for noise-limited systems and interference and noise-limited systems operating in either Rayleigh or Nakagami fading with lognormal shadow fading. Secondly, we derived expressions for systems with fixed number of interferers and random number of interferers using geometric mean and shifted gamma approximations respectively. The geometric mean approximation presented upper bounds the communication range. In Chapter 5, we present the network performance analysis using outage probability for

both fixed number and random number of interferers. We derived closed-form expressions for outage probability using a PDF-based approach and MGF-based approach in a Rayleigh or Nakagami fading environments. In Chapter 6, we explored a few applications and systems that may benefit from the analysis discussed in this thesis. Computer simulations were developed and performed in a MATLAB based environment to validate our analytical results. The results presented show that the analytical results obtained are in good agreement with the simulations. The parameters used reflect a realistic wireless network deployment scenario. We can deduce that an increase in the number of devices and communication range improves connectivity by comparing the two graphs in Figure 8. However, there still some devices that are isolated in both cases, mainly, those close to the borders are more likely to be isolated due to the fact that the disk area will be smaller compared to those in the center of the network. In (4.8), the effects of multipath and shadow fading, and path-loss are clearly observable and decoupled and in (4.45), it is evident that log-normal shadowing positively impacts the isolation probability that is there is a gain realized.

In Figure 29, we observe that a device is more likely to experience outage as the number of interferers present increases; which is expected in practical application. We also observe that the results obtained by either the PDF approach or MGF approach are in good agreement.

8.2 Conclusion

The main contributions from this thesis are highlighted here as follows:

- 1) Investigated how channel impairments affect communication in various application using device isolation probability and outage probability.
- 2) Developed a unified mathematical model which incorporates the main factors i.e. channel fading, number of interferers, and transmitter-receiver distances that impact successful receptions at receiver end.
- 3) Derived in closed-form numerical expressions for isolation probability in noise-limited systems and interference and noise-limited systems operating in either Rayleigh or Nakagami fading with lognormal shadow fading. These derived closed-form approximations are useful for evaluating the overall network connectivity and fidelity in a wireless channel with co-channel interference. Simulation results have been presented, which show the soundness of the proposed techniques.
- 4) Derived isolation probability expressions for systems with fixed number of interferers and random number of interferers using geometric mean and shifted gamma approximations respectively.
- 5) Explored also is the outage probability where closed-form expressions were derived using PDF-based approach and MGF-based approach in a Rayleigh or Nakagami fading environments. Aggregate interference was considered to be either gamma distributed or alpha-stable distributed. The special cases that were considered confirmed the correctness of the analysis.

8.3 Suggestions for Future Work

We plan to extend the outage probability analysis to networks where the path-loss exponent is random. We also plan to extend the path-loss model to address the peculiar behavior when $r < 1$. We plan to generalize the results to more general device placement distributions and investigate the impact of device mobility on connectivity.

APPENDIX A

Derivation of (4.37) and (4.44)

$$\mathbb{E}[\mathcal{R}^2] = \left(\frac{1}{\beta}\right)^{2/\eta} \mathbb{E}\left[\sum_{i=1}^N \left\{ \frac{1}{(\alpha_0^2/\alpha_i^2)(u_0/u_i)} r_i^{-\eta} \right\}\right]^{-2/\eta} \quad (\text{A.1})$$

Let $\Phi^{-1} = (\alpha_0^2/\alpha_i^2)(u_0/u_i)$ account for fading, then we obtain (4.33). Observe that $\Phi = 1$ for (4.37). Since $N \sim \text{Poisson}(\lambda)$, then compound Poisson sum is approximated using a

shifted gamma function. Let $Z = \sum_{i=1}^N \frac{1}{\Phi} r_i^{-\eta}$, then $Z = k + S$; where $k \in \mathbb{R}$ and

$S \sim \Gamma(\varphi, \theta)$. It follows that Z has a sifted gamma distribution given in (4.34) and

$$\varphi = \frac{4\lambda\mu_2^3}{\mu_3^2}, \quad \theta = \frac{2\mu_2}{\mu_3}, \quad k = \lambda \left(\mu_1 - \frac{2\mu_2^2}{\mu_3} \right) \quad (\text{A.2})$$

To compute the means, we let $\mathcal{G} = \Phi^{-1} r^{-\eta}$; where Φ is a constant; thus

$\mu_b = \mathbb{E}\left\{\left[(1/\Phi)r^{-\eta}\right]^b\right\}$ where $b \in \mathbb{R}$. The PDF of $\xi = r^{-\eta}$ is given as

$$p_{\xi}(\xi) = \frac{2}{\eta C^2} \xi^{-(2/\eta+1)}; \quad 0 < \xi \leq C^{-\eta} \quad (\text{A.3})$$

Thus, $\mu_b = \frac{2(1/\Phi)^b}{\eta C^2} \int_0^{C^{-\eta}} \xi^{b-(2/\eta+1)} d\xi = \frac{2(1/\Phi)^b}{\eta C^2} \left[\frac{\xi^{b-(2/\eta)}}{(b-2/\eta)} \right]_0^{C^{-\eta}} = \frac{2(1/\Phi)^b C^{-\eta b}}{(\eta b - 2)}$ where $b \in \mathbb{R}$. It

follows that the first, second, and third moments are obtained as

$$\mu_1 = \frac{2C^{-\eta}}{\Phi(\eta-2)}; \quad \mu_2 = \frac{C^{-2\eta}}{\Phi^2(\eta-1)}; \quad \mu_3 = \frac{2C^{-3\eta}}{\Phi^3(3\eta-2)} \quad (\text{A.4})$$

Substituting (A.4) into (A.2), we obtain the results in (4.40). Then we find the expectation using (4.34) yielding

$$\mathbb{E}_{\Phi, N, r} \{Z^{-\nu} \mid N, r\} = \mathbb{E}_{\Phi} \left[\int_k^{\infty} z^{-\nu} \frac{(z-k)^{\varphi-1}}{\theta^{\varphi} \Gamma(\varphi)} \exp\left(-\frac{(z-k)}{\theta}\right) dz \right]$$

where $\nu \in \mathbb{R}$. The integral can be computed by first changing variable; that is let $\zeta = z - k$. Then, we have

$$\mathbb{E}_{\Phi, N, r} \{Z^{-\nu} \mid N, r\} = \mathbb{E}_{\Phi} \left[\frac{1}{\theta^{\varphi} \Gamma(\varphi)} \int_0^{\infty} \zeta^{\varphi-1} (\zeta + k)^{-\nu} \exp\left(-\frac{\zeta}{\theta}\right) d\zeta \right]$$

We perform another change of variable to $t = \zeta/k$, which yields

$$\mathbb{E}_{\Phi, N, r} \{Z^{-\nu} \mid N, r\} = \mathbb{E}_{\Phi} \left[\frac{k^{\varphi}}{\theta^{\varphi} \Gamma(\varphi) k^{\nu}} \int_0^{\infty} t^{\varphi-1} (t+1)^{-\nu} \exp\left(-\frac{kt}{\theta}\right) dt \right]$$

Using [4, eq.(13.2.5)], we have

$$\mathbb{E}_{\Phi, N, r} \{Z^{-\nu} \mid N, r\} = \mathbb{E}_{\Phi} \left[\frac{1}{\theta^{\varphi} \Gamma(\varphi) k^{\nu}} k^{\varphi} \Gamma(\varphi) \mathbf{U}\left(\varphi, \varphi+1-\nu, \frac{k}{\theta}\right) \right]$$

The above equation can be rearranged to obtain

$$\mathbb{E}_{\Phi, N, r} \{Z^{-\nu} \mid N, r\} = \mathbb{E}_{\Phi} \left[k^{-\nu} \left(\frac{k}{\theta}\right)^{\varphi} \mathbf{U}\left(\varphi, \varphi+1-\nu, \frac{k}{\theta}\right) \right] \quad (\text{A.5})$$

Observe the Φ appears in k and θ only, thus, we have

$$\mathbb{E}_{\Phi} \left[k^{-\nu} \left(\frac{k}{\theta} \right)^{\varphi} \mathbf{U} \left(\varphi, \varphi+1-\nu, \frac{k}{\theta} \right) \right] = \mathbb{E}_{\Phi} \left[\Phi^{-\nu} \psi^{\varphi} \mathbf{U} (\varphi, \varphi+1-\nu, \psi) \right] \quad (\text{A.6})$$

where $\psi = \lambda \left(\frac{2(3\eta-2)}{(\eta-2)(\eta-1)} - \frac{(3\eta-2)^2}{(\eta-1)^3} \right)$, which results in (4.42). But

$$\Phi^{-1} = (\alpha_0^2 / \alpha^2) (u_0 / u), \text{ thus we have } \mathbb{E}_{\Phi} [\Phi^{-\nu}] = \mathbb{E} \left[(\alpha_0^2 / \alpha^2)^{\nu} \right] \mathbb{E} \left[(u_0 / u)^{\nu} \right].$$

To perform the first expectation, we use the PDF for the ratio given in (9.7) to obtain

$$\mathbb{E} \left[(\alpha_0^2 / \alpha^2)^{\nu} \right] = \frac{\Gamma(m_0 + m)}{\Gamma(m_0) \Gamma(m)} \left(\frac{m_0}{\Lambda m} \right)^{m_0} \int_0^{\infty} \zeta^{\nu+m_0-1} \left(1 + \frac{m_0}{\Lambda m} \zeta \right)^{-(m_0+m)} d\zeta$$

Thus using [30, eq.(3.194.3,8.384.1)], we obtain the result in (4.41) when $\nu = 2/\eta$.

To perform the second expectation, we use the log-normal PDF given in (2.10) with zero mean yielding

$$\mathbb{E} \left[(u_0 / u)^{\nu} \right] = \frac{1}{\sqrt{2\pi}} \int_0^{\infty} \zeta^{\nu} \exp \left(-\frac{[\ln \zeta / \sigma_R]^2}{2} \right) d\zeta \text{ where } \sigma_R^2 = \sigma_0^2 + \sigma^2$$

Performing a change of variable and using [30, eq.(3.323.2.10)], we have the result

presented in (4.31) where $\nu = 2/\eta$. Substituting (4.31) and (4.30) into (A.6) and the result

of (A.6) into (A.5). The outcome is substituted into (A.1) yields the result given in (4.44).

To obtain (4.37), just substitute the fading parameter $\Phi = 1$ in (A.6).

Derivation of (5.16).

Using equation (5.14) and (5.15), the derivative can be expressed and simplified as below

$$\begin{aligned}
 \mathcal{D}_s^{m_0} \mathbb{M}_Z \left[\left(t + \frac{m_0 \beta}{\bar{\gamma}_0} \right)_s \right] \Big|_{s=1} &= \mathcal{D}_s^{m_0} \left(1 + \frac{\bar{\gamma}_z (t + m_0 \beta / \bar{\gamma}_0) s}{m_z} \right)^{-Nm_z} \Big|_{s=1} \\
 \mathcal{D}_s^{m_0} \mathbb{M}_Z \left[\left(t + \frac{m_0 \beta}{\bar{\gamma}_0} \right)_s \right] \Big|_{s=1} &= (-1)^{m_0} (Nm_z)_{m_0} \left(\frac{m_z}{\bar{\gamma}_z (t + m_0 \beta / \bar{\gamma}_0)} \right)^{-m_0} \\
 &\quad \times \left(1 + \frac{\bar{\gamma}_z (t + m_0 \beta / \bar{\gamma}_0)}{m_z} \right)^{-Nm_z - m_0}
 \end{aligned} \tag{A.8}$$

where $(a)_n = \frac{\Gamma(a+n)}{\Gamma(a)}$ is the Pochhammer symbol and $(a)_{-k} = \frac{(-1)^k}{(1-a)_k}$ were used.

Substituting (A.8) into (5.14), we have

$$\mathcal{Q}_{\alpha_0^2} = 1 - \frac{(Nm_z)_{m_0}}{\Gamma(m_0)} \left(\frac{\bar{\gamma}_z}{m_z} \right)^{m_0} \int_0^\infty \left(t + \frac{m_0 \beta}{\bar{\gamma}_0} \right)^{m_0-1} \left(1 + \frac{\bar{\gamma}_z}{m_z} \left(t + \frac{m_0 \beta}{\bar{\gamma}_0} \right) \right)^{-Nm_z - m_0} dt \tag{A.9}$$

Making the change of variable $\zeta = \left(t + \frac{m_0 \beta}{\bar{\gamma}_0} \right)$, the integral in (A.9) becomes

$$\mathcal{Q}_{\alpha_0^2} = 1 - \frac{(Nm_z)_{m_0}}{\Gamma(m_0)} \left(\frac{\bar{\gamma}_z}{m_z} \right)^{m_0} \int_{m_0 \beta / \bar{\gamma}_0}^\infty \zeta^{m_0-1} \left(1 + \frac{\bar{\gamma}_z}{m_z} \zeta \right)^{-Nm_z - m_0} d\zeta \tag{A.10}$$

With the help of [30, eq.(3.194.2.6)], the integral in (A.10) is performed to yield the result in (5.16).

Derivation of (5.20)

To simplify (5.18), we use the following moment generating function (MGF) identities.

$$\mathbb{M}_Z(-s) = \left(1 + \frac{\bar{\gamma}_z s}{m_z}\right)^{-Nm_z} = \left(\frac{\bar{\gamma}_z}{m_z}\right)^{-Nm_z} \left(\frac{m_z}{\bar{\gamma}_z} + s\right)^{-Nm_z}; \mathbb{M}_Z(-(s+a)) = e^{-as} \mathbb{M}_Z(-s);$$

$$\mathbb{M}_{aZ}(-s) = \mathbb{M}_Z(-as)$$

so that the differentiation term becomes

$$\begin{aligned} \mathcal{D}_s^{m_0} \mathbb{M}_{\frac{m_0 \beta y (D+Z)}{\bar{\gamma}_0}}(-s) &= \mathcal{D}_s^{m_0} \left\{ \exp\left(-\frac{m_0 \beta y D}{\bar{\gamma}_0} s\right) \mathbb{M}_Z\left(-\frac{m_0 \beta y}{\bar{\gamma}_0} s\right) \right\} \\ &= (-1)^{m_0} \left(\frac{m_0 \beta y D}{\bar{\gamma}_0}\right)^{m_0} \left(\frac{m_0 \beta y}{\Lambda m_z}\right)^{-Nm_z} \exp\left(-\frac{m_0 \beta y D}{\bar{\gamma}_0} s\right) \\ &\quad \times \sum_{k=0}^{\infty} \binom{m_0}{k} \left(-\frac{m_0 \beta y D}{\bar{\gamma}_0} s\right)^{-k} \mathcal{D}_s^k \left\{ \left(s + \frac{\Lambda m_z}{m_0 \beta y}\right)^{-Nm_z} \right\} \end{aligned} \quad (\text{A.11})$$

where $\Lambda = \bar{\gamma}_0 / \bar{\gamma}_z$. Considering the last term in (A.11), we have

$$\begin{aligned} \mathcal{D}_s^k \left\{ \left(s + \frac{\Lambda m_z}{m_0 \beta y}\right)^{-Nm_z} \right\} &= (-1)^k (-Nm_z)_k \left(s + \frac{\Lambda m_z}{m_0 \beta y}\right)^{-Nm_z-k} \\ &= (-1)^k (-Nm_z)_k \left(\frac{\Lambda m_z}{m_0 \beta y}\right)^{-Nm_z-k} \left(1 + \frac{m_0 \beta y}{\Lambda m_z} s\right)^{-Nm_z-k} \end{aligned} \quad (\text{A.12})$$

where $(a)_{-k} = \frac{(-1)^k}{(1-a)_k}$ was used. Thus, substituting (A.12) into (A.11); we have

$$\begin{aligned}
\mathcal{D}_s^{m_0} \mathbb{M}_{\frac{m_0 \beta y (D+Z)}{\bar{\gamma}_0}}(s) \Big|_{s=1} &= (-1)^{m_0} \left(\frac{m_0 \beta y D}{\bar{\gamma}_0} \right)^{m_0} \exp \left(-\frac{m_0 \beta y D}{\bar{\gamma}_0} \right) \sum_{k=0}^{\infty} \frac{(-m_0)_k (-Nm_z)_k}{k!} \\
&\quad \times \left(-\frac{m_z D}{\bar{\gamma}_z} \right)^{-k} \left(1 + \frac{m_0 \beta y}{\Lambda m_z} \right)^{-Nm_z - k} \\
&= (-1)^{m_0} \left(\frac{m_0 \beta y D}{\bar{\gamma}_0} \right)^{m_0} \left(\frac{m_0 \beta y}{\Lambda m_z} \right)^{-Nm_z} \exp \left(-\frac{m_0 \beta y D s}{\bar{\gamma}_0} \right) \sum_{k=0}^{\infty} \binom{m_0}{k} \\
&\quad \times \left(-\frac{m_0 \beta y D}{\bar{\gamma}_0} s \right)^{-k} (-1)^k (-Nm_z)_k \left(\frac{\Lambda m_z}{m_0 \beta y} \right)^{-Nm_z - k} \left(1 + \frac{m_0 \beta y}{\Lambda m_z} s \right)^{-Nm_z - k}
\end{aligned} \tag{A.13}$$

where $\binom{m_0}{k} = \frac{\Gamma(m_0 + 1)}{k! \Gamma(m_0 + 1 - k)} = \frac{(-m_0)_k}{(-1)^k k!}$ was used. Inserting (A.13) into (5.18), we obtain

the outage probability as

$$\begin{aligned}
\mathcal{Q}_{\alpha_0^2} &= \frac{1}{\Gamma(m_0)} \left(\frac{m_0 \beta D}{\bar{\gamma}_0} \right)^{m_0} \int_0^1 y^{m_0-1} \exp \left(-\frac{m_0 \beta y D}{\bar{\gamma}_0} \right) \left(1 + \frac{m_0 \beta y}{\Lambda m_z} \right)^{-Nm_z} \\
&\quad \times {}_2F_0 \left(Nm_z, -m_0; -; -\bar{\gamma}_z / m_z D \left(1 + \frac{m_0 \beta y}{\Lambda m_z} \right) \right) dy
\end{aligned} \tag{A.14}$$

But by using [4, eq.(13.1.10)], (A.14) can be expressed as (5.20).

Derivation of (5.30)

The exponential function in (5.29) can be expressed as contour integral as below

$$\exp \left(-\Theta \left(t + \frac{m_0 \beta}{\bar{\gamma}_0} \right)^{2/\eta} s^{2/\eta} \right) = \frac{1}{2\pi j} \int_{\varsigma-j\infty}^{\varsigma+j\infty} \Gamma(\nu) \left(\Theta \left(t + \frac{m_0 \beta}{\bar{\gamma}_0} \right)^{2/\eta} s^{2/\eta} \right)^{-\nu} d\nu \tag{A.15}$$

Substituting (A.15) into (5.29), we have

$$\begin{aligned}
\mathcal{D}_s^{m_0} \left\{ \exp \left(-\Theta \left(t + \frac{m_0 \beta}{\bar{\gamma}_0} \right)^{2/\eta} s^{2/\eta} \right) \right\} \Big|_{s=1} &= \frac{1}{2\pi j} \int_{\varsigma-j\infty}^{\varsigma+j\infty} \left[\Theta \left(t + \frac{m_0 \beta}{\bar{\gamma}_0} \right)^{2/\eta} \right]^{-\nu} \\
&\quad \times \frac{\Gamma(\nu) \Gamma(1-2\nu/\eta)}{\Gamma(1-2\nu/\eta - m_0)} s^{-2\nu/\eta - m_0} d\nu \Big|_{s=1}
\end{aligned} \tag{A.16}$$

Using $\frac{\Gamma(1-a)}{\Gamma(1-a-n)} = (-1)^n \frac{\Gamma(a+n)}{\Gamma(a)}$, the above equation can be simplified and evaluated

to yield

$$\mathcal{D}_s^{m_0} \left\{ \exp \left(-\Theta \left(t + \frac{m_0 \beta}{\bar{\gamma}_0} \right)^{2/\eta} s^{2/\eta} \right) \right\} \Big|_{s=1} = (-1)^{m_0} \times H_{1,2}^{1,1} \left(\Theta \left(t + \frac{m_0 \beta}{\bar{\gamma}_0} \right)^{2/\eta} \middle| \begin{matrix} (0, 2/\eta) \\ (0, 1), (m_0, 2/\eta) \end{matrix} \right) \quad (\text{A.17})$$

Substituting (A.17) in (5.14), making a change of variable $\zeta = t + \frac{m_0 \beta}{\bar{\gamma}_0}$, and using [46,

eq.(2.54)], we have the outage probability as

$$Q_{SIR} = 1 - \frac{1}{\Gamma(m_0)} \left(\frac{m_0 \beta}{\bar{\gamma}_0} \right)^{m_0} H_{2,3}^{2,1} \left(\left(\frac{m_0 \beta}{\bar{\gamma}_0} \right)^{2/\eta} \middle| \begin{matrix} (0, 2/\eta), (1-m_0, 2/\eta) \\ (-m_0, 2/\eta), (0, 1), (m_0, 2/\eta) \end{matrix} \right) \quad (\text{A.18})$$

where $H_{p,q}^{k,l}(\cdot)$ is Fox's H -function defined in (B.1). For the special case of

$\eta = 2n$; $n \in \mathbb{N}^+$ and using [46, eq.(1.59)], equation (A.18) becomes

$$Q_{SIR} = 1 - \frac{1}{\Gamma(m_0)} \left(\frac{m_0 \beta}{\bar{\gamma}_0} \right)^{m_0} n H_{2,3}^{2,1} \left((\Theta')^n \left(\frac{m_0 \beta}{\bar{\gamma}_0} \right) \middle| \begin{matrix} (0, 1), (1-m_0, 1) \\ (-m_0, 1), (0, n), (m_0, 1) \end{matrix} \right) \quad (\text{A.19})$$

where $\Theta' = \pi \lambda \alpha \mathbb{E}_k [A^{1/n}] \Gamma(1-1/n)$. Then, using (B.1) and [30, eq.(8.335.7)]; the Fox's

H -function term in equation (A.19) can be expressed as

$$n H_{2,3}^{2,1} \left((\Theta')^n \left(\frac{m_0 \beta}{\bar{\gamma}_0} \right) \middle| \begin{matrix} (0, 1), (1-m_0, 1) \\ (-m_0, 1), (0, n), (m_0, 1) \end{matrix} \right) = \frac{\left(n (2\pi)^{(1-n)} \right)^{\frac{1}{2}}}{2\pi j} \times \oint_{\zeta} \frac{\Gamma(\nu - m_0) \prod_{k=0}^{n-1} \Gamma(\nu + k/n) \Gamma(1-\nu)}{\Gamma(1-m_0+\nu) \Gamma(1-m_0-\nu)} \left((\Theta'/n)^n \left(\frac{m_0 \beta}{\bar{\gamma}_0} \right) \right)^{-\nu} d\nu \quad (\text{A.20})$$

Then, we use the definition of the Meijer's G -function (B.2) to simplify (A.20) as

$$\begin{aligned}
 nH_{2,3}^{2,1} \left(\left(\Theta' \right)^n \left(\frac{m_0 \beta}{\bar{\gamma}_0} \right) \middle| \begin{matrix} (0,1), (1-m_0,1) \\ (-m_0,1), (0,n), (m_0,1) \end{matrix} \right) &= \sqrt{n(2\pi)^{(1-n)}} \\
 \times G_{2,n+2}^{n+1,1} \left(\left(\Theta'/n \right)^n \left(\frac{m_0 \beta}{\bar{\gamma}_0} \right) \middle| \begin{matrix} 0, (1-m_0) \\ -m_0, \Delta(n,0), m_0 \end{matrix} \right) & \quad (A.21)
 \end{aligned}$$

where $\Delta(a,b) = \left(\frac{b}{a}, \frac{b+1}{a}, \dots, \frac{b+a-1}{a} \right)$. Substituting (A.21) into (A.19) yields the outage probability in (5.30)

APPENDIX B

B.1 Fox's H -function [46]

H -function is defined using Mellin-Barnes type integral as

$$H_{p,q}^{m,n}[z] = H_{p,q}^{m,n} \left[z \left| \begin{matrix} (a_p, T_p) \\ (b_q, B_q) \end{matrix} \right. \right] = \frac{1}{2\pi j} \oint_{\epsilon} \Xi_H(s) z^{-s} ds \quad (\text{B.1})$$

where $\Xi_H(s) = \frac{\prod_{j=1}^m \Gamma(b_j + B_j s) \prod_{j=1}^n \Gamma(1 - a_j - T_j s)}{\prod_{j=n+1}^p \Gamma(a_j + T_j s) \prod_{j=l+1}^q \Gamma(1 - b_j - B_j s)}$ and z may be real or complex

but not zero, m, n, p , and q are integers such that $1 \leq m \leq q, 0 \leq n \leq p$; $T_j, B_j > 0$, a_j and b_j are complex parameters.

B.2 Meijer's G -function [30]

The Meijer G -function is a special case of the H -function (B.1) and is obtained by letting $T_j = B_j = 1$, thus G -function is expressed as

$$G_{p,q}^{m,n}[z] = G_{p,q}^{m,n} \left[z \left| \begin{matrix} a_1, \dots, a_p \\ b_1, \dots, b_q \end{matrix} \right. \right] = \frac{1}{2\pi j} \oint_{\epsilon} \Xi_G(s) z^{-s} ds \quad (\text{B.2})$$

where $\Xi_G(s) = \frac{\prod_{j=1}^m \Gamma(b_j + s) \prod_{j=1}^n \Gamma(1 - a_j - s)}{\prod_{j=n+1}^p \Gamma(a_j + s) \prod_{j=l+1}^q \Gamma(1 - b_j - s)}$.

APPENDIX C

The MATLAB code used for simulation is given below.

```
clear all;clc;close all;
tic;
att_coef=3.5;
W=10^-4;
Ptx=1;
L = 100;
Kx=1;
Ky=1;
Mx=3;
pwr0 = 5;
pwri = 1;
sigm=1;
Gx=1;
My=2;
Gy=10;
do=0; %Exclusion zone
Thresh =10; % Minimum Sensor sensitivity
N_dens=10^-3; % Sensor density
N_itera=1500; % Number of iterations
iso_prob=zeros(1,N_itera);
bin_prob=zeros(1,N_itera);

for k=1:N_itera
clear dist topl s Px;
N=poissrnd(N_dens*L^2);
dist=zeros(N+2,N+2);
netXloc = unifrnd(-50,50,N+2,1);
netYloc = unifrnd(-50,50,N+2,1);
B=[netXloc netYloc];
for i = 1:N+2
dist(i,:)=sqrt((B(i,1)-B(:,1)).^2 +(B(i,2)-B(:,2)).^2);
end;
for i = 1:N+2
dist(i,i)=0;
end;
topl=zeros(N+2,N+2);
Px=zeros(N+2,N+2);
for i=1:N+2
for j=1:N+2
if (i~=j)
topl(i,j)=Kx*gamrnd(Mx,Gx)*lognrnd(0,sigm)*(dist(i,j)^(-
att_coef));
```

```

        LDist=dist(j,:);
        LDist(i)=0;
        CC=find(LDist>do);
        DD=Ky*gamrnd(My,Gy).*lognrnd(0,sign);
        VV= LDist(CC)';
        s = VV.^(-att_coef) .*DD;
        BBo=sum(s);
        Bo=BBo+W;
        AB=(top1(i,j)/Bo);
        if (AB >= Thresh)
            Px(i,j)=1;
        else
            Px(i,j)=0;
        end
    end
end

end

UU=sum(Px)';
III=sum(Px,2);
JJ=UU+III;
z=length(find(JJ==0));
iso_prob(k)=z/N;
end

CCC=isnan(iso_prob);
iso_prob(CCC)=0;
PP=sum(iso_prob)/length(iso_prob);
toc;

```

BIBLIOGRAPHY

- [1] V. A. Aalo, T. Piboongunon and C. D. Iskander, "Bit-error rate of binary digital modulation schemes in generalized gamma fading channels," *IEEE Communications Letters*, vol. 9, pp. 139-141, 2005.
- [2] V. A. Aalo and J. Zhang, "Performance analysis of maximal ratio combining in the presence of multiple equal-power cochannel interferers in a Nakagami fading channel," *IEEE Transactions on Vehicular Technology*, vol. 50, pp. 497-503, 2001.
- [3] A. Abdi and M. Kaveh, "On the utility of gamma PDF in modeling shadow fading (slow fading)," in *IEEE 49th Vehicular Technology Conference*, 1999, pp. 2308-2312.
- [4] M. Abramowitz and I. A. Stegun, *Handbook of Mathematical Functions with Formulas, Graphs, and Mathematical Tables*. New York: Dover Publications, Inc., 1972.
- [5] D. P. Agrawal and Q. Zeng, *Introduction to Wireless and Mobile Systems*. Stamford, CT: Cengage Learning, 2011.
- [6] O. Akan, O. Karli and O. Ergul, "Cognitive radio sensor networks," *IEEE Network*, vol. 23, pp. 34-40, 2009.
- [7] I. F. Akyildiz, W. Y. Lee, M. C. Vuran and S. Mohanty, "A survey on spectrum management in cognitive radio networks," *IEEE Communications Magazine*, vol. 46, pp. 40-48, 2008.
- [8] I. F. Akyildiz and X. Wang, "A survey on wireless mesh networks," *IEEE Communications Magazine*, vol. 43, pp. S23-S30, 2005.
- [9] S. A. Aldosari and J. M. F. Moura, "Detection in Sensor Networks: The Saddlepoint Approximation," *IEEE Transactions on Signal Processing*, vol. 55, pp. 327-340, 2007.
- [10] S. Atapattu, C. Tellambura and H. Jiang, "A Mixture Gamma Distribution to Model the SNR of Wireless Channels," *IEEE Transactions on Wireless Communications*, vol. 10, pp. 4193-4203, 2011.

- [11] A. V. Babu and M. K. Singh, "Node Isolation Probability of Wireless Adhoc Networks in Nakagami Fading Channel," *International Journal of Computer Networks & Communications*, vol. 2, pp. 21-36, 03-05, 2010.
- [12] X. Bai, S. Kumar, D. Xuan, Z. Yun and T. H. Lai, "Deploying wireless sensors to achieve both coverage and connectivity," in *Proceedings of the 7th ACM International Symposium on Mobile Ad Hoc Networking and Computing*, Florence, Italy, 2006, pp. 131-142.
- [13] N. C. Beaulieu and C. Cheng, "Efficient Nakagami-m fading channel Simulation," *IEEE Transactions on Vehicular Technology*, vol. 54, pp. 413-424, 2005.
- [14] N. C. Beaulieu and A. A. Abu-Dayya, "Bandwidth efficient QPSK in cochannel interference and fading," *IEEE Transactions on Communications*, vol. 43, pp. 2464-2474, 1995.
- [15] C. Bettstetter and C. Hartmann, "Connectivity of Wireless Multihop Networks in a Shadow Fading Environment," *Wireless Networks*, vol. 11, pp. 571-579, 2005.
- [16] P. Cardieri, "Modeling Interference in Wireless Ad Hoc Networks," *IEEE Communications Surveys & Tutorials*, vol. 12, pp. 551-572, 2010.
- [17] Y. C. Cheng and T. G. Robertazzi, "Critical connectivity phenomena in multihop radio models," *IEEE Transactions on Communications*, vol. 37, pp. 770-777, 1989.
- [18] C. D. Cordeiro, D. P. Agrawal and D. H. Sadok, "Interference modeling and performance of Bluetooth MAC protocol," *IEEE Transactions on Wireless Communications*, vol. 2, pp. 1240-1246, 2003.
- [19] A. J. Coulson, A. G. Williamson and R. G. Vaughan, "Improved fading distribution for mobile radio," *IEEE Proceedings Communications*, vol. 145, pp. 197-202, 1998.
- [20] D. J. Daley and D. Vere Jones, *An Introduction to the Theory of Point Processes*. New York: Springer, 2002.
- [21] M. Derakhshani and T. Le-Ngoc, "Aggregate Interference and Capacity-Outage Analysis in a Cognitive Radio Network," *IEEE Transactions on Vehicular Technology*, vol. 61, pp. 196-207, 2012.
- [22] N. Devroye, M. Vu and V. Tarokh, "Cognitive radio networks," *IEEE Signal Processing Magazine*, vol. 25, pp. 12-23, 2008.
- [23] O. Dousse, F. Baccelli and P. Thiran, "Impact of interferences on connectivity in ad hoc networks," *IEEE/ACM Transactions on Networking*, vol. 13, pp. 425-436, 2005.

- [24] V. Erceg, L. J. Greenstein, S. Tjandra, S. R. Parkoff, A. Gupta, B. Kulic, A. Julius and R. Jastrzab, "An empirically-based path loss model for wireless channels in suburban environments," in *IEEE The Bridge to Global Integration, Global Telecommunications Conference (GLOBECOM)*, 1998, pp. 922-927.
- [25] B. A. Fette, *Cognitive Radio Technology*. Amsterdam ; Boston: Newnes/Elsevier, 2006.
- [26] A. Fragkiadakis, E. Tragos and I. Askoxylakis, "A Survey on Security Threats and Detection Techniques in Cognitive Radio Networks," *IEEE Communications Surveys & Tutorials*, vol. PP, pp. 1-18, 2012.
- [27] V. K. Garg, *Wireless Communications and Networking*. Amsterdam ; Boston: Elsevier Morgan Kaufmann, 2007.
- [28] A. Ghasemi, "Interference aggregation and sensing in cognitive radio networks," in *Second International Workshop on Cognitive Radio and Advanced Spectrum Management (CogART)*, 2009, pp. 86-90.
- [29] A. Goldsmith, *Wireless Communications*. Cambridge University Press., 2005.
- [30] I. S. Gradshteyn, A. Jeffrey and I. M. Ryzhik, *Table of Integrals, Series, and Products*. Boston: Academic Press, 1994.
- [31] J. Griffiths and J. P. McGeehan, "Interrelationship between some statistical distributions used in radio-wave propagation," *IEEE Proceedings F Communications, Radar and Signal Processing.*, vol. 129, pp. 411-417, 1982.
- [32] R. Hekmat and P. Van Mieghem, "Interference in Wireless Multi-Hop Ad-Hoc Networks and Its Effect on Network Capacity," *Wireless Networks*, vol. 10, pp. 389-399, 2004.
- [33] A. Hossain, P. K. Biswas and S. Chakrabarti, "Sensing models and its impact on network coverage in wireless sensor network," in *IEEE Region 10 and the Third International Conference on Industrial and Information Systems (ICIIS)*, 2008, pp. 1-5.
- [34] C. Huang, Y. Tseng and H. Wu, "Distributed protocols for ensuring both coverage and connectivity of a wireless sensor network," *ACM Trans.Sen.Netw.*, vol. 3, March, 2007.
- [35] J. Ilow and D. Hatzinakos, "Analytic alpha-stable noise modeling in a Poisson field of interferers or scatterers," *IEEE Transactions on Signal Processing.*, vol. 46, pp. 1601-1611, 1998.

- [36] H. Inaltekin, S. B. Wicker, M. Chiang and H. V. Poor, "On unbounded path-loss models: effects of singularity on wireless network performance," *IEEE Journal on Selected Areas in Communications.*, vol. 27, pp. 1078-1092, 2009.
- [37] J. Karedal, A. J. Johansson, F. Tufvesson and A. F. Molisch, "A Measurement-Based Fading Model for Wireless Personal Area Networks," *IEEE Transactions on Wireless Communications.*, vol. 7, pp. 4575-4585, 2008.
- [38] M. Khabazian, S. Aissa and M. Mehmet-Ali, "Performance modeling of message dissemination in vehicular ad hoc networks," in *IEEE 5th International Symposium on Wireless Pervasive Computing (ISWPC)*, 2010, pp. 174-179.
- [39] I. M. Kostic, "Analytical approach to performance analysis for channel subject to shadowing and fading," *IEEE Proceedings Communications.*, vol. 152, pp. 821-827, 2005.
- [40] S. Kusaladharma and C. Tellambura, "Aggregate Interference Analysis for Underlay Cognitive Radio Networks," *IEEE Wireless Communications Letters.*, vol. 1, pp. 641-644, 2012.
- [41] S. Lee and A. Lim, "Reliability and performance of IEEE 802.11n for vehicle networks with multiple nodes," in *International Conference on Computing, Networking and Communications (ICNC)*. 2012, pp. 252-256.
- [42] W. C. Y. Lee, *Wireless and Cellular Telecommunications*. New York, NY: McGraw-Hill, 2006.
- [43] X. Liu and M. Haenggi, "Throughput analysis of fading sensor networks with regular and random topologies," *EURASIP J. Wirel. Commun. Netw.*, vol. 2005, pp. 554-564, sep, 2005.
- [44] Z. Liu, H. Liu, W. Xu and Y. Chen, "Exploiting Jamming-Caused Neighbor Changes for Jammer Localization," *IEEE Transactions on Parallel and Distributed Systems*, vol. 23, pp. 547-555, 2012.
- [45] S. B. Lowen and M. C. Teich, "Power-law shot noise," *IEEE Transactions on Information Theory.*, vol. 36, pp. 1302-1318, 1990.
- [46] A. M. Mathai, H. J. Haubold and R. K. Saxena, *The H-Function Theory and Applications*. New York: Springer, 2009.
- [47] V. P. Mhatre, C. Rosenberg, D. Kofman, R. Mazumdar and N. Shroff, "A minimum cost heterogeneous sensor network with a lifetime constraint," *IEEE Transactions on Mobile Computing.*, vol. 4, pp. 4-15, 2005.

- [48] D. Miorandi, "The Impact of Channel Randomness on Coverage and Connectivity of Ad Hoc and Sensor Networks," *IEEE Transactions on Wireless Communications.*, vol. 7, pp. 1062-1072, 2008.
- [49] A. Mudesir, M. Bode, K. W. Sung and H. Haas, "Analytical SIR for self-organizing wireless networks," *EURASIP J. Wirel. Commun. Netw.*, vol. 2009, pp. 18:1-18:8, Jan, 2009.
- [50] M. Naserian, K. Tepe and T. Mohammed, "On the connectivity of nodes in wireless ad hoc and sensor net," in *Canadian Conference on Electrical and Computer Engineering*, 2005, pp. 2073-2075.
- [51] R. Niu and P. K. Varshney, "Performance Analysis of Distributed Detection in a Random Sensor Field," *IEEE Transactions on Signal Processing.*, vol. 56, pp. 339-349, 2008.
- [52] T. Piboongunon, V. A. Aalo and C. D. Iskander, "Average error rate of linear diversity reception schemes over generalized gamma fading channels," in *IEEE SoutheastCon. Proceedings*. 2005, pp. 265-270.
- [53] P. C. Pinto and M. Z. Win, "Communication in a poisson field of interferers," in *40th Annual Conference on Information Sciences and Systems*, 2006, pp. 432-437.
- [54] R. Rajagopalan and P. Varshney, "Connectivity analysis of wireless sensor networks with regular topologies in the presence of channel fading," *IEEE Transactions on Wireless Communications.*, vol. 8, pp. 3475-3483, 2009.
- [55] T. S. Rappaport, *Wireless Communications : Principles and Practice*. Upper Saddle River, N.J: Prentice Hall PTR, 2002.
- [56] T. Riley, "Modeling of licensed PCS self-interference." in *IEEE Military Communications Conference (MILCOM). Communications for Network-Centric Operations: Creating the Information Force*. 2001, pp. 408-412.
- [57] A. Salmasi and K. S. Gilhousen, "On the system design aspects of code division multiple access (CDMA) applied to digital cellular and personal communications networks," in *IEEE Vehicular Technology Conference, 41st. Gateway to the Future Technology in Motion*, 1991, pp. 57-62.
- [58] H. Schmidli, "Risk Theory," 1996.
- [59] R. K. Schmidt, B. Kloiber, F. Schuttler and T. Strang, "Degradation of communication range in VANETs caused by interference 2.0 - real-world experiment," in *Proceedings of the Third International Conference on Communication Technologies for Vehicles*, Oberpfaffenhofen, Germany, 2011, pp. 176-188.

- [60] S. Shakkottai, R. Srikant and N. B. Shroff, "Unreliable sensor grids: coverage, connectivity and diameter," *Ad Hoc Networks*, vol. 3, pp. 702-716, 11, 2005.
- [61] P. Shankar, "Statistical Models for Fading and Shadowed Fading Channels in Wireless Systems: A Pedagogical Perspective," *Wireless Personal Communications*, vol. 60, pp. 191-213, 2011.
- [62] P. Shankar, "Performance Analysis of Diversity Combining Algorithms in Shadowed Fading Channels," *Wireless Personal Communications*, vol. 37, pp. 61-72, 2006.
- [63] P. M. Shankar, "Error Rates in Generalized Shadowed Fading Channels," *Wireless Personal Communications*, vol. 28, pp. 233-238, 2004.
- [64] R. Shorey, A. Ananda, M. C. Chan and W. T. Ooi, *Mobile, Wireless, and Sensor Networks : Technology, Applications, and Future Directions*. Piscataway : Hoboken, N.J: IEEE Press ; Wiley-Interscience, 2006.
- [65] M. K. Simon and M. S. Alouini, *Digital Communication Over Fading Channels*. Hoboken, N.J: Wiley-Interscience, 2005.
- [66] E. W. Stacy, "A Generalization of the Gamma Distribution," *The Annals of Mathematical Statistics*, vol. 33, pp. pp. 1187-1192, Sep., 1962.
- [67] G. L. Stüber, *Principles of Mobile Communication*. Boston: Kluwer Academic, 2001.
- [68] M. Torrent-Moreno, D. Jiang and H. Hartenstein, "Broadcast reception rates and effects of priority access in 802.11-based vehicular ad-hoc networks," in *Proceedings of the 1st ACM International Workshop on Vehicular Ad Hoc Networks*, Philadelphia, PA, USA, 2004, pp. 10-18.
- [69] I. Trigui, A. Laourine, S. Affes and A. Stephenne, "Performance analysis of mobile radio systems over composite fading/shadowing channels with co-located interference." *IEEE Transactions on Wireless Communications.*, vol. 8, pp. 3448-3453, 2009.
- [70] Y. R. Tsai, "Sensing Coverage for Randomly Distributed Wireless Sensor Networks in Shadowed Environments," *IEEE Transactions on Vehicular Technology.*, vol. 57, pp. 556-564, 2008.
- [71] Q. Tse and B. Landfeldt, "Interference-aware geocasting for VANET," in *IEEE International Symposium on a World of Wireless, Mobile and Multimedia Networks (WoWMoM)*, 2012, pp. 1-6.

- [72] J. Venkataraman, M. Haenggi and O. Collins, "Shot noise models for outage and throughput analyses in wireless ad hoc networks," in *IEEE Military Communications Conference (MILCOM)*, 2006, pp. 1-7.
- [73] Y. Wen, S. Loyka and A. Yongacoglu, "On distribution of aggregate interference in cognitive radio networks," in *25th Biennial Symposium on Communications (QBSC)*, 2010, pp. 265-268.
- [74] M. Z. Win, P. C. Pinto and L. A. Shepp, "A Mathematical Theory of Network Interference and Its Applications," *Proceedings of the IEEE*, vol. 97, pp. 205-230, 2009.
- [75] W. Xu, K. Ma, W. Trappe and Y. Zhang, "Jamming sensor networks: attack and defense strategies," *IEEE Network*, vol. 20, pp. 41-47, 2006.
- [76] T. Yang, G. Mao and W. Zhang, "Connectivity of Large-Scale CSMA Networks," *IEEE Transactions on Wireless Communications*, vol. 11, pp. 2266-2275, 2012.
- [77] X. Yang and A. P. Petropulu, "Co-channel interference modeling and analysis in a Poisson field of interferers in wireless communications," *IEEE Transactions on Signal Processing.*, vol. 51, pp. 64-76, 2003.
- [78] Y. D. Yao and A. U. H. Sheikh, "Investigations into cochannel interference in microcellular mobile radio systems," *IEEE Transactions on Vehicular Technology*, vol. 41, pp. 114-123, 1992.
- [79] M. Zorzi and S. Pupolin, "Outage probability in multiple access packet radio networks in the presence of fading," *IEEE Transactions on Vehicular Technology.*, vol. 43, pp. 604-610, 1994.